PETROLOGY AND GEOCHEMISTRY OF A PROGRESSIVELY METAMORPHOSED SEDIMENTARY FORMATION IN BIG THOMPSON CANYON, LARIMER COUNTY, COLORADO

By

Charles Martell

Submitted in Partial Fulfillment
of the Requirements for the Degree of
Master of Science in Geology

New Mexico Institute of Mining and Technology

Socorro, New Mexico

May, 1982

ABSTRACT

Big Thompson Canyon is located along the eastern flank of the dominantly high grade gneissic terrain of the Front Range. A lower metamorphic grade enclave is exposed in this localized area, representing a progressively metamorphosed sedimentary formation (phyllites and schists, 1.70 - 1.75 b.y.) with metamorphic isograds, approximately perpendicular to the strike of an isoclinally folded sequence, intruded by syntectonic igneous bodies.

A clastic assemblage consisting of polycrystalline quartz aggregates, monocrystalline quartz, plagioclase and alkali feldspar is present in rocks of the biotite and garnet zones. Grain size is similar in the two zones, although the garnet zone varies from the biotite zone in the following ways: clastic grains decrease in abundance, monocrystalline quartz grains and individual grains of polycrystalline quartz aggregates are more rounded and show greater development of mortar texture and feldspar grains show greater development of sieve texture. As the clastic assemblage recrystallizes, metamorphic minerals quartz, plagioclase, biotite, muscovite and alkali feldspar increase in abundance, in size, in frequency of idioblastic grains, and become more polygonal in nature. Metamorphic index minerals garnet, staurolite and sillimanite are not abundant. Presence of andalusite and sillimanite suggests low- to medium- pressure metamorphism.

Samples from zones of progressively higher grades

show that the following occurs: Al2O3, Fe2O3T, MgO, K2O, Cs, Rb, Ba, Sc and Ce increase, SiO2, CaO and Zr decrease, rare earth elements and Na2O remain approximately constant and Hf, Cr, U, Th and Sr behave erratically. Variations in original sedimentary composition and metasomatic effects resulting from the igneous intrusions in the area contribute to these chemical changes. Correlation exists between mineralogy and of the bulk chemistry of the rocks with increasing grades of metamorphism, except for the relation between Na2O and plagioclase. Effects from metasomatism, sedimentary chemical variation and progressive metamorphism cannot be individually determined. Possible transposition of sedimentary layers during isoclinal folding places doubt on whether a single unit was sampled.

Polycrystalline quartz aggregates are interpreted as quartzite rock fragments and serve as a constraint for provenance. Clastic monocrystalline quartz, plagioclase and alkali feldspar suggest a granitic rock source. This is confirmed by X-Y element pair, CaO-Al2O3-MgO and CaO-Na2O-K2O plots.

Detrital sandstone grain plots suggest a lack of magmatic arc provenances in the original tectonic setting. The SiO2-Na2O-K2O plot suggests a miogeoclinal setting.

ACKNOWLEDGEMENTS

Thanks go out to many people who assisted me in the analytical procedures and the writing of this thesis. Kent Condie, principal thesis advisor provided guidance and a forum for discussion. Advisors J. Robertson and A. Budding read this thesis and offered suggestions for its improvement. Sandia Laboratories of Albuquerque irradiated the rock samples used in instrumental activation analysis and P. Allen assisted with the analytical techniques. K. Faris assisted with X-Ray Fluorescence analytical procedures. J. Renault assisted with the X-Ray Fluorescence data reduction. C. Taplin typed this manuscript. J. Brannan drafted the figures included in this report. T. and M. McCrink and A. Simcox reviewed this manuscript.

TABLE OF CONTENTS

LIST OF FIGURES

15- CaO-K2O-Na2O plot delineating position witin the Granitic field

16- Al2O3-CaO-MgO plot illustrating presence of plutonic rock types

17- K-Rb plot

18- Average REE distributions in metasediments from each metamorphic zone in Big Thompson Canyon. Subscript N refers to chondrite-normalized ratios

19- Envelope of REE variation for the Big Thompson Canyon metasediments compared to average North American Shale (NASC) and to the envelope of REE variation in graywackes

20- Triangular quartz-feldspar-unstable lithic fragments plot showing different types of provenance as a function of framework mode

21- Triangular monocrystalline quartz-total feldspar-lithic fragments plot showing different types of provenance as a function of framework mode

22- Tectonic setting as a function of SiO2, K2O, and Na2O content of Big Thompson Canyon biotite zone-samples

LIST OF TABLES

6-14,17)

19-References for constructed rock fields of X-Y element plots

20-Source rock proportions calculated from X-Y element plots

D1-Elements determined by neutron activation analysis

E1-X-Ray Fluorescence instrument settings and error calculations

E2-Standards (concentraions in %) used in constructing calibration curves

E3-Influencing elements affecting analyte concentrations

E4-Mass absorption coefficients of standards used in determining Rb, Sr, and Zr concentrations

INTRODUCTION

Location

The Colorado Front Range is a northward-trending mountainous uplift, approximately 50 to 55 kilometers wide. It extends from Canyon City, Colorado, north to the Wyoming state border where it merges with the Laramie Range (Figure 1). The eastern slope of the Front Range is characterized by broad, dissected, terraces that descend in steps to the plains.

The entrance to Big Thompson Canyon coincides with the Front Range - Denver Basin border, west of Loveland, Colorado. This entrance way is the beginning of a 17.5 km traverse through the canyon, that is situated between west longitudes 105 22. 30" and 105 12. 30.. and north latitudes 40 27. 30" and 40 23. 30" in the Drake and Masonville 7.5 quadrangles (Plate 1).

Objectives of the Study

Samples were collected along this traverse from the progressively metamorphosed sedimentary Idaho Springs Formation of Proterozoic age (1.70 to 1.75 b.y.) for petrographic study and geochemical analysis. Chemical analyses were obtained using Instrumental Neutron Activation and X-Ray Fluorescence techniques. (Refer to the Appendix

for sampling and analytical procedures.)

The main objectives of this study are to determine

1) Changes in mineralogy and chemistry with increasing metamorphic grade.
2) Provenance of the sediments utilizing petrologic and chemical data.
3) Path of progressive metamorphism on a pressure-temperature diagram, and
4) Petrologic and chemical constraints for tectonic setting.

Early literature by Fuller (1924), Lovering (1929) and Lovering and Goddard (1950) describes the occurrences of the Idaho Springs Formation throughout the Front Range, which is an uplift of Proteozoic basement rocks. This formation consists chiefly of biotitic and pelitic schists and sillimanite gneisses of sedimentary origin. Proterozoic granites, granite gneisses, pegmatites, migmatites and tonalites are locally abundant, and are usually conformable with metasedimentary rock structures.

Tweto (1977) appraised existing nomenclature of Precambrian rocks in Colorado and he urged dropping the use of the term "Idaho Springs Formation". Throughout the Front Range, schists and gneisses of sedimentary origin have been indiscriminately included in this formation without regard to their stratigraphic position. He also recommends

assigning lithic unit names to individual localities of the Idaho Springs Formation. Braddock et al (1970a) and (1970b) assign the name "Metasedimentary rocks" to the formation in the Drake and Masonville 7.5 quadrangles. According to Braddock, this unit consists of interbedded quartzo-feldspathic schist and gneiss and mica schist and gneiss. Thin beds of granular to pebbly metaconglomerate and knotted mica schist are also present. This sequence is isoclinally folded with axial traces trending northwest-southeast, according to Fuller (1924), Lovering (1929), Lovering and Goddard (1950) and Braddock (1966).

Big Thompson Canyon Study Area

A geologic map (see pocket and Figure 2) of the Drake and Masonville quadrangles, after Braddock et al (1970a) and (1970b) illustrates a progressive metamorphic sequence. Garnet, staurolite and sillimanite isograds are approximately perpendicular to the general east-west strike of the beds. The biotite isograd is not exposed in the study area. Metamorphic zones are defined as the areas between adjacent isograds. Samples were collected from all four metamorphic zones. Collection sites are primarily concentrated in the canyon. The only exception was the biotite zone, which was collected at higher elevations, out of the canyon. All samples were collected away from faults and shear zones.

In this type of study it is necessary to sample a succession that records part of a facies series. A sample collecting traverse should be made along strike of a homogeneous succession on the scale of tens of kilometers. The isograds should be at a steep angle to the strike of the unit.

Suitable sample sites were difficult to find in the sillimanite zone because of the abundance of Pegmatitic Granite bodies. A fluid phase eminating from this intrusive body may affect the chemistry of the host metasedimentary rocks and obscure the effects of progressive metamorphism.

Biotite-muscovite granite, pegmatitic granite, tonalite and amphibolite are the other Proterozoic rock units present besides "Metasedimentary rocks". Paleozoic and Mesozoic undifferentiated strata occur in the eastern region of the geologic map, dipping at steep angles to the east. Quaternary sediments occur throughout the study area. The contact between Proterozoic and Phanerozoic rocks represents the eastern limit of the dominantly Proterozoic, Front Range.

Geologic History

The following geologic history of the Big Thompson Canyon area is based on works by Lovering (1929), Lovering and Goddard (1950), Braddock (1966), Hedge et al (1967), Peterman et al (1968), Braddock (1970) and Tweto (1977).

The Big Thompson Canyon area represents a lower metamorphic grade enclave in the Front Range high grade gneissic terrain.

1) Sediments were deposited about 1.8 billion years ago.
2) The first stage of deformation produced large scale (amplitude = 5 km) isoclinal folds and formed a penetrative cleavage.
3) Albite-muscovite-chlorite-phyllites are a product of the first period of metamorphism.
4) The second stage of deformation produced superposed folds and a crenulation cleavege.
5) A third stage of deformation deformed the earlier two generations and produced a second crenulation cleavage. This stage of deformation was accompanied by a second period of regional metamorphism about 1.70 to 1.75 billion years ago (presently exposed biotite, garnet, staurolite and sillimanite zones) and intrusion of syntectonic igneous rocks. Peterman et al (1968) determined this age using the Rb-Sr method. These igneous rocks (tonalite, biotite-muscovite granite, pegmatitic granite) are mostly concordant and unfoliated.
6) Post-tectonic, mostly discordant, unfoliated granite to quartz monzonite bodies were emplaced in the Front Range about 1.4 billion years ago. These bodies are not exposed in the study area.
7) The Ancestral Rocky Mountains were formed during

Mid-Carboniferous to Mid-Triassic time.

8) During the Laramide orogeny (Late Cretaceous-early Eocene), the fault-bounded Precambrian basement was once again uplifted, forming the Front Range and adjacent Denver Basin with a facies distribution representing a proximal to distal piedmont tract.

Petrography

Introduction

This study focuses on a quartzo-feldspathic schist and phyllite (metasedimentary) unit of the (13,000 ft. thick) Idaho Springs Formation of central Colorado (Figure 1). Major metamorphic minerals are quartz, plagioclase, biotite, muscovite, chlorite, garnet, sillimanite, staurolite and alkali feldspar. Unmetamorphosed clastic grains present in the biotite and garnet zones are alkali feldspar, plagioclase, quartzite rock fragments (polycrystalline quartz aggregates), monocrystalline quartz, apatite, tourmaline and magnetite. Grain size varies from 0.05 mm for metamorphic quartz and plagioclase to 4.5 mm for the quartzite rock fragments and clastic alkali feldspar.

Biotite, garnet, staurolite and sillimanite are the index minerals for the progressively increasing metamorphic zones. Biotite is ubiquitous in all four zones. Garnet, staurolite and sillimanite are not present in every sample of their respective zones.

Not all of the Big Thompson Canyon samples are bedded on a hand specimen scale. (Since all of the beds present are less than one centimeter thick they will subsequently referred to as laminations.) The fresh surfaces of the laminated hand specimens show alternating grey to black and silver to white bands (Plate 1). Non-laminated

hand specimens are gray, black, silver and speckled white. The laminations are rich in mica, which alternates with feldspar and quartz. This cyclic repitition of laminations in the low grade samples and the presence of graded bedding throughout the entire area indicate a sedimentary origin (Braddock et al, 1970a and 1970b). In the biotite zone the mica-rich layers are less than 1 mm thick; they are 2 mm thick in the sillimanite zone, but with less quartz and feldspar. With increasing grades of metamorphism, the alternating laminations respectively become richer in mica and feldspar plus quartz. Additionally, the thicknesses of the laminations become more regular and consistent. Grain size is too small for these samples to be classisied as gneisses.

Three generations of foliation surfaces are present. The first two generations are dominant. In the study samples, each generation is at a constant small acute angle with the sedimentary laminations. A weak, third generation bisects the earlier foliations. These three foliation surfaces do not cross cut the poikiloblastic biotite porphyroblasts that are present, indicating mineral growth occurred after the last deformational period.

The two dominant foliation surfaces are characterized by the following:

1) Each generation is well defined by parallel mica grains.

2) When present, long axes of clastic plagioclase, clastic

monocrystalline quartz, polycrystalline quartz aggregates and clastic alkali feldspar are sub-parallel to parallel to the foliation surfaces. These grains exhibit pronounced undulose extinction.

3) Foliation surfaces are not well defined by metamorphic plagioclase, alkali feldspar and quartz in the biotite and garnet zones, but are when these grains acquire a more polygonal shape in the staurolite and sillimanite zones. The third generation is well defined by the micas but not by the other mineral grains.

Biotite Zone

Rocks of this zone exhibit varying degrees of metamorphic recrystallization of a clastic assemblage consisting of monocrystalline quartz, polycrystalline quartz aggregates (quartzite rock fragments), plagioclase and alkali feldspar. Ubiquitous accessory minerals are apatite, tourmaline and magnetite. Metamorphic minerals are quartz, plagioclase, biotite and muscovite. Biotite commonly is partially transformed to chlorite.

The following is a list of general criteria that were used to distinguish clastic from metamorphic grains in rocks of the study area:

1) Clastic grains tend to be coarser in size.

2) Metamorphic grains are xenoblastic and are truncated against the boundaries of the clastic grains.

3) Clastic grains are usually more rounded than metamorphic grains.

4) Mortar texture is developed along the boundaries of the monocrystalline quartz grains.

5) Polycrystalline quartz aggregates contain rounded to subangular grains, some with mortar texture.

Results of the modal analysis are listed in Table 1. Mean values and ranges of the mineral percentages are listed in Table 5. Possible inconsistancies between the modal analysis and major element chemistry may result. Causes for this are listed in Appendix B. Mean values for the metamorphic and clastic components are, respectively, 55% and 45%. The quartz group (metamorphic and clastic components) comprises about 66% of the rock assemblage. Muscovite and biotite together contribute 20%, biotite usually predominating. The feldspar group (mostly metamorphic plagioclase, clastic alkali feldspar and plagioclase) contributes 11%. Of the clastic assemblage, plagioclase and alkali feldspar contribute a minor amount (3%), monocrystalline and polycrystalline quartz contribute the major part (39%).

The terminology used to describe metamorphic textures is from Spry (1969). Since schistosity is well developed and metamorphic isograds were assigned by Braddock, et al (1970a and b) to document progressive metamorphism in the Big Thompson Canyon Area, textures of regional metamorphism will be used.

Quartz a dominant mineral in the Big Thompson Canyon samples, was subdivided into three groups on the basis of grain size, form and crystals per grain. Polycrystalline quartz aggregates (1 - 4.5 mm in size) usually contain five to ten crystals per grain (Plate 2). The contained crystals have curved to straight boundaries, are 0.2 to 0.7 mm in size, are subangular to subrounded in shape and do not exhibit preferred orientation. Under crossed nicols, extinction is not uniform for the individual crystals. In a few polycrystalline quartz aggregates, secondary quartz occurs as thin strips rimming the contained quartz crystals. These strips may be rim cement. The polycrystalline aggregates, when subangular to rounded in shape, do not exhibit preferred orientation. Preferred orientation is probably the result of stretching of polycrystalline aggregates during deformation.

The lack of major metamorphic textures in the quartzite rock fragments suggests a sedimentary origin. Alternatively, they may have formed during deformation of quartz-rich laminations. But in many samples the aggregates are isolated from each other and from quartz rich laminations. In either case, it is important to consider that the rock has been subjected to three perdiods of deformation and metamorphism (Braddock, 1967). In addition to the stretching, mortar texture is present in varying degrees of development. Certain aggregates appear stable but others show varying degrees of disaggregation.

The second category of clastic quartz is referred to as monocrystalline quartz (Plate 2). A minor constituent of this category is the result of the disaggregation of the polycrystalline aggregates. Monocrystalline quartz grains are nearly adjacent to the aggregate. In certain aggregates, fractures are evident.

Sizes of monocrystalline clastic quartz grain range from 0.2 ot 0.75 mm (fine to coarse sand); grain shape varies from rounded to subangular. Most grains do not show preferred orientation. Certain grains are elongated, possibly resulting from deformation. Under crossed nicols a small percentage of the grains show pronounced undulose extinction. Other mineral grains are truncated against or appear to grow around the monocrystalline quartz grains.

The physical nature of these monocrystalline grains has been modified to some degree by deformation and metamorphism. Mortar texture is present in various stages of development. Certain grains appear to have taken on a stretched, polygonal shape. Metamorphic imprinting may straighten the boundaries on the larger clastic grains. The grain size variation is a function of the original clastic size, the degree of mortar texture development and the amount of secondary grain growth.

The third category of quartz is metamorphic. These grains are the result of the recrystallization of polycrystalline and monocrystalline quartz. Grain size ranges from 0.05 to 0.1 mm. Therefore a size division

between obvious clastic and metamorphic quartz appears to be between 0.1 and 0.2 mm. A subgroup is clastic monocrystalline quartz that has been subjected to cataclasis and consequently has been reduced in grain size.

Most metamorphic quartz grains are xenoblastic, with some idioblastic grains. Growth forms for adjacent metamorphic quartz grains are varied due to the presence of granular and heteroblastic textures on a thin section scale. Granoblastic, polygonal to elongate textures result when granular textures are present.

Granular textures are more prevalent for groups of metamorphic quartz grains when there is less mica. This complexity of grain shape and growth form is the result of deformation and metamorphism.

Plagioclase is present in metamorphic and clastic forms. It is characterized by size, presence of twinning, grain shape, growth forms, degree of pitting of grains and presence of saussurite alteration products.

Clastic plagioclase ranges in size from 0.2 to 2.0 mm (Plate 3). Grains are rounded to sub-angular laths with long axes showing preferred orientation within the two strong schistosity planes. Varying degrees of sericite alteration are present. Muscovite laths less than 0.05 mm are present. Twinning laws include albite and Carlsbad types but there are statistically too few clastic plagioclase grains present to allow an anorthite content determination. Boundaries of metamorphic minerals are

truncated against the mostly straight to curved boundaries of the clastic plagioclase grains.

Polyphase deformation does not appear to have appreciably affected the shape of the grains and fracturing is not observed. Size of grains may be related to original clastic size range. Obvious overgrowths are not present. Feldspar grains do not fracture easily but have been rounded to a degree with the original crystal development still evident. If an igneous origin is assumed, with no metamorphic overprints affecting the shape, grains should be subhedral to anhedral. Metamorphic imprints are evident internally from the presence of muscovite laths and sieve texture.

Metamorphic plagioclase ranges in size from 0.05 to 0.15 mm. The grains are pitted giving a cloudy appearance. Boundaries are mostly curved to straight reflecting the presence of more xenoblastic than idioblastic crystals. Twinning is absent and cleavage traces are subdued.

Alkali feldspar is present only in clastic form in the biotite zone (Plate 3). Grain size ranges from 0.7 to 3.0 mm. Alkali feldspar grains are rounded (anhedral) to subangular (subhedral) with crystal development similar to plagioclase. These grains are visible in thin section due to the yellow spotted appearance from staining. Sericite alteration is present. Varying degrees of sieve texture are present, including cases where only outlines of former clastic alkali feldspar grains remain. Deformational

features are not present, although the long axis of each grain is generally parallel to the schistosity. When present, cleavage is parallel to the {010} direction. Individual grains are characterized by low first order interference colors and very low relief.

Grain size for biotite ranges from 0.1 to 0.5 mm and is not a function of generation of schistosity in any of the four metamorphic zones. Boundaries are mostly straight to curved. Idioblastic grains are more abundant than xenoblastic grains. Most of the grains show perfect cleavage in one direction {001}. The few grains present not showing cleavage, (grains cut parallel to {001}), exhibit a tabular habit. Grains showing {001} cleavage are pleochroic, mostly showing shades of brown, with some green (not chlorite). Kink bands are uncommon with nearly all the grains exhibiting small extinction angles (less than 3). Zircon inclusions are present in some biotite grains.

The nature of biotite shape and size appears to depend partially on its abundance with respect to metamorphic quartz and metamorphic plagioclase. Samples with greater abundance of biotite show smaller length to width ratios. The resulting columnar shapes control the growth patterns of adjacent feldspar and quartz grains. Samples with less biotite show larger length to width ratios (blades), with growth patterns that are controlled by the presence of clastic monocrystalline quartz and feldspar as well as metamorphic quartz and feldspar. The latter growth

pattern is analogous to a sandstone containing less matrix (clay minerals) between its grain boundaries. Samples with an overall smaller grain size tend to show biotite grains with greater length to width ratios. These grains are at the lower end of the biotite size range.

Muscovite varies in grain size from 0.1 to 0.5 mm. It occurs as blades with greater length to width ratios than biotite, as thin tabular crystals and as scaly aggregates, mostly of idioblastic shape but not as well developed as biotite crystals. These colorless grains have one perfect cleavage direction ⊥001 with parallel extinction.

Varying proportions of mica with respect to quartz and feldspar illustrate a greatly varying matrix to framework ratio in the original sediments. Variations in overall mean size for various samples indicate that the original sediment consisted primarily of sand with lesser amounts of silt- and clay- sized grains.

Examples of syntectonic crystallization include: the preferred orientation of the mica grains; the degree of grain growth in one preferred orientation (with muscovite tending to show very pronounced growth patterns); and metamorphic plagioclase and quartz possibly showing a slightly elongate pattern. Post-tectonic crystallization is illustrated by biotite porphyroblasts that are not cut by any of the three generations of schistosity. The growth of these grains follow the other foliation surfaces, enclosing finer grained muscovite grains and illustrating a

poikiloblastic texture.

Retrograde metamorphism is illustrated by alteration of biotite to chlorite. Effects range from biotite rimmed by chlorite to chlorite pseudomorphs after biotite. The latter effect is suggested by the various degrees of alteration. Retrograde chlorite grains are characterized by their "Berlin Blue" interference color.

Accessory minerals are tourmaline and apatite. Magnetite is also present. Tourmaline and apatite do not appear to be a result of the metamorphism. Low oxygen fugacity favors the formation of magnetite during regional metamorphism. In trace amounts, magnetite appears to alter to chlorite. Spry (1969) reports this apparent alteration. Physical properties of these are similar throughout the four zones.

Apatite is colorless in thin section, is less than 0.2 mm in size, occurs as six-sided prismatic and bladed crystals and shows moderate relief. Grains are disseminated throughout the samples.

Tourmaline is pleochroic with colors ranging from colorless to green. Crystals are generally 0.2 mm in size, occurs as columns, showing high relief and irregular fractures with no cleavage. Extinction is parallel with moderate to strong birefringence. These grains are also disseminated throughout the samples.

Magnetite is opaque with triangular, square and rhombic sections. The grains are angular to subrounded,

ranging in size from 0.1 to 0.2 mm in size. Angular to subangular grains are aligned with the schistosity.

Garnet Zone

The rocks of the garnet zone, in addition to the minerals of the biotite zone, contain the index mineral garnet. Results of the modal analyses are listed in Table 2. Mean values and ranges of the mineral percentages are listed in Table 5. Mean values for the metamorphic and clastic components are 65% and 35% respectively. The increased degree of recrystallization is reflected by the decreased clastic abundance of garnet zone rocks.

Metamorphic quartz increases to 34%, clastic monocrystalline quartz decreases to 17% and polycrystalline quartz aggregates decrease to 6%. As a group, total quartz decreases to 57%, which indicates clastic quartz decreases faster than metamorphic quartz increases. Muscovite and biotite both increase to 17% and 9% respectively, while magnetite, tourmaline and apatite decrease.

Metamorphic plagioclase decreases slightly to 7%, clastic plagioclase increases to 1.0%, clastic alkali feldspar increases slightly to 4%. This suggests that the garnet zone rocks originally had a greater feldspar to quartz ratio, since the amount of clastic feldspar is expected to decrease with increasing metamorphism.

The minerals of the garnet zone do not show any

significant changes in form, shape and size as compared with rocks of the biotite zone. Within the garnet zone samples are approximately the same distance from the garnet isograd. Variations in texture and abundance may be a result of variability in the original sediments and not the result of metamorphism.

Polycrystalline quartz aggregates range in size from 1.0 to 3.5 mm. This slight decrease in size for the garnet zone may reflect originally smaller clasts in the sediments or further disaggregation of the grains. In the biotite zone the aggregates are mostly stable with few apparent disaggregated monocrystalline clastic grains adjacent to aggregates. This process is more evident in the garnet zone. Therefore, with increasing metamorphic grade a larger percentage of the aggregates break down with the subsequent recrystallization of the individual monocrystalline grains.

Besides disaggregation, the intact grains of the polycrystalline aggregates show a greater development of mortar texture development. Dissaggregation and development of mortar texture may have begun while the rocks of the garnet zone were at lower temperature and pressures. The polycrystalline aggregates of the biotite zone may have continued to recrystallize under garnet zone metamorphic conditions before completely breaking down. Boundaries and shapes of polycrystalline grains are similar in the biotite and garnet zone.

Total clastic quartz decreases in the garnet zone

but the mean ratio of the monocrystalline to polycrystalline quartz ratio increases from 1.3 to 2.8. This results from dissaggregation-recrystallization or from the presence of less polycrystalline quartz originally.

Monocrystalline clastic quartz ranges in size from 0.2 to 0.8 mm which is nearly equivalent to the range of the biotite zone. Grain shape ranges from mostly subangular to rounded, with most grains showing preferred orientation. This may reflect further growth on the original clastic grains during syntectonic crystallization or deformation. However, since the size ranges are similar in the two zones, deformation is probably more dominant.

Metamorphic quartz ranges in size from 0.05 to 0.1 mm for the finer grained rocks and from 0.4 to 0.6 mm for rock samples which are coarser grained and have mostly to completely recrystallized. Shape and boundaries of smaller grains are similar to those found in the biotite zone but the coarser grains tend to be sub-idioblastic.

Clastic alkali feldspar ranges in size from 0.15 to 3.0 mm with mostly rounded boundaries. The proportion of clastic alkali feldspar to clastic quartz varies throughout the garnet zone samples. The amount of original clastic grains may control the presence of clastic alkali feldspar more than selective deformation and recrystallization.

In addition to considering the constant percentage of alkali feldspar, increased development of sieve texture implies that clastic alkali feldspar is not significantly

recrystallized until it has passed through the garnet zone.

Clastic plagioclase ranges in size from 0.15 to 1.5 mm with mostly rounded grains. These grains are more rounded than biotite zone grains and both zones have approximately the same size range, degree of sericite alteration and twinning. Sieve texture is present, but is not developed to the degree that it is in alkali feldspar. Clastic plagioclase recrystallizes in a manner analogous to alkali feldspar.

Metamorphic plagioclase ranges in size from 0.05 to 0.75 mm, with the lower range corresponding to finer grained rocks and the upper range corresponding to coarser grained rocks. Its grain shape, boundaries and growth patterns are similar to those in the biotite zone.

Biotite ranges in size from 0.15 to 1.25 mm. The higher end of the range represents nearly recrystallized samples while the lower end of the range represents samples that contain clastic components. In the biotite zone (where all samples contain clastic components), biotite ranges in size from 0.15 to 0.5 mm. Therefore, while recrystallization occurs in both zones, biotite grains are larger in the garnet zone than in the biotite zone.

Grains in the biotite zone are more bladed than in the garnet zone, and grains in the garnet zone more columnar than in the biotite zone. Chloritization of the biotite grains does not occur in samples 10 and 15, but occurs in trace amounts to more than trace amount in some grains.

Small amounts also occur in the biotite zone. The development of schistosity does not change with garnet zone metamorphic conditions.

Muscovite ranges in grain size from 0.1 to 0.8 mm, with the upper limit corresponding to the coarser- grained, recrystallized samples. The grains are mostly bladed, illustrating a pronounced growth pattern in one direction, parallel to the foliation surface. For the mica group,a correlation between grain size and generation of schistosity is not obvious. All mica grains increase in size as they pass into the garnet zone.

Garnet does not appear in all samples. When it does occur, there are only a few grains present (less than or equal to 0.2%). It ranges in size from 0.2 to 0.7 mm (Plate 4). The smallest grains are colorless, subidioblastic, unzoned dodecahedrons. They are roughly pitted and may show parting. Larger grains in the range are xenoblastic with the grain form obscurred. Quartz inclusions are present in grains of all sizes. Chloritization is present in various degrees, ranging from rimmed to completely chloritized garnet dodecahedrons.

Helicitic textures are not present in the internal structure of the garnet grains. Larger grains exhibit fractures while the smaller grains do not. These features do not support conclusively a pre-tectonic origin of these grains.

Staurolite Zone

With passage into the staurolite zone, the mineral assemblage changes with the elimination of the clastic components and the addition of staurolite and metamorphic alkali feldspar. Results of the modal analysis are listed in Table 3. Mean values and ranges of the mineral percentages are listed in Table 5. Metamorphic minerals now make up 100% of the system. Therefore, complete recrystallization of the obvious clastic grains began to occur in the garnet zone and ended before the staurolite isograd was reached.

The following are changes in mineral percentages: total quartz drops from 57% to 40%, metamorphic alkali feldspar appears (1.8%), plagioclase increases from 7% to 14%, biotite increases from 18% to 23%, muscovite increases from 10% to 18%, magnetite increases from 1.1% to 1.7%, garnet increases from 0.1% to 0.3%, staurolite appears in a few samples (0.1%), sillimanite anomalously appears in sample 65, retrograde chlorite is abundant in two samples (2.5% and 3.5% in samples 3 and 4, respectively); and the accessories drop from 0.8% to 0.4%.

Besides the changing values of the modal analyses, general trends include increasing grain size, better development of crystal faces (more idioblastic grains) and increasing segregation of irregularly spaced laminations that are rich in micas and quartz plus feldspar. Only one

sample (75) is characterized by the lack of laminations and layers in a hand specimen . Quartz plus feldspar rich laminations are about 2 mm thick. Mica rich laminations are from 1 to 2 mm thick.

Quartz ranges in size from 0.15 to 0.5 mm. There is a greater tendency towards forming a granoblastic elongate texture but this is counteracted by the increasing percentage of mica grains. Where quartz impinges upon mica grains, its boundary conforms to the mica grain and it grows only in the available space present. Boundaries of quartz grains are straight. There are more sub-idioblastic quartz grains present than in the previously described zones.

Plagioclase ranges in size from 0.05 to 0.35 mm. A greater abundance of larger and idioblastic grains are found with lesser amounts of xenoblastic grains.

Alkali feldspar ranges in size from 0.1 to 0.5 mm. These grains resemble the clastic grains of the biotite and garnet zones, but there are important differences. Grain size is smaller with boundaries suggestive of well-developed crystal faces. Metamorphic grains impinge upon these clastic alkali-feldspar grains. In contrast, the metamorphic grains are mostly xenoblastic (space fillers). Grains are developed by growing around finer grains, resulting in a sieve texture. Sericite alteration is less abundant in alkali feldspar than in plagioclase.

Biotite grains range in size from 0.2 to 1.0 mm. This is similar to the garnet zone. Shape, boundaries and

growth patterns of biotite do not vary with passage to the staurolite zone for most grains. Biotite porphyroblasts (larger grains) occur which are not cross-cut by the micas and are poikiloblastic. These grains may have grown after the last deformational period. Chloritization of biotite in various degrees occur. Physical properties of muscovite do not change with passage into the staurolite zone.

Garnet occurs as sub-idioblastic dodecahedrons (some chloritized, 0.1 to 0.2 mm), that are isolated and in chloritized linear aggregates, parallel to the preferred orientation. Locally (sample 75), fractured xenoblastic porphyroblasts occur that range in size from 0.7 to 2.0 mm and are mostly unaffected by chloritization.

A problematic mineral in this study is staurolite. The presence of possible sericite pseudomorphs after staurolite in the Big Thompson Canyon is indirect evidence that retrograde conditions existed (Plate 4). vPorphyroblastic grains ranging up to 2.5 mm in size are pale yellow, contain quartz inclusions, show high relief and are xenoblastic elongate sections. Under cross nicols the grains are a sericite matrix.

Sillimanite is found in one sample in the central area of the staurolite zone. This finding is contrary to the metamorphic zones mapped by Braddock, et al (1970a, b). It accounts for 0.8% of sample 65. It is found in felted fibrous masses (grains are 0.05 to 0.2 mm) contained in

muscovite grains. The fibers are colorless, show high relief and show parallel extinction with second order interference colors. The occurrence is anomalous and can not be explained by the author. It is not near any igneous intrusions in the area. Samples closer to the tonalite body in the western region of the staurolite zone do not contain sillimanite.

Very fine grained regions, 1 to 3 centimeters wide, containing primarily sericite with grains less than 0.05 mm in size are found in zones in two samples. In sample 4, a large section of the thin section consists of this very fine grained matrix. In sample 3, smaller fragments are found. The matrix appears to be a finer grained version of the sample, but the presence of feldspar and quartz could not be conclusively determined. Although an origin for this matrix is uncertain it may have originally been a lens of clay to silt size particles or andalusite that has been subjected to retrograde metamorphism. According to Braddock (1970a and 1970b), andalusite is present in the study area.

Sillimanite Zone

Results of the modal analysis are listed in Table 4. Mean values of the mineral percentages are listed in Table 5. The mean values for mineral abundance do not change as significantly from the staurolite to sillimanite zone as garnet to the staurolite zone . From the garnet to the

staurolte zone, quartz decreases from 40% to 38%. Alkali feldspar increases slightly from 1.8% to 2.0%, plagioclase increases from 14% to 20%, biotite decreases from 23% to 19%, muscovite increases slightly from 18% to 20%, magnetite decreases from 1.7% to 1.2%, garnet decreases slightly from 0.3% to 0.2%, apatite and tourmaline increase slightly from 0.4% to 0.6%. Staurolite is not present and sillimanite appears (3.0%). Sillimanite zone transistions occur at a lateral distance of 13 km along the traverse through the four metamorphic zones.

The following mineralogic transformation may possibly explain the changes with passage into the sillimanite zone:

1) Muscovite + Quartz = Alkali feldspar + Sillimanite + H_2O

(Equation 4-3 from Turner (1981)). In various degrees of development muscovite breaks down to domains of alkali feldspar or sillimanite. Plate 5 illustrates the breakdown of muscovite to form sillimanite and the replacement of biotite by sillimanite.

In this reaction, quartz is consumed which may explain the decrease in quartz upon passing into the sillimanite zone. Since muscovite breaks down, its percentage should decrease, although it does not. Alkali feldspar is produced in the breakdown of muscovite, but it only increases slightly. Variability in mineralogical composition of the original sediments may explain the

apparent contradictions in trends of increasing and decreasing mineral abundances. In a latter section, geochemical arguments are considered.

Quartz ranges in size from 0.25 to 0.70 mm. Grain shape and boundaries are quite variable but shape tends to be sub-idioblastic and boundaries are straight to curved. Plagioclase ranges in size from 0.15 to 0.75 mm. Grain shape is sub-idioblastic. Grain boundaries tend to be straight. Alkali feldspar ranges in size from 0.15 to 0.75 mm. Boundaries and shapes of alkali feldspar grains indicate that they grew in available space. As expected, their irregular shapes reflect varying degrees of breakdown of muscovite. Grain sizes increase for quartz, plagioclase and alkali feldspar upon passing into the sillimanite zone.

Biotite and muscovite are quite variable in size due to the breakdown reactions, ((0.05 to 0.75 mm) and (0.25 to 2.0 mm)), and in boundary and in shape. Certain initial idioblastic muscovite grains show partial transformation to sillimanite and alkali feldspar. Biotite occurs once again as idioblastic and sub-idioblastic grains.

Garnet occurs as mostly chloritized, sub-idioblastic dodecahedrons, ranging in size from 0.1 to 0.3 mm. Sillimanite occurs in felted fibrous masses, ranging in size from 0.05 to 0.25 mm.

Petrologic Constraints For Provenance Determination

Recrystallization and deformational processes hinder provenance determination. Polycrystalline quartz aggregates are interpreted as quartzite rock fragments with medium to coarse sand-sized quartz grains. In some rock fragments different extinction patterns rim the quartz grains; these are interpreted as cement. Variations in grain size and metamorphic imprinting make it impossible to determine how many sources are responsible for the quartzite component.

Other clastic components are contributed from a granitic source or sources. This is supported by the presence of clastic alkali feldspar in fine to mostly medium grained (igneous classification) particles and clastic plagioclase. Clastic quartz grains are not small enough to be considered volcanic grains. Variation in grain size for these feldspar and quartz grains is probably the result of weathering and transport. Also, quartz grain size may be modified as a result of the development of mortar texture. Apatite and tourmaline grains may occur in a wide range of igneous compositions and do not help delineate the igneous type.

Therefore, there are two major sources: sedimentary quartzite and granitic or gneissic rocks. Proportions of the clastic components change from sample to sample, reflecting recrystallization processes and varying contributions from different sources. Mineralogically, there is no evidence for a volcanic source since volcanic grains recrystallize before attaining greenschist facies metamorphism. In a

later section, provenance is considered from geochemical arguments, using the presence of quartzite rock fragments as a constraint.

Mineralogically, the sediments are suggestive of quartz-rich graywackes, but preferential recrystallization changes the proportions of the original clastic assemblage minerals. A formerly poorly sorted matrix and framework rich in quartz and poor in feldspar is inferred by the presence of mica, clastic quartz, metamorphic quartz and low abundance of feldspar. On the basis of texture and mineralogy these samples are classified as arkosic wackes, according to Pettijohn et al (1973).

Conclusions

The following is a list of petrologic changes with zones of increasing grades of metamorphism:

1) Clastic grains (from a former arkosic wacke) decrease in abundance past the garnet isograd and recrystallize completely before reaching the staurolite isograd.

2) Clastic grain size stays the same or decreases slightly past the garnet isograd.

3) A greater abundance of monocrystalline quartz grains are rounded with greater development of mortar texture past the garnet isograd.

4) Sieve texture becomes more developed in clastic feldspar

grains with passage into the garnet zone.

5) Metamorphic grains increase in size, show a greater abundance of idioblastic grains and become more polygonal in shape.

6) The reactions that are responsible for the formation of index minerals biotite, garnet and staurolite went to completion.

7) The breakdown reaction of muscovite producing the minerals sillimanite and alkali feldspar records the highest temperature, pressure conditions reached in the study area.

8) Three foliation surfaces are well defined by the mica grains and are not well defined by the other mineral grains.

9) Metamorphic grains quartz, plagioclase, biotite and muscovite increase in abundance. Metamorphic alkali feldspar grains appear in staurolite zone with abundances remaining constant past the sillimanite isograd.

GEOCHEMISTRY

Introduction

Tables 6 through 9 list chemical analyses of the biotite, garnet, staurolite and sillimanite zones. With these data compositional trends are described within metamorphic zones and with increasing grades of metamorphism. Petrographic results explain these findings.

Changes With Zones Of Increasing Grades of Metamorphism

Tables 10 and 11 list the mean values and ranges of element concentrations in the four metamorphic zones. Figures 4 and 5 illustrate the chemical variation that exists between the four metamorphic zones. Certain oxides increase systematically, some decrease and others show similar concentrations within biotite plus garnet and staurolite plus sillimanite zones.

Systematic increases are recorded for K2O%. Al2O3, Fe2O3T, Na2O, MgO and TiO2 increase to the staurolite zone and then decrease slightly. CaO and SiO2 decrease to the staurolite zone and then increase slightly.

La concentration systematically increases through all four zones. Other light rare earth elements (Ce, Sm, Eu) increase systematically from the biotite to staurolite zone and decrease above the sillimanite isograd. Heavy rare-

earth elements do not systematically change with increasing grades of metamorphism.

Of the other trace elements, Cs, Ba and Sc show systematic increases with zones of progressively higher grades of metamorphism. Rb and Sr increase to the staurolite zone, followed by a decrease to the sillimanite zone. Zr and U exhibit decreases from the biotite to the staurolite zone followed by no change above the sillimanite isograd. Th is present in greater concentrations in the biotite and garnet zones, but systematic changes are not present with further increases in metamorphic grade. Systematic changes in Cr and Hf concentrations are not present throughout the four metamorphic zones.

Rb/Sr and Ti/Zr increase in going from the biotite to sillimanite zone. Nonsystematic changes are present for the Th/U and Ba/Sr values. The (La/Yb)N value increases to the staurolite zone then decreases to the sillimanite zone, but these changes are very small. Consistent values are recorded for K/Rb through the staurolite zone. A large increase is recorded by the sillimanite zone K/Rb value which is due to three samples with low Rb abundances.

Figure 18 is a chondrite-normalized, rare-earth plot with curves representing each of the four individual metamorphic zones. Each curve exhibits enriched, light rare earth and flat heavy rare earth element patterns. In a superficial sense, patterns for the four metamorphic zones resemble each other but there are slight numerical

differences as illustrated by Table 11. The (La/Yb)N value increases to the staurolite zone and then decreases above the sillimanite isograd. (La/Sm)N stays constant throughout all four metamorphic zones. The Eu anomaly value decreases to the staurolite zone and increases slightly above the sillimanite isograd. All three parameters indicate very minor changes which are within analytical uncertainty for data derived from instrumental neutron activation analysis. These slight changes indicate that the degree of light to heavy rare-earth-element enrichment increases, light rare-earth- element enrichment stays constant and the Eu anomaly increases with increasing grades of metamorphism. Because of analytical uncertainty, it is suggested that rare- earth-element concentrations may not be affected by progressive metamorphism.

Sample Distributions With Respect To Chemical Variation

In the biotite, staurolite and sillimanite zones, sample - collecting traverses are approximately perpendicular to the isograds. Samples in these zones do not show systematic changes in chemical abundances with respect to position. Sample positions in the garnet zone are nearly the same distance from the garnet isograd. It is assumed that all the samples were subjected to similar metamorphic conditions in this zone but the ranges of SiO2, Al2O3, Fe2O3T, and K2O abundances show greater variation

than exhibited in the other three metamorphic zones. These non-systematic changes illustrate the variability in composition of the sediments and variable effects resulting from gradual increasing of metamorphic grade. This suggests that an undeterminable variation also also existed in the sediments throughout the study area before the onset of metamorphism. The actual role of each of these three mechanisms is uncertain with the data obtained in this study.

Correlations With Mineralogy

Mineral assemblages of the four metamorphic zones are similar. Therefore, changes in abundance are more relevant than the appearance of low abundance index minerals. Biotite is present in greater than trace abundances for all metamorphic zones, while index minerals garnet and staurolite are usually less than 1% in abundance. Sillimanite is present in greater than trace amounts in two samples.

Partitioning of major and trace elements between various mineral phases can only be considered qualitatively, because of the variation in composition resulting from solid solution and trace element substitution. Resolution of this problem requires individual mineral analysis. This may be performed using an electron-probe microanalyzer (as discussed by Mason (1978)) since the average grain size is

less than 1 mm.

The following is a list of suggested correlations between the mineralogic and chemical data, resulting from passing through increasing zones of metamorphism including effects of original sedimentary compositional variation, metasomatic effects from the igneous intrusions and progressive metamorphism:

1) The abundances of garnet, staurolite, magnetite, apatite and tourmaline are too low to affect the overall chemical trends resulting from progressive metamorphism.

2) A steady increase of Fe is paralleled by an increase in biotite. This obscures the decrease of Fe_2O_3T/MgO normally reported for biotite by Engel and Engel (1962).

3) The nonchanging Mg concentration with passage from biotite to the garnet zone contradicts the corresponding increase in biotite. Increases in Mg concentration are paralleled by increases in biotite for continued increasing grades of metamorphism in the study area.

4) A steady increase in Al is paralleled by an increase in muscovite.

5) The $Al_2O_3 + Fe_2O_3T$ percentage total is highest for the two samples containing sillimanite in the sillimanite zone. Fe may substitute into some of the Al sites.

6) The decrease in Ca at the biotite-garnet zone transition contradicts the increase of anorthite content in plagioclase , as reported by Turner and Verhoogen (1960). As

plagioclase increases above the staurolite and sillimanite isograds, Ca does not increase; it instead, decreases above the staurolite isograd and remains unchanged above the sillimanite isograd. This may be explained by the substitution of Ca for K in biotite, muscovite and alkali feldspar.

7) Samples from zones of progressively higher grades show that the abundance of Na does not parallel the increasing abundance of plagioclase. Insead, Na may substitute for K in biotite, muscovite and alkali feldspar.

8) An increase in K is paralleled by increases in muscovite, biotite and alkali feldspar. Since K2O is present in the study rocks, staurolite is deficient.

Conclusions

1) Most of the chemical variation within the individual metamorphic zones and between zones is due to the variation in the original sedimentary composition with an undeterminable contribution resulting from progressive metamorphism and metasomatism.

2) The following elements generally increase with increasing grades of metamorphism: K, Al, Fe, Mg, Ti, Cs, Ba, Sc, Rb, Sr, La, Ce and Sm. Ca, Si and Zr generally decrease with progressive metamorphism. The following elements do not systematically change: Na, U, Th, Cr, Hf, Yb and Lu. Rare-earth-element (chondrite normalized)

patterns are not affected by progressive metamorphism.

3) Correlations between petrologic and chemical data are generally preserved with increasing grades of metamorphism except for the relationships between Ca, Na and plagioclase.

SEDIMENT PROVENANCE

Introduction

Obvious clastic components (quartzite rock fragments, monocrystalline quartz, plagioclase and alkali feldspar) are present in the biotite and garnet zones. As staurolite zone metamorphic conditions are reached in the Big Thompson Canyon area, the last clastic grains are recrystallized. Clastic grains suggest the presence of quartzite and granitic rocks in the source area(s). A portion of the original clastic assemblage has recrystallized and consequently, evidence for other potential sources is no longer available.

Three methods of treating chemical data were used to determine the source(s) present and the composition of the igneous source(s), regardless of the degree of recrystallization of the clastic grains. Since the study area samples exhibit the effects of progressive metamorphism (refer to Geochemistry: Compositional Trends With Increasing Metamorphism), only the biotite-zone samples are used for provenance determination. Only minor chemical changes result from greenschist facies metamorphism (refer to Discussion of Progressive Metamorphism section). The presence of samples from the other three zones further illustrates increasing K2O with progressive metamorphism.

Method one employs two triangular plots (Figures 16

and 15): A CaO-MgO-Al2O3 plot identifies the presence of the various plutonic rock types and, the CaO-Na2O-K2O plot identifies their position within the granitic field. In both of these plots SiO2 content is not considered. This is equivalent to removing the quartzite source and considering what is left.

Method two uses X-Y element plots. Fields of various rock types are represented in the individual plots. Mixing lines connect the various possible source rocks passing through the sample points of the Big Thompson Canyon samples. The known presence of a quartzite source places a constraint on the position of the mixing line. Possible percentages of various sources are determined from this method.

Method three subtracts the chemical contributions from the clastic components for biotite zone samples and determines the igneous rock type from the composition of what remains. Most of the surviving clastic grains are either monocrystalline quartz or quartzite rock fragments. Since, the subtraction of the chemical contribution from alkali feldspar and plagioclase only imposes minor changes upon the chemistry of what remains, this method was not used in this study. The triangular plots of method one and the X-Y element plot achieve the
desired results.

Triangular Element Plots

The CaO-Al2O3-MgO triangular plot from Bavinton and Taylor (1980) represented in Figure 16. Biotite-zone samples lie slightly outside the granite and granodiorite fields. With increasing grades of metamorphism the cluster of points tighten and are nearly adjacent to the granite field.

Several alternatives may explain the point distribution of the biotite-zone samples. Mixing lines, parallel to the Al2O3-MgO side of the triangle infer an ultramafic mafic or contribution. The second alternative calls for the enlargement of the granite and granodiorite fields to enclose biotite zone sample points. The third alternative disallows this mixing-line method on the assumption that progressive metamorphism has significantly changed the bulk chemistry. A fourth alternative connects granite and granodiorite fields with tholeiites and basaltic komatiites.

A lack of petrographic evidence for a volcanic mafic or ultramafic contribution hinders the resolution of this problem. Volcanic grains and fragments recrystallize before biotite-zone metamorphic conditions are reached. The second alternative, which calls for the enlargement of the granite and granodiorite fields, is favored by the author.

It is possible that this question can be resolved from observations from the CaO-Na2O-K2O plot represented in Figure 15. The CaO abundances of all the samples are too low to reflect a possible contribution from a mafic or

ultramafic source. Values of CaO abundance are well within the 5% level that defines the upper limit of the granitic field.

The CaO-Na2O-K2O plot exhibits a bimodal distribution of points, representing the granite and granodiorite fields. Several alternatives may account for this bimodal distribution with the constraint that the position of a sample on the plot is not a function of location (referring to geologic map). An alternative calls for two distinct sources with each sample receiving one of the two sources, but this is contrary to the sample locations. Alternatively a statistically low number of samples could have resulted in a sampling gap. An alternative that is supported by the modal analysis data attributes point distribution on the plot to the degree of preservation of clastic components during transport from the original source(s). Varying proportions of clastic grains from sample to sample support this idea. Earlier, in the Petrology section(Biotite Zone, Conclusion) it was stated that grain- size distributions of clastic minerals do not suggest bimodal populations, suggestive of two sources. Recrystallization processes obscure the original size population. A location sampling gap may contribute to the gap on the plot.

This study does not conclusively determine the number of igneous sources. Integration of petrologic with triangular- plot data supports the presence of quartzite and

granitic igneous sources. Granite field points may represent samples with more alkali feldspar that survived transportation to the Big Thompson Canyon area.

X-Y Element Plots

The objective of this section is to determine the relative proportion of source rocks present, using biotite zone samples. Values from the literature define the constructed fields for the following rock types: granites, granodiorites, tonalite-tronhjemites, Mid Ocean Ridge Basalts, calc-alkaline basalts, rift tholeiites, average continental crust, graywackes and orthoquartzites. Symbols for these rock types are listed in Table 18. References for these values are listed in Table 19. Each individual study area sample point serves as a pivot point for mixing lines connecting two or more rock types. Petrologic data supporting a quartzite source serves as a constraint for the positioning of a mixing line.

Triangular plots of chemical elements suggest a dominant granitic igneous source. The level of CaO % abundance was well within the granitic range. If a basalt source contributed to the study area rocks, its existence is obscured and is probably very minor. Therefore these mixing lines should only connect the quartzite and granitic fields. If a mixing line also connects the study area sample points to one of the basalt fields an unrealistically high

abundance of 25% is recorded for basalt.

The following assumptions were made in the calculations:

1) The fields that represent the various rock types, constructed from values from the literature, are accurate representations.

2) Metamorphism has not greatly affected the positions of the biotite zone sample points.

v3) Mixing lines originate from the center of the orthoquartzite field and pass through the sample points to the granitic field.

4) If orthoquartzite and basalts overlap, use orthoquartzite as a source.

5) Due to the ranges in concentrations of each element pair, only relative abundances can be calculated.

Accurate deteminations of source proportions and position within the granitic field are not possible with each X-Y element plot. Comparison between the Big Thompson Canyon biotite-zone field and constructed graywacke field allows a determination of former sediment type.

Calculations of the proportion of source rocks were carried out with the following X-Y plots: K2O-Na2O, Al2O3-Fe2O3T, Al2O3-K2O and Rb-Sr(Figures 6,7,8 and 11). The results are listed in Table 24. Average values from the four plots for all samples indicate an approximate 50% contribution of orthoquartzite and a 50% contribution of granite to tonalite-trondhjemite (mostly granodiorite).

The K-Rb (Fig. 17) and U-Th (Fig. 13) plots are not useful in determining the proportion of source rocks because most of the fields for various rock types lie in a linear trend. The Fe2O3-MgO, Fe-Sc, U-Th and La-Sm (Figures 9,10,13,14) plots exhibit coincident biotite zone and granitic rock fields. This does not allow the proportion of source rocks to be determined.

Delineation of position within the granitic field is exhibited by all the plots which allow source rock proportion to be determined, except for the Al2O3-Fe2O3T plot. This particular plot illustrates that Fe2O3T is mobile and should not be used for this purpose. On the Fe-Sc plot, the biotite zone points are clustered in the granodiorite area of the granitic field on the side away from the orthoquartzite field. The Fe2O3T-MgO plot similarly illustrates scatter of both elements in the granitic field.

Both the La-Sm and U-Th plots show divisions within the granitic field. Low levels of La and Sm are present in orthoquartzites. Biotite zone samples are in the tonalite-trondhjemite/granodiorite segment of the linear trend (of rock types) for La-Sm. Perhaps the presence of orthoquartzite contributed to lowering the overall levels (of La and Sm) thus, depressing the linear trend of sample points downward from the granite to tonalite-trondhjemite linear trend. La and Sm are especially useful in considering provenance because of their relative immobility.

This is reviewed in the " Discussion of Progressive Metamorphism, Geochemistry" section. The positions of biotite-zone samples on the U-Th plot indicate that both of these elements are mobile.

Mixing lines cannot be constructed through all the sample points on the Ca-Sr plot (Fig.12). The field containing the sample points overlaps the granitic field, which itself contains a scattering of granite, granodiorite and tonalite-trondhjemite points from the literature.

Subdivisions of the granitic field are well exhibited on the K-Rb plot. Biotite-zone samples exhibit the granitic trend. The orthoquartzite presence may have shifted the trend to the tonalite-trondhjemite to granodiorite position.

The fields representing graywacke on the X-Y plots are a compilation of values from the Sheba Formation (Condie, 1970), Belvue Road Formation (Condie, 1970), Wyoming graywackes, Paleozoic graywackes ((Mattiat, 1960), (Pettijohn, 1963), (Onrdrick and Griffiths, 1969)) and Mesozoic graywackes ((Reed, 1957) and (Baily and others, 1964). The average composition of the Big Thompson Canyon biotite zone differs from the average of the constructed graywacke field in the following ways:

1) Na2O, Al2O3, Fe2O3T, Sr, CaO, La, and Sm concentrations are lower.

2) Sc and Rb concentrations are nearly equivalent, although K2O concentrations are higher and lower.

3) U and Th concentrations are nearly equivalent.

4) MgO concentrations are less than in Precambrian graywackes and greater than in Paleozoic and Mesozoic graywackes.

The presence of an approximately 50% orthoquartzite clastic component suggests that the concentrations of the major elements (other than SiO2), La and Sm, have been lowered and, hence, exhibit lower concentrations than in the graywacke field. Therefore, the Big Thompson Canyon samples appear to represent "proto-graywackes", graywackes originally enriched in quartz (SiO) and, sometimes enriched in K2O. Part of this enrichment may have resulted from low grade metamorphism. REE patterns in the metasediments are similar to Phanerozoic shales with large negative Eu anomalies and are enriched in light REE. This contrasts with REE patterns of graywackes (Figure 19).

According to Pettijohn, Potter and Siever (1973) the distinguishing criteria between graywacke and arkose include: dominance of MgO over CaO and of Na2O over K2O. For the biotite zone samples, these element pairs are nearly equivalent. This imparts an arkosic nature to the graywacke. Further statements by these authors indicate that MgO and FeO are related to a chloritic nature. Big Thompson Canyon samples contain high levels of mica which is probably related to the presence of a chloritic matrix in the original sediment.

Conclusions

1) Triangular plots illustrate the probable lack of a mafic and ultramafic source.The positions of samples are well within the CaO, 5% level of the granitic field.

2) The K2O-Na2O, Al2O3-Fe2O3T, Al2O3-K2O and Rb-Sr X-Y plots allow use of the mixing line method. This determines the presence of nearly equal components of orthoquartzite and tonalite-trondhjemite to granite (mostly granodiorite) sources.

3) Both methods suggest that the granitic (chemical) trend reflects the varying degrees of preservation of clastic component grains.

4) Low levels of the major elements, La and Sm, with respect to the constructed graywacke field suggest a quartz-rich graywacke, with high levels of K2O and CaO concentrations imparting an arkosic nature.

DISCUSSION OF PROGRESSIVE METAMORPHISM

Introduction

The following are problems inherent in a comparative study: often only small segments of facies-series are preserved, isograds are not always at a steep angle to individual lithologic units, metamorphosed sediments exhibit variations in chemical composition and mineralogical assemblages between units, and sedimentary units are laterally discontinuous. These problems restrict the number of progressive (biotite to sillimanite zone) metasedimentary sequences of other areas that can be compared with the Big Thompson Canyon sequence. A further complication can occur when the effects of progressive metamorphism are overprinted by metasomatism. Based on inspection in the field and detailed petrographic analysis, textural effects and petrological changes resulting from metasomatism are not present in Big Thompson Canyon samples.

Petrology

Mineral assemblages from Big Thompson Canyon and from classic localities are listed in Table 14 (with a listing of the localities in Table 15). In the text that follows, differences in mineral assemblages and possible

reactions that are responsible for the formation of the metamorphic index minerals (biotite, garnet, staurolite and sillimanite) are discussed.

The Big Thompson Canyon biotite- zone mineral assemblages differ from the examples in that chlorite is present only as a retrograde mineral and sphene is absent. The absence of prograde chlorite may be explained by polyphase metamorphism. Biotite may contain the necessary Ti that sphene requires.

Possible reactions from combined field and petrochemical data for the appearance of biotite in meta-arkose and some graywackes are as follows:

Microcline + chlorite = biotite + muscovite (Mather, 1970)

In metapelites metagraywackes:

Chlorite + phengite = biotite + muscovite (Brown, 1971)

Muscovite + stilpnomelane = biotite (Fe-rich) + epidote DeButhune (1976)

Clastic microcline, chlorite and epidote grains are not present. Sufficient Ca is not present to permit epidote formation. The presence of clastic alkali feldspar grains may support the first reaction.

In contrast to the garnet zone assemblages of other localities, Big Thompson Canyon samples lack epidote, chlorite, chloritoid and sphene. According to Winkler (1979), the following chemical factors are necessary for chloritoid formation: a large Fe/Mg ratio, a relatively high Al content and, simultaneously, low contents of K, Na and

Ca. These conditions lead to the absence of chloritoid from assemblages involving biotite, albite and alkali feldspar. The presence of chlorite, epidote and sphene were discussed earlier.

Since chlorite is absent in the biotite zone, its role in the formation of garnet is uncertain. The following garnet producing reactions are based on petrographic observations:

Chlorite + biotite + quartz = almandine-rich garnet + biotite (Chakraborty and Sen, 1967)

Chlorite + muscovite + epidote = almandine-rich garnet + biotite (Brown, 1969)

Chlorite + muscovite + quartz = almandine + biotite (Thompson and Norton, 1969)

Since the study rocks are low in CaO, the second reaction is unimportant. Therefore, the present mineralogy may support the first or third reaction.

Miyashiro (1958) recognized the appearance of alkali feldspar at temperatures below those associated with the muscovite breakdown reaction. He predicted its occurrence as a result of a reaction between biotite, muscovite and quartz. In contrast, Deer, Howie and Zussman (1966) proposed that alkali feldspar should not appear in pelitic rocks until pressure-temperature conditions favor the instability of the micas. The reaction producing alkali feldspar under staurolite- zone metamorphic conditions in the study area went to completion.

Comparison of the staurolite zone mineral assemblage in the study area with those of the examples illustrates a lack of kyanite and cordierite in the Big Thompson Canyon area samples. As discussed earlier, andalusite may have been present before the onset of retrograde metamorphism.

Occurrence of staurolite and cordierite depends on a suitable chemical composition and range of pressures and temperatures. Based on experimental data, Hoscheck (1969) proposes the following reaction:

Chlorite + muscovite = staurolite + biotite + quartz

From petrographic observations, Froese and Gasparrini (1975) propose:

Chlorite + muscovite + almandine = staurolite + biotite + quartz

Since the bulk composition is not favorable for chloritoid formation, reactions using it in the formation of staurolite are not relevant. Chlorite also is not present.

According to Winkler (1979), staurolite and cordierite generally do not coexist in medium grade rocks. Staurolite and almandine may coexist in rocks with a low (Mg/(Fe+Mg)) ratio.

The Big Thompson Canyon sillimanite zone assemblage developed at temperatures between those that produced examples 12(a, b, c and d) and those that produced examples 13(a, b and c). Evidence required for the delineation of an alkali feldspar isograd within the sillimanite zone is not conclusive in the study area. As discussed in the

Petrology(Sillimanite zone) section, a distinct reaction is responsible for the formation of sillimanite. Alkali feldspar and sillimanite are not always associated together as the breakdown products of muscovite. This reaction serves as a constraint for the path of progressive metamorphism. Evidence is not available to suggest that kyanite is or was ever present in the study samples; this serves to constrain the upper end of the pressure range, 4 kb (13 km). Additionally, the presence of andalusite is a further constraint for the path of progressive metamorphism.

In the Big Thompson Canyon area, progressive metamorphism follows a path that is intermediate to Miyashiro.s (1973) low- to medium-pressure metamorphism series (Figure 3). Explanation of the symbols on this figure are listed in Table 17. It is not possible to assign strict lower limits to the pressure-temperature range for the study area because of the lack of exposure of the biotite isograd. Therefore, the approximate temperature and pressure conditions are 300o to 650o C and 2 to 3.5 kb for the path of progressive metamorphism in the Big Thompson Canyon study area.

Geochemistry

Analyses documenting progressive metamorphism in sedimentary rocks are not abundant in the literature. Table 20 is a compilation of available data from various

localities. Elements are categorized according to whether they increase, decrease, stay approximately constant or exhibit variable, but significant, changes.

Conclusive statements can not be made pertaining to major and trace element behavior for all regional metamorphic systems except that the REE concentrations stay approximately constant. Analyses for other localities exhibit conflicting trends. This behavior is not surprising for trace elements (excluding the rare earth element group) since an earlier conclusion of this study states "trace elements exhibit greater variation in concentration than the major elements". This is probably due to variations in the original sedimentary composition.

Of the other studies, only Engel and Engel (1958), (1960), (1962) report progressive changes that are analogous to those of this study. Differences include K2O and Na2O. From Table 16 only this study reports increasing K2O as a function of increasing grades of metamorphism. As suggested earlier in this study, K2O (and other alkali elements) enrichment may be a consequence of fluid eminations from the pegmatitic granite (refer to map in pocket).

Based on a compilation of progressive metamorphic chemical changes, suggested in the literature, is apparent that regional metamorphism is generally not an isochemical process (except for rare earth elements). Effects of sedimentary compositional variation are not clearly documented in these studies. This variation in sediment

composition throughout an area is a major obstacle to the solution of this problem. The author recommends that closer-spaced samples be taken from selected areas in future studies.

The REE group is of special interest in determining the original sediment type and its source rocks. The REE patterns of the study area samples are compared with NASC and graywacke REE patterns in Figure 19. REE patterns of metamorphic rocks are a function of REE concentrations in the original source rocks and the effects of weathering, transportation, deposition and metamorphic processes.

Nesbitt (1979) states "rare-earth-element patterns in sediments may be indicative of parent material only when all fractions of the weathering products derived from the parent rock are included in the sediment sample". Also, the lack of fractionation in REE patterns from the parent rock to the sediment is caused by mechanical mixing of the detritus. Ronov, Balashov and Migdisov (1967) state that "sedimentary cycle plays insignificant role in fractionation of rare earths". Their study is based on 30,000 samples from the Russian platform. REE paterns become more enriched in light- rare- earth elements in the progression from ultramafic to alkalic igneous rocks. Sediments, therefore, mirror the REE patterns of their igneous parents.

Various studies in the literature have determined the composition of the upper continental crust from REE patterns in sedimentary rocks ((McLennan, Fryer and Young,

1979), (Nance and Taylor, 1977), (Condie, 1970)). Other studies have demonstrated rare earth immobility as a function of increasing metamorphic grade. Muecke, Pride and Sakar (1979) looked at the White Rock Formation (amphibolite facies) of southwestern Novia Scotia, Canada. Cullers, Yeh and Chaudhuri (1974) analyzed Silurian pelitic schists (greenschist to amphibolite facies) from northwestern Maine. Green, Brunfelt and Heir (1972) analyzed gneisses (amphibolite and granulite facies) from the Precambrian Lofoten high grade metamorphic terrain in Norway.

Conclusions

1) Biotite, garnet, staurolite and sillimanite (sillimanite-muscovite and sillimanite-alkali feldspar) zones are present in the Big Thompson Canyon area.
2) Staurolite and sillimanite are not present in all samples of their respective zones.
3) Based on data from this study, delineation of the isograd dividing two subzones of the sillimanite zone is not possible.
4) The path of progressive metamorphism is similar to a path intermediate to Miyashiro.s (1973) low pressure- and medium- pressure metamorphism and represents the upper greenschist to upper amphibolite facies segment.
5) Approximate temperature and pressure ranges are 300o to 650o C and 2 to 3.5 kbs.

6) Progressive metamorphism is not isochemical in the study area. TiO2, Al2O3, Fe2O3T, MgO, K2O, Cs, Rb, Ba, Sc and Ce increase with increasing grades of metamorphism, while SiO2, CaO and Zr decrease.

7) With comparison to other regional metamorphic systems, increase of K2O is the most obvious systematic difference. Fluid eminations from the pegmatitic granite in the study area may be responsible for this enrichment of K2O.

8) Rare-earth elements are relatively immobile during progressive metamorphism and mirror the REE patterns of the original sediment and parent rock.

TECTONIC SETTING

The role of plate tectonics in the Proterozoic is a subject of considerable debate. A recent study by Kroner (1980) reviews the topic. Various workers use a uniformitarian approach by comparing Proterozoic rock assemblages with Phanerozoic petrotectonic assemblages.

Existence of rock age-belts in the southwestern United States is discussed by various workers including Hills and Houston (1979), Van Schmus and Bickford (1980) and Condie (1982) (Figure 1). On a regional scale Archean granitic gneiss (2.5 b.y.) of the Wyoming Province is separated from lower Proterozoic (1.70 to 1.80 b.y.) gneisses by a shear zone trending northeasterly throughout southern Wyoming.

All three cited studies propose a convergent plate boundary to account for the shear zone. Hills and Houston (1979) propose a plate- tectonic model in which an Atlantic-type continental margin collided with and was partially subducted beneath a volcanic arc. Van Schmus and Bickford (1980) propose convergent processes (involving volcanic arcs) occurring against a nonrifted continental margin. Condie (1982) proposes a model that calls for back-arc basin closure with a resulting Andean type orogeny, combining rifting and volcanic arc models.

In this study Phanerozoic plate tectonic processes

are assumed. This assumption allows the use of plots that characterize tectonic setting as a function of sedimentary mineralogical composition proposed by Dickinson and Suczek (1979). Continental Block, Recycled Orogen and Magmatic Arc Provenances are represented in these plots.

In figures 20 and 21, Big Thompson Canyon samples are represented on plots with total clastic quartz-feldspar-unstable lithic fragments and monocrystalline quartz-feldspar-total lithic fragments end members. Unstable lithic fragments, including volcanic, metavolcanic, sedimentary and metavolcanic varieties are considered as very minor consitiuents in the original clastic assemblage (refer to Provenance section). In Figure 20, decreasing maturity or stability indicates less influence from Cratonic interior provenances and more influence from Uplifted basement provenances. In Figure 21, increasing ratio of chert to quartz indicates more influence from a subduction complex and less influence from a collision orogen and foreland uplift. Continental Block Provenances (Cratonic Interior) and Recycled Orogen Provenances are the dominant fields represented respectively in the two plots (Magmatic Arc Provenances are not represented in either plot).

The appearance of two dominant provenance fields is explainable in the following ways:

1) Recrystallization of the clastic mineral grain types affects the original clastic grain proportions. Clastic

mineral assemblages vary in their proportions from sample to sample.

2) Phanerozoic petrotectonic assemblages are not applicable to the classification of Proterozoic rock assemblages.

3) Continental Block and Recycled Orogen Provenances are indistinguishable in the Proterozoic assemblages.

4) More than one provenance contributes to the sediments.

5) Magmatic Arc Provenance sediments are not in the study area. The lack of unstable lithic fragments is consistent with a granitic-quartzitic provenance.

6) Representation of the Recycled Orogen Provenance field may be accounted for by the grouping of polycrystalline quartz aggregates with the unstable lithic fragments end member. Dickinson and Suczek (1979) do not clearly indicate which category these coarse - grained polycrystalline quartz aggregates should be grouped with. The author recommends that these aggregates be grouped with monocrystalline quartz.

Schwab (1975) relates the chemical composition of sandstones to miogeocline, eugeocline and rift, continental-margin types. This is represented by a triangular plot (Figure 22) with SiO2/10, K2O and Na2O end members; it assumes that these elements are immobile for metamorphic temperature-pressure conditions ranging up to greenschist facies. The average of biotite zone samples plots in the miogeocline field. This chemical plot shows a closer association to the eugeocline field than the mineralogical plots do with the Magmatic Arc Provenances. The Big

Thompson Canyon biotite zone samples, with K2O/Na2O ¢ 1 and SiO2 ¢70% are analogous to Schwab.s quartz-rich modern deep sea sand and ancient graywackes from a miogeoclinal setting.

SUMMARY AND CONCLUSIONS

The objectives of this study were to determine the changes in mineralogy and chemistry with increasing metamorphic grade, provenance of the sediments, pressure and temperature conditions during metamorphism and constraints for tectonic setting. However, the first objective was not conclusively achieved.

Sedimentation occurred in a miogeoclinal setting with sedimentary quartzite and granodiorite sources. A clastic assemblage, including quartzite rock fragments, monocrystalline quartz, plagioclase and alkali feldspar contributed to the formation of an arkosic wacke.

Low- to medium- pressure facies metamorphism (with temperature and pressure ranges 300o to 650o and 2 to 3.5 kb) caused the recrystallization of this assemblage before the staurolite zone conditions were reached. This path of progressive metamorphism is constrained by the absence of kyanite and the presence of andalusite and the Muscovite + quartz = sillimanite + alkali feldspar + H2O reaction.

Compositional changes with zones of increasing grades of metamorphism are the result of sedimentary compositional variation throughout the area, metasomatic effects resulting from igneous intrusions in the area and progressive metamorphism. Alkali enrichment of the sediments in the higher grade metamorphic zones is the most apparent effect of metasomatism. REE abundances

remain approximately constant although LREE total abundances increase slightly. These factors place doubt on whether progressive chemical changes suggested in the literature are solely due to progressive metamorphism. Regional metamorphism in general does not appear to be an isochemical process.

However there are problems in this study that are probably insurmountable with the current data and sampling practices.

1) Possible transposition of sedimentary laminations during isoclinal folding places a degree of uncertainty on whether a single sedimentary layer was sampled. A detailed structural analysis of an area is required for this type of study.

2) There is no sure way in determining if a sedimentary layer was chemically homogeneous along its lateral extent.

3) The low number of samples analyzed does not allow the determination of statistically valid results. A greater number of samples need to be collected in future studies.

4) Presence of igneous intrusions in higher metamorphic grade zones affects the original sedimentary composition.

5) This work assumes that the metamorphic zones of Braddock (1970a and 1970b) are correctly mapped.

APPENDIX A: SAMPLE COLLECTION

During the period beginning July 25, 1980 and ending August 8, 1980, a total of 103 samples were collected in the Big Thompson Canyon area from the four exposed metamorphic zones. From these hand specimens 60 were cut for thin sections with 33 of these prepared for X-Ray Fluorescence and Neutron Activation analysis.

Since the strike of the beds is approximately east-west, samples were collected within a narrow latitude range (1.5 km) to minimize compositional variation that may have occured in the original sedimentary unit. Samples near shear zones or subject to oxidation were not collected.

APPENDIX B: PETROGRAPHIC TECHNIQUES

Modal analyses are obtained by counting 1000 grains per thin section, using a Swift 14 key point counter and a Leitz Wetzlar microscope. The following factors affect the accuracy of the results:

1)The staining process is not always effective in delineating alkali feldspar.

2) A conclusive distinction between metamorphic quartz and feldspar is not possible when the grain size is less than 0.1 mm.

3)Minerals may not be randomly distributed throughout the sample.

4) Error ranges are larger than the actual abundances of trace minerals.

APPENDIX C: SAMPLE PREPARATION

Rock samples were crushed to 10 mu sized particles in a series of steps without sieving, for use in X-Ray Fluorescence and Neutron Activation analysis. A large Allis-Chalmers "Chipmunk" grinder and smaller model reduced the particles to granule size. These particles were reduced to sand size with a Westinghouse Rotary Grinder Mill. In the final step a Microjet 5 - High Speed Grinder with a Tungsten Carbide pestle reduces the particle size to the 10 mu range.

Powdered samples were weighed out to 0.5 gram by a Mettler H 10 TW, placed in polyethylene vials and sealed for Neutron Activation analysis. Three gram briquettes were made for X-Ray Fluorescence.

APPENDIX D: NEUTRON ACTIVATION ANALYTICAL PROCEDURES

The method described by Gordon et al(1968) was performed with a Nuclear Data Inc. - 6600 gammma-ray spectrometer equiped with an LSI-11 computer and a Ge(Li) detector. Table D1 lists the elements with associated chondrite and peak energy values, determined with this method.

Polyethylene vials (containing powdered sample) were irradiated at Sandia Laboratories, in Albuquerque, New Mexico for 30 minutes at a power of approximately 600 kilowatts. U.S.G.S. standards AGV1, G1 and inhouse standard LOSP were used in constructing the calibration curve. The error range of this method is plus or minus 5% for the major elements and 10% for the trace elements.

APPENDIX E: X-RAY FLUORESCENCE ANALYTICAL TECHNIQUES

The method described by Noorish and Hutton (1969) performed with a Phillips X-Ray Spectrometer. Table E1 lists the X-Ray Fluorescence instrument settings and error calculation for the calibration curve of each individual element. The drift pellet position was filled by U.S.G.S. standard AGV1.

Renault (personal communication) reviewed the following variables that affect the proportional relationship between the count rate of an analytical line and the concentration of the analyte:

I. Physical Variables
   - A. Sample preparation (grain size variation, homogeneity, and briquette pressure variations)
   - B. Instrumental errors (Kv/mA variability, spectrometer alignment, temperature and atmospheric pressure, vacumn variation and miscellaneous electronic instabilities)
   - C. Counting Error
   - D. Operator Error

II. Compositonal Variables
   - A. Absorption

B. Enhancement

C. Peak interference

The Altair 8800b computer was used for data reduction involving the major element concentrations. Table E2 lists the standards used in constructing the calibration curves for the major element. These curves reduce instrumental error. Error due to compositional variables was reduced by calculating the effects of influencing elements on analyte concentration. These elements are listed in Table E3.

The equation of a calibration curve was determined from the standard deviations of count ratios, R, and concentrations, X, and arranged for solution of the concentration of an unknown is:

$$X=(R-b)/(S(R)/S(X)) \quad . . . . . (1)$$

where R comes from equation (2), b is the intercept on the R axis, and S(R) and S(x) are respectively the Gaussian standard deviations of the count ratios and the concentrations of the standards.

If S(p) and S(b) and D(p) and D(b) are respectively the peak and backqround counts of a sample and the drift pellet, then

$$R=(S(p)-S(b))/(D(p)-D(b)) \quad . . . . . (2)$$

Both equations were described by Renault (personal communication).

The RMS% error of a calibration curve is determined by evaluating the difference between concentrations of standards calculated from the curve and concentrations used to construct the curve:

$$\text{RMS\% error} = \frac{\sum_{i=1}^{n} ((C(i)-M(i))/M(i))^2}{n} \times 100$$

where C(i) and M(i) are the calculated and measured concentrations of the ith element and there are n standards. This error is a measure of the total error associated with the analytical procedure (Renault, personal communication).

An X-Ray fluorescence method described by Reynolds (1963) was used for the determination of Rb, Sr and Zr concentrations. Overall errors in trace element analysis by this method amount to plus of minus 3%. In this method the intensity of the compton scattered protion of a Mo-K, alpha primary beam and the values of the mass absorption coefficients for U.S.G.S. rock standards are related through linear regression. In the second step, the concentration of some element Z of unknown X was directly determined from the

following equation:

$$\text{ppm } Z(x) = Icsi(x)/Icsi(std) \text{ X } Mu(x)/Mu(std) \text{ x ppm } Z(std)$$

where Mu(x)/Mu(std) refers to the mass absorption coefficients at 0.9 Ao of unknown and standard, ppm Z(std) refers to the concentration of an element in a specific standard and Icsi(x) and Icsi(std) refer to the intensity of the compton scattered intensity of the unknown and standard. Mass absorption coefficients of standards used in determining Rb, Sr and Zr concentrations are listed in Table E4.

Table 1 - Modal analyses of biotite zone rocks (in %).

	8	33	34	37	38
Metamorphic Minerals					
Quartz	33	30	31	26	36
Alkali Feldspar	-	-	-	-	-
Plagioclase	4	15	14	2	11
Biotite	10	19	13	13	11
Muscovite	16	0.2	1.0	14	0
Magnetite	1.4	1.2	0.6	0.1	2.0
Garnet	-	-	-	-	-
Staurolite	-	-	-	-	-
Sillimanite	-	-	-	-	-
Clastic Minerals					
Quartz	6	32	7	9	27
Plagioclase	0.0	0.0	0.1	0.1	0.0
Alkali Feldspar	5	0.3	10	3	0.7
Quartzite Fragments	24	1.7	23	32	12
Accessories	0.6	0.6	0.3	0.8	0.3
Total	100	100	100	100	100

	46	53	55	26	Mean
Metamorphic Minerals					
Quartz	32	19	17	26	27
Alkali Feldspar	-	-	-	-	-
Plagioclase	4	10	6	8	8
Biotite	13	8	10	16	13
Muscovite	11	9	6	10	7
Magnetite	0.7	0.6	1.1	0.3	1.0
Garnet	-	-	-	-	-
Staurolite	-	-	-	-	-
Sillimanite	-	-	-	-	-
Clastic Minerals					
Quartz	21	35	51	7	22
Plagioclase	0.9	0.0	0.0	0.3	0.2
Alkali Feldspar	2	0.1	0.2	5	3
Quartzite Fragments	15	18	0.7	27	17
Accessories	0.3	0.3	8	0.4	1.3
Total	100	100	100	100	100

Table 2 - Modal analysis of garnet zone rocks (in %)

	7	10	12	15	19
Metamorphic Minerals					
Quartz	38	30	19	49	14
Alkali Feldspar	-	-	-	-	-
Plagioclase	9	8	3	14	0.4
Biotite	6	6	20	35	15
Muscovite	12	1.3	16	1.5	1.5
Magnetite	1.2	1.3	0.4	0.0	0.0
Garnet	0.1	0.1	0.2	0.0	0.0
Staurolite	-	-	-	-	-
Sillimanite	-	-	-	-	-
Clastic Minerals					
Quartz	32	28	20	-	23
Plagioclase	0.0	0.1	0.0	-	40
Alkali Feldspar	0.1	2	7	-	6
Quartzite Fragments	0.1	23.0	13	-	0.0
Accessories	1.5	0.2	1.4	0.5	0.1
Total	100	100	100	100	100

	21	24	25	Mean
Metamorphic Minerals				
Quartz	28	21	60	34
Alkali Feldspar	-	-	-	-
Plagioclase	7	7	10	7
Biotite	30	20	8	18
Muscovite	24	8	18	10
Magnetite	1.6	2.0	2.0	1.1
Garnet	0.2	0.1	0.0	0.1
Staurolite	-	-	-	-
Sillimanite	-	-	-	-
Clastic Minerals				
Quartz	0.0	24	0.0	17
Plagioclase	0.0	6	0.0	1.0
Alkali Feldspar	9	6	1.0	4
Quartzite Fragments	0.0	5	0.6	6
Accessories	0.2	0.9	0.4	0.8
Total	100	100	100	100

Table 3 - Modal analysis of staurolite zone rocks (in %)

	3	4	63	65	68
Metamorphic Minerals					
Quartz	41	34	39	37	49
Alkali Feldspar	5	0	0.6	0	0
Plagioclase	8	18	10	14	24
Biotite	25	26	12	30	22
Muscovite	16	19	36	14	0.6
Magnetite	1.0	0.8	1.7	3	4
Garnet	1.0	0.1	0.3	0.1	0.2
Staurolite	0.0	0.1	0.0	0.8	0.0
Sillimanite	-	-	-	0.8	-
Clastic Minerals					
Quartz	-	-	-	-	-
Plagioclase	-	-	-	-	-
Alkali Feldspar	-	-	-	-	-
Quartzite Fragments	-	-	-	-	-
Accessories	3	4	0.4	0.3	0.2
Total	100	100	100	100	100

	71	75	76	Mean
Metamorphic Minerals				
Quartz	42	38	42	40
Alkali Feldspar	3	4	3	1.8
Plagioclase	13	11	10	14
Biotite	21	26	18	23
Muscovite	20	19	23	18
Magnetite	0.8	1.1	3	1.7
Garnet	0.1	0.4	0.4	0.3
Staurolite	0.0	0.1	0.0	0.1
Sillimanite	-	-	-	-
Clastic Minerals				
Quartz	-	-	-	-
Plagioclase	-	-	-	-
Alkali Feldspar	-	-	-	-
Quartzite Fragments	-	-	-	-
Accessories	0.1	0.4	0.5	1.1
Total	100	100	100	100

Table 4 - Modal analysis of sillimanite zone rocks (in%)

	2	82	85	89	96
Metamorphic Minerals					
Quartz	31	34	30	39	50
Alkali Feldspar	10	0.7	0.5	0.5	0.5
Plagioclase	14	18	15	11	17
Biotite	23	21	23	20	13
Muscovite	20	21	11	28	19
Magnetite	0.4	1.7	1.0	0.0	0.0
Garnet	0.1	0.4	0.3	0.0	0.1
Staurolite	0.0	0.0	0.0	0.0	0.0
Sillimanite	0.0	4	19	0.0	0.0
Clastic Minerals					
Quartz	-	-	-	-	-
Plagioclase	-	-	-	-	-
Alkali Feldspar	-	-	-	-	-
Quartzite Fragments	-	-	-	-	-
Accessories	0.5	0.2	0.2	1.5	0.4
Total	100	100	100	100	100

	97	100	101	Mean
Metamorphic Minerals				
Quartz	48	29	47	38
Alkali Feldspar	1.6	5	0.4	2
Plagioclase	20	14	15	16
Biotite	17	19	16	19
Muscovite	10	31	18	20
Magnetite	3.0	0.6	3.0	1.2
Garnet	0.3	0.2	0.2	0.2
Staurolite	0.0	0.0	0.0	0.0
Silllimanite	0.0	0.0	0.0	3.0
Clastic Minerals				
Quartz	-	-	-	-
Plagioclase	-	-	-	-
Alkali Feldspar	-	-	-	-
Quartzite Fragments	-	-	-	-
Accessories	0.1	1.2	0.4	0.6
Total	100	100	100	100

Table 5 - Mean values (ranges) of modal analysis of the four metamorphic zones for the Big Thompson Canyon samples (in %)

	Biotite Zone	Garnet Zone	Staurolite Zone	Sillimanite Zone
Metamorphic Minerals				
Quartz	27(17-36)	31(14-60)	40(34-42)	38(29-50)
Plagioclase	8(1.0-15)	7(0.4-14)	14(8-24)	16(11-20)
Alkali Feldspar	-	-	-	2(0.4-10)
Biotite	13(8-19)	17(6-35)	23(12-30)	19(13-23)
Muscovite	7(0.0-16)	9(1.3-24)	18(0.6-36)	20(10-31)
Magnetite	1.0(0.1-2.0)	1.1(0.0-2.0)	1.7(0.8-4)	1.2(0.0-3.0)
Garnet	-	0.1(0.0-2.0)	0.3(0.1-0.4)	0.2(0.0-0.4)
Staurolite	-	-	0.1(0.0-0.8)	-
Sillimanite	-	-	-	3(0.0-19)
Clastic Minerals				
Quartz	22(6-51)	17(0.0-32)	-	-
Plagioclase	0.2(0.0-0.9)	1(0.0-6)	-	-
Alkali Feldspar	3(0.1-5)	4(0.1-9)	-	-
Quartzite Fragments	17(1.7-24)	6(0.0-23)	-	-
Accessories	0.5(0.3-0.8)	0.8(0.1-1.5)	1.1(0.1-4)	0.6(0.1-1.5)
Total% For Mean	100	100	100	100

Table 6 - Composition of biotite zone rocks (oxides in weight percent, trace elements in parts per million)

	8	33	34	37	38	46	53	55	26	MEAN
SiO_2	75.8	76.7	74.4	75.7	76.5	77.1	82.8	77.7	75.1	76.9
TiO_2	0.45	0.50	0.51	0.47	0.52	0.55	0.48	0.37	0.44	0.48
Al_2O_3	12.0	9.67	10.7	12.7	10.1	9.51	8.19	11.2	12.9	10.8
Fe_2O_{3T}	3.53	2.99	3.92	3.69	3.17	3.35	1.95	4.21	3.63	3.38
MgO	1.59	1.63	1.85	3.36	2.25	1.38	0.91	1.59	1.26	1.82
CaO	0.84	2.22	1.74	0.42	2.01	5.02	0.79	0.21	0.60	1.54
Na_2O	1.26	2.23	2.67	0.67	3.09	1.14	1.38	0.71	0.81	1.55
K_2O	2.84	1.34	1.74	3.49	0.92	0.78	2.10	2.52	3.34	2.12
TOTAL %	98.3	97.3	97.5	100.6	98.5	98.9	98.6	98.4	98.1	98.5
Cs	8.11	7.94	9.74	7.65	4.69	4.98	9.30	6.24	7.75	7.61
Rb	100	70.4	72.1	117	48.1	39.2	64.1	79.6	113	78.2
Sr	76.4	168	149	29.8	170	154	78.8	46.7	40.9	102
Zr	109	232	145	144	182	263	292	184	137	188
U	2.61	5.00	2.83	3.03	3.49	5.05	3.74	3.19	2.51	4.47
Th	11.3	13.2	9.04	11.8	8.76	13.8	12.2	8.67	11.3	11.1
Ba	372	137	177	438	740	151	433	403	647	315
Cr	47.8	46.6	48.7	39.7	81.6	N.D.	60.8	36.8	33.5	49.4
Sc	9.77	7.01	9.49	10.8	8.79	8.95	9.13	8.21	9.14	9.03
Hf	5.56	9.26	5.18	5.63	6.87	9.41	12.1	6.44	5.37	6.44
La	23.4	23.8	15.9	30.0	26.8	43.6	41.7	27.9	22.8	28.4
Ce	37.5	56.7	53.6	49.4	58.8	78.6	74.7	47.6	54.5	56.8
Sm	4.75	5.38	4.00	5.09	5.06	7.10	6.01	5.68	3.77	5.20
Eu	0.68	0.54	1.18	1.18	1.21	1.23	1.55	0.79	0.79	1.02
Tb	1.13	0.99	0.98	0.83	0.50	0.71	0.63	1.27	0.74	0.86
Yb	2.33	2.90	2.40	1.84	1.94	2.98	3.94	2.66	1.38	2.48
Lu	0.28	0.46	0.37	0.39	0.32	0.67	0.58	0.35	0.28	0.44

N.D. - Not Detectable

Table 7 - Composition of garnet zone rocks (oxides in weight percent, trace elements in parts per million)

	7	10	12	15	21	24	25	MEAN
SiO_2	74.1	83.5	75.2	61.9	64.3	76.1	77.8	73.3
TiO_2	0.49	0.48	0.49	0.73	0.41	0.53	0.46	0.51
Al_2O_3	13.2	6.55	13.5	17.1	20.2	11.2	11.9	13.4
Fe_2O_{3T}	3.25	1.78	3.88	7.92	6.27	3.74	3.22	4.29
MgO	2.13	0.66	1.34	3.39	2.16	1.76	1.33	1.82
CaO	1.08	1.32	0.41	1.32	0.41	1.21	0.66	0.92
Na_2O	1.87	1.91	0.62	2.48	1.06	2.16	1.14	1.61
K_2O	2.84	1.12	3.92	4.03	4.80	2.26	3.05	3.15
TOTAL %	98.9	97.3	99.3	98.8	99.6	98.9	99.5	98.9
Cs	8.99	4.07	9.93	19.1	12.3	11.6	8.68	10.7
Rb	107	44.9	141	210	180	97.3	108	127
Sr	135	119	38.4	199	91.1	104	78.6	109
Zr	174	257	127	152	193	159	165	175
U	3.1	4.96	3.66	5.15	4.48	3.46	3.72	3.61
Th	11.2	13.7	12.9	21.7	11.5	9.28	12.1	13.2
Ba	358	180.6	391	395	798	466	398	427
Cr	64.1	55.4	36.8	49.6	14.1	63.2	63.7	49.5
Sc	10.5	6.85	10.7	13.8	15.5	11.4	11.5	11.5
Hf	6.37	10.1	6.40	5.33	6.01	5.22	6.29	6.53
La	34.1	28.9	29.7	44.3	45.2	25.6	29.9	34.0
Ce	57.9	57.9	69.4	76.4	98.5	47.8	63.9	66.4
Sm	6.03	5.60	5.05	8.39	7.97	4.54	5.19	6.11
Eu	1.28	0.93	0.84	1.55	1.06	1.28	1.50	1.12
Ib	0.68	0.70	0.49	1.13	0.85	0.89	1.00	0.82
Yb	2.54	2.62	2.00	2.76	2.54	1.54	2.24	2.31
Lu	0.47	0.38	0.37	0.55	0.59	0.44	0.41	0.46

Table 8 - Composition of staurolite zone rocks (oxides in weight percent, trace elements in parts per million)

	3	4	63	65	68	71	75	76	MEAN
SiO_2	65.9	59.2	62.3	62.2	64.7	62.9	66.2	66.7	63.8
TiO_2	0.51	0.55	0.61	0.69	0.64	0.73	0.65	0.85	0.65
Al_2O_3	18.6	21.9	20.9	20.4	14.9	20.2	18.7	17.5	19.1
Fe_2O_{3T}	5.88	7.99	6.47	6.63	7.40	6.38	6.05	6.35	6.64
MgO	1.82	2.65	2.33	2.83	2.52	2.68	2.16	2.50	2.44
CaO	0.53	0.58	0.61	0.81	1.37	0.74	0.57	0.54	0.72
Na_2O	1.06	1.45	1.12	1.52	4.01	1.37	N.D.	1.88	1.77
K_2O	4.47	5.39	5.57	4.58	2.46	5.48	5.01	4.68	4.71
TOTAL %	98.9	99.7	99.5	99.7	98.0	100.4	99.3	101.0	98.6
Cs	11.2	16.7	32.5	39.7	N.D.	38.2	35.0	29.4	29.0
Rb	172	212	204	198	158	196	174	170	186
Sr	72.7	107	85.3	103	353	135	103	132	137
Zr	165	119	150	164	184	160	141	145	154
U	2.70	2.40	3.54	3.94	3.06	4.21	3.78	3.73	3.42
Th	12.3	12.6	11.0	13.1	11.9	11.1	9.44	10.8	11.5
Ba	686	695	711	628	210	415	377	557	535
Cr	59.5	70.7	72.6	70.5	158	196	174	170	121
Sc	15.2	17.8	18.8	18.1	14.2	14.9	18.4	17.0	16.8
Hf	7.08	3.21	4.97	5.77	5.72	3.69	4.57	4.43	4.93
La	39.9	34.6	35.2	43.0	35.8	39.4	29.0	46.6	37.9
Ce	95.0	96.1	57.4	108	87.3	56.5	83.0	72.3	81.9
Sm	7.19	6.45	6.00	6.77	6.70	6.70	6.23	7.70	6.71
Eu	0.76	0.88	0.53	1.21	2.35	1.70	1.19	1.69	1.23
Tb	1.06	0.68	0.88	1.19	0.41	0.74	1.14	1.13	0.90
Yb	2.44	2.18	2.54	2.46	2.10	1.94	3.08	3.40	2.52
Lu	0.48	0.34	0.48	0.49	0.46	0.46	0.51	0.68	0.49

N.D. - Not Detectable

Table 9 - Composition of sillimanite zone rocks (oxides in weight percent, trace elements in parts per million)

	2	82	85	89	96	97	100	101	MEAN
SiO_2	64.2	61.7	63.1	64.8	67.5	65.4	60.5	66.5	64.2
TiO_2	0.86	0.79	0.87	0.67	0.49	0.67	0.72	0.71	0.72
Al_2O_3	18.0	20.8	19.2	19.0	17.5	16.1	21.2	16.7	18.6
Fe_2O_{3T}	6.71	6.97	6.99	5.99	4.12	6.20	6.53	6.16	6.21
MgO	2.83	3.09	3.27	2.24	2.38	2.85	2.59	2.41	2.71
CaO	0.55	0.68	0.55	0.70	1.14	2.81	0.81	0.71	0.74
Na_2O	1.93	1.61	1.12	1.47	1.60	1.82	1.32	2.09	1.62
K_2O	6.15	5.24	4.67	4.98	4.81	4.40	6.05	4.58	5.11
TOTAL %	101.2	100.9	99.8	99.9	99.7	98.8	99.7	99.9	99.9
Cs	17.0	17.6	17.8	36.7	16.3	44.6	89.3	70.6	38.7
Rb	234	68.9	68.8	66.9	156	152	251	185	148
Sr	107	130	96.2	143	82.3	129	97.2	119	113
Zr	98.7	158	155	169	171	144	157	177	154
U	2.59	4.46	3.83	3.62	3.19	2.18	3.53	3.71	3.39
Th	8.39	11.2	10.9	10.7	10.3	10.0	12.7	11.7	10.8
Ba	948	652	597	329	877	533	809	433	647
Cr	86.0	105.3	82.9	87.0	N.D.	72.6	81.0	74.0	84.1
Sc	18.3	25.1	18.2	18.6	10.7	14.6	19.1	16.6	17.4
Hf	3.00	6.74	4.57	3.75	6.85	4.73	5.71	6.44	5.22
La	24.6	47.2	39.9	37.4	42.7	27.1	39.6	55.7	39.3
Ce	71.7	107	90.2	71.2	87.2	46.6	72.8	93.6	79.8
Sm	5.16	7.22	7.26	6.29	6.51	5.29	6.64	8.23	6.58
Eu	1.34	0.95	0.55	1.16	1.48	0.53	0.71	0.83	0.94
Tb	1.06	0.83	0.75	1.53	0.84	0.37	0.51	0.43	0.79
Yb	1.80	3.54	3.40	2.36	3.38	2.56	2.38	3.98	2.93
Lu	0.25	0.42	0.41	0.50	0.64	0.34	0.50	0.49	0.44

N.D. - Not Detectable

Table 10 - Mean values (ranges) of major (in %) and trace (in ppm) elements

	Biotite Zone	Garnet Zone	Staurolite Zone	Sillimonite Zone
SiO_2	76.9 (65.5 - 82.1)	73.3 (61.9 - 83.5)	63.8 (59.2 - 66.7)	64.2 (60.5 - 67.5)
TiO_2	0.48 (0.37 - 0.61)	0.51 (0.41 - 0.73)	0.65 (0.51 - 0.85)	0.72 (0.49 - 0.87)
Al_2O_3	10.8 (8.19 - 12.9)	13.4 (6.55 - 20.2)	9.1 (14.9 - 21.9)	18.6 (16.1 - 21.2)
Fe_2O_{3T}	3.38 (1.95 - 7.98)	4.29 (1.78 - 7.92)	6.64 (5.88 - 7.99)	6.21 (4.12 - 6.99)
MgO	1.82 (0.91 - 3.36)	1.82 (0.66 - 3.39)	2.44 (1.82 - 2.83)	2.71 (2.24 - 3.27)
CaO	1.54 (0.21 - 5.02)	0.92 (0.41 - 1.32)	0.72 (0.53 - 1.37)	0.74 (0.55 - 1.14)
Na_2O	1.55 (0.67 - 3.09)	1.61 (0.62 - 2.48)	1.77 (N.D. - 4.01)	1.62 (1.12 - 2.09)
K_2O	2.12 (0.78 - 3.49)	3.15 (1.12 - 4.80)	4.71 (2.46 - 5.57)	5.11 (4.40 - 6.15)
Cs	7.61 (4.69 - 9.74)	10.7 (4.07 - 19.1)	29.0 (N.D. - 39.7)	38.7 (16.3 - 89.3)
Rb	78.2 (39.2 - 117)	127 (44.9 - 210)	186 (158 - 212)	148 (66.9 - 251)
Sr	102 (29.8 - 170)	109 (38.4 - 199)	137 (72.7 - 353)	113 (82.3 - 143)
Zr	188 (109 - 292)	175 (127 - 257)	154 (119 - 184)	154 (98.7 - 177)
U	4.47 (2.51 - 5.05)	3.61 (3.10 - 5.15)	3.42 (2.40 - 4.21)	3.39 (2.18 - 4.46)
Th	11.1 (8.67 - 13.8)	13.2 (9.28 - 21.7)	11.5 (9.44 - 13.1)	10.8 (8.39 - 12.7)
Ba	315 (74 - 647)	427 (181 - 798)	535 (210 - 711)	647 (329 - 948)
Cr	49.4 (N.D. - 81.6)	49.5 (14.1 - 64.1)	121 (59.5 - 80.4)	84.1 (N.D. - 105)
Sc	9.03 (7.01 - 10.8)	11.5 (6.85 - 15.5)	16.8 (14.2 - 18.8)	17.4 (10.7 - 25.1)
Hf	6.44 (5.18 - 12.1)	6.53 (5.22 - 10.1)	4.93 (3.21 - 7.08)	5.22 (3.00 - 6.85)

Table 11 - Mean values (ranges) of rare earth elements (in ppm) and selected elemental ratios

	Biotite Zone	Garnet Zone	Staurolite Zone	Sillimanite Zone
La	28.4 (15.9 - 43.6)	34.0 (25.6 - 45.2)	37.9 (34.6 - 46.6)	39.3 (24.6 - 55.7)
Ce	56.8 (37.5 - 80.7)	66.4 (47.8 - 92.5)	81.9 (56.5 - 108)	79.8 (46.6 - 107)
Sm	5.20 (3.77 - 7.10)	6.11 (4.54 - 8.39)	6.71 (6.00 - 7.70)	6.58 (5.16 - 8.23)
Eu	1.02 (0.54 - 1.87)	1.12 (0.84 - 1.50)	1.23 (0.53 - 2.35)	0.94 (0.53 - 1.48)
Tb	0.86 (0.53 - 1.27)	0.82 (0.49 - 1.13)	0.90 (0.41 - 1.19)	0.79 (0.37 - 1.53)
Yb	2.48 (1.38 - 3.94)	2.31 (1.54 - 2.76)	2.52 (1.94 - 3.08)	2.93 (1.80 - 3.54)
Lu	0.44 (0.28 - 0.67)	0.46 (0.37 - 0.59)	0.49 (0.34 - 0.68)	0.44 (0.25 - 0.64)
Th/U	3.30 (2.51 - 4.49)	3.23 (2.58 - 4.21)	3.51 (2.50 - 5.23)	3.27 (2.50 - 4.60)
Ba/Sr	6.86 (0.43 - 15.8)	4.95 (1.98 - 10.2)	5.24 (0.59 - 9.44)	10.8 (2.30 - 41.3)
Rb/Sr	1.32 (0.25 - 3.93)	1.46 (0.38 - 3.67)	1.69 (0.45 - 2.39)	1.88 (0.47 - 2.58)
K/Rb	216 (158 - 272)	209 (159 - 234)	209 (129 - 239)	366 (200 - 631)
Ti/Zr	16.6 (12.1 - 24.8)	18.5 (11.2 - 28.8)	25.8 (18.5 - 35.2)	29.6 (17.2 - 52.3)
(La/Yb)N	7.13 (4.01 - 9.97)	8.79 (6.69 - 10.8)	9.32 (5.69 - 12.3)	8.54 (6.40 - 11.4)
(La/Sm)N	3.00 (2.60 - 3.50)	3.00 (2.90 - 3.20)	3.10 (2.60 - 3.50)	3.20 (2.50 - 3.70)
(Eu/Eu*)N	0.69 (0.23 - 1.11)	0.64 (0.42 - 0.83)	0.47 (0.32 - 0.87)	0.52 (0.28 - 0.75)

Table 12 - Elemental ratios for the biotite and garnet zone samples

	8	33	34	37	38	46	53	55	26
Th/U	4.33	2.63	3.19	3.89	2.51	2.73	3.26	2.71	4.49
Ba/Sr	4.87	0.82	1.19	14.7	0.43	9.81	5.49	8.62	15.8
Rb/Sr	1.31	0.42	0.48	3.93	0.28	0.25	0.81	1.70	2.76
K/Rb	236	158	200	248	159	165	272	263	245
Ti/Zr	24.8	12.9	21.1	19.6	17.1	12.5	9.87	12.1	19.3
(La/Yb)N	6.32	4.97	4.01	9.88	8.36	7.85	6.42	6.36	9.97
(La/Sm)N	3.33	2.40	2.20	3.20	2.90	3.00	3.80	2.70	3.30
EuEf = (Eu/Eu*)	0.39	0.75	0.75	1.12	0.93	0.23	1.11	0.90	0.84
K_2O/Na_2O	2.25	0.60	0.65	5.21	0.30	0.68	1.52	3.55	4.12

	7	10	12	15	21	24	25
Th/U	3.62	2.76	3.51	4.21	2.58	2.68	3.24
Ba/Sr	2.65	1.52	10.2	1.98	8.76	4.48	5.06
Rb/Sr	0.79	0.38	3.67	1.06	1.98	0.94	1.37
K/Rb	220	207	231	159	221	193	234
Ti/Zr	16.9	11.2	23.1	28.8	12.7	20	16.7
(La/Yb)N	7.61	6.69	8.62	9.75	10.8	10.0	8.11
(La/Sm)N	2.90	2.80	3.10	2.90	3.10	3.10	3.20
EuEf(Eu/Eu*)	0.74	0.69	0.42	0.61	0.45	0.76	0.83

Table 13 - Elemental ratios for the staurolite and sillimanite zone samples

	3	4	63	65	68	71	75	76
Th/U	4.56	5.23	3.10	3.31	3.89	2.63	2.50	2.90
Ba/Sr	9.44	6.50	8.36	6.10	0.59	3.07	3.66	4.22
Rb/Sr	2.37	1.98	2.39	1.92	0.45	1.45	1.69	1.29
Ti/Zr	18.5	27.7	24.4	25.2	20.9	27	27.7	35.2
K/Rb	216	211	227	192	129	232	239	228
(La/Yb)N	9.88	9.48	8.36	10.6	10.3	12.3	5.69	7.97
(La/Sm)N	3.00	2.90	3.20	3.50	2.90	3.20	2.60	3.30
Eu/Eu*	0.32	0.50	0.29	0.50	0.49	0.87	0.40	0.46

	2	82	85	89	96	97	100	101
Th/U	3.24	2.50	2.85	2.95	3.23	4.60	3.61	3.16
Ba/Sr	8.86	5.02	6.20	2.30	10.7	41.3	8.32	3.64
Rb/Sr	2.19	0.53	0.72	0.47	1.90	1.18	2.58	1.55
Ti/Zr	52.3	30.0	33.7	23.8	17.2	27.9	27.5	24.1
K/Rb	218	631	563	618	256	240	200	205
(La/Yb)N	8.00	8.07	7.10	9.60	7.66	6.40	10.1	11.4
(La/Sm)	2.50	3.60	3.00	3.30	3.60	2.80	3.30	3.70
(Eu/Eu*)	0.73	0.43	0.28	0.69	0.75	0.41	0.44	0.44

Table 14 - Mineral assemblages from other progressive metamorphic compleses ((X) signifies trace amounts)

	1	2	3	4	5a	5b	6a	7a	7b	8a	8b	9a	10a	10b	11a	11b	11c	12a	12b	12c	12d	13a	13b	13c
Quartz	X	X	X	X	X	X	X	X	X	X	X	X	X	X	X	X	X	X	X	X	X	X	X	X
Albite					X	X	X	(X)	(X)	X		X												
Biotite	X	X	X	X	X	X	X		X	X	X	X	X	X	X	X	X	X		X	X	X	X	X
Muscovite	X	X	X	X	X		X	X	X	X	X	X	X	X			X	X	X	X	X	(X)		
Chlorite					X	X		X	(X)	(X)	X				X	X								
Epidote					X	X	(X)			(X)		(X)												
Sphene					X	X						(X)												
Clinozoisite							X																	
Magnetite							(X)																	
Ankerite							X																	
Calcite							X																	
Retrograde Chlorite	X																							
Almandine		X	X	X						X	X	(X)	X	X				X	X		X	X	X	
Chloritoid											X													
Oligoclase										(X)		X		X										
Alkali Feldspar			X	X																				
Andesine													X											
Stauolite			(X)										(X)	X			X	X	X	X				
Sericite															X	X								
Kyanite													X											
Andalusite	X															X	X							
Plagioclase		X	X	X													X					X	X	X
Sillimanite				(X)															X	X		X	X	X
Orthoclase																					X	X		

Table 15 - Localities of other progressive metamorphic complexes

1)	Big Thompson Canyon Biotite Zone
2)	Big Thompson Canyon Garnet Zone
3)	Big Thompson Canyon Staurolite Zone
4)	Big Thompson Canyon Sillimanite Zone
5a,b)	Haast Schist Terrane, New Zealand (Brown, 1971) - metagraywackes
6a)	Hanover quadrangle, western Vermont and New Hampshire (Lyons, 1955) - pelitic rocks
7a)	Southern Daldradian, Scotland (Tiley, 1925), (Elles and Tilley, 1930), (Atherthon, 1964) - pelitic rocks
7b)	Psammopelitic rocks
8a)	Dalradian sequence (Williamson, 1953), (Atherthon, 1964), (Brown, 1967) - pelitic rocks
8b)	Psammopelitic rocks
9a)	Western Haas Schist Terrane, New Zealand (Cooper) - Metagraywackes
10a,b)	Staurolite -kyanite, New Hampshire - Vermont (Lyons, 1955) - pelitic rocks
11)	Western region of Northeastern Dalradian, Scotland (Reed, 1955) - pelitic rocks
11a)	Biotite Zone
11b)	Garnet Zone
11c)	Staurolite Zone
11d)	Sillimanite Zone
12a,b,c,d)	Sillimanite - Muscovite Zone, New Hampshire (Thompson, 1957) - pelitic rocks
13a,b,c)	High grade sillimanite zones of Scottish Highlands and New Hampshire (Turner, 1981) - pelitic and quartzo - feldspathic assemblages

Note:

(5a, 5b, 6a, 7a, 7b, & 11a are biotite zone rocks)
(8a, 8b, 9a, & 11b are garnet zone rocks)
(10a, 10b, & 11c are staurolite zone rocks)
(11d, 12a, 12b, 12c, 12d, 13a, 13b & 13c are sillimanite zone rocks)

Table 16: Changes in chemistry from other progressive metamorphic complexes as a function of increasing metamorphic grade

	Engel and Engel (1960), (1958)	Binns et al (1976)	Sighinofi and Gorgoni (1978)
Metamorphic facies	Amphibolite/ Granulite	Amphibolite/ Granulite	Amphibolite/ Granulite
Rock type/ Location	Paragneiss Adirondack Mts.	Paragneiss West. Aust.	Acid,sub-acid rocks Western Alps
Increases	CaO,MgO, Al2O3, TiO2,Na2O,Cr,Ga, Ni,Pb,Sc,V,Y	Alkalis (K,Rb,Cs, Li),U,Th	Fe2O3T,MgO CaO,Cu,Sr
Decreases	SiO2,K2O,H2O, Cu,B	Sr,Ba,REE, Zr,Nb,Y,Hf, Transition Metals	K2O,Li,Zn,Rb Zn,Rb
No changes	Co,Sr,Zr,Yb	-	Mno,Na2O,Ga Cr,Ni,Cu,

Table 17 - Explanation of symbols for Figure 3

Symbol(s)	Explanation	Source
L.P.,M.P	Low- and medium-pressure metamorphism	Miyashiro (1973)
K.A.,K.S., A.S	Kyanite-Andalusite, Kyanite-Sillimanite and Andalusite-Sillimanite stability curves	Holdaway (1971)
W.S.S	Water-saturated granite solidus	Winkler (1979)
P.P.M	Path of progressive metamorphism	
GA	Greenschist-Amphibolite facies boundary	Condie (1976)
ST	Chlorite + muscovite = Staurolite + quartz + biotite	Hoschek (1969)
SI	Muscovite + quartz + Na-rich plagioclase = Aluminosilicate + orthoclase + more Ca-rich plagioclose	Luth (1976)

Table 18 - Explanation of symbols on X - Y element plots (Figures 6-14, 17)

Symbol	Explanation*
BTC	Big Thompson Canyon biotite-zone
ORTH	Orthoquartzites
GR.FD	Granitic Field
GRA	Granites
GRAN	Granodiorites
T.TR.	Tonalite - Trondhjemites
CAB	Calc - alkaline basalts
R.T.	Rift Tholeiites
MORB	Mid Ocean Ridge Basalts
CC	Continental Crust
GRY	Graywackes
PGY	Precambrian graywackes
PMGY	Paleozoic and Mesozoic graywackes
.	Biotite-zone samples
O	Garnet-zone samples
⊕	Staurolite-zone samples
+	Sillimanite-zone samples
*	References for these rock fields are in Table 23

Table 19: References for constructed rock fields of X-Y element plots

Continental Crust: Eade and Fahrig (1973), Eade and Fahrig (1971), Heir (1965), Holland and Lambert (1972), Shaw et al (1976) and Shaw et al (1967)

Orthoquartzites: Haskin and Wildeman (1966), Mahdavi (1964), Murray et al (1958), Nance and Taylor (1977) and (1976), Piller and Adams (1962), Rogers et al (1964), and Wildeman and Haskin (1973)

Tonalite-Trondjhemite: Arth and Hanson (1975), Collerson and Bridgwater (1979), Glikson (1979), McGregor (1979) and Oversby (1976)

Granites and Granodiorites: Brown (1967), Condie and Budding (1979), Heir and Rhodes (1966), Tilling and Gottfried (1969) and Turkekian and Wedepohl (1961)

Mid Ocean Ridge Basalts: Engel and Engel (1964), Engel et al (1965), Hart (1971), Heir and Carter (1964), Heir et al (1964, Heir and Rogers (1963), Kay et al (1970), Larsen and Gottfried (1969), MacLeod and Pratt (1973), Tasumoto et al (1965)

Rift Tholeiites: Gunn and Watkins (1970), Helmke and Haskin (1973), Hawkins (1970), Kay and Gast (1973), McDougall (1976) and Waters (1962)

Calc-alkaline basalts: Fryclund and Fleischer (1963), Norman and Haskin (1968), Taylor (1969), Taylor et al (1969), Taylor and White (1966)

Table 20: Source rock proportions calculated from X-Y element plots (Orthoquartzite is present in remaining fraction of each sample)

Plot	K20-Na2O	Al2O3-Fe2O3T	Al2O3-K2O	Rb-Sr	Average
Sample					
8	0.4 (GRA)	0.6 (GRAN)	0.8 (GRAN)	0.7 (GRA)	0.6
26	X	0.75 (GRA)	0.9 (GRAN)	0.3 (GRAN)	0.7
33	0.5 (GRAN)	0.5 (GRAN)	0.4 (GRAN)	0.7 (GRAN)	0.5
34	0.4 (GRAN)	0.6 (GRAN)	0.6 (GRAN)	0.7 (GRAN)	0.6
37	X	0.7 (GRA)	0.9 (GRA)	0.2 (T.TR.)	0.8
38	0.6 (T.TR.)	0.5 (GRAN)	0.6 (T.TR.)	.5 (T.TR.)	0.5
46	0.2 (T.TR.)	0.6 (GRAN)	0.4 (T.TR.)	.3 (T.TR.)	0.4
53	0.3 (GRA)	0.4 (GRA)	0.5 (GRAN)	0.4 (GRA)	0.4
55	0.2 (GRA)	0.6 (GRA)	0.75 (GRAN)	X	0.5

X- Mixing line calculation is not possible

Table D-1 - Elements determined by Neutron Activation Analysis

Element	Chondrite Value	Peak Energy (keV)
Na_2O - 24		1368.65
Fe_2O_{3T} - 59 *		1099.30
La - 140	0.330	1596
Ce - 141	0.880	145.50
Sm - 153	0.181	103.23
Eu - 152	0.069	1408.10
Tb - 160	0.047	879.30
Yb - 175	0.200	396.10
Lu - 177	0.034	208.36
Np - 239(U)		277.56
Pa - 233(Th)		311.90
Rb - 86 *		1077.20
Cs - 134		797.00
Cr - 51		320.10
Sc - 46		889.30
Ba - 131		496.30
Hf - 181		482.20
Zr - 95 *		756.70

*Values determinded by X-Ray Fluorescence used in lieu of these values

Table E-1 - X-Ray Fluorescence instrument settings and error calculations

Element	KV/MA	Tube	Collimator	Detector	Crystal	RMS%Error
Si	50/45	Cr	Coarse	FPC	Gypsum	1.201073
Ti	50/45	Cr	Fine	FPC	Quartz	0.0500179
Al	50/45	Cr	Coarse	FPC	Gypsum	0.172109
Fe	50/45	Cr	Fine	FPC	Quartz	0.337055
Mg	50/45	Cr	Coarse	FPC	Gypsum	0.712054
Ca	50/45	Cr	Fine	FPC	Quartz	0.538462
K	50/45	Cr	Fine	FPC	Quartz	0.0894233
Mo Comp	50/45	Mo	Fine	Scin	LiF(200)	
Rb	50/45	Mo	Fine	Scin	LiF(200)	
Sr	50/45	Mo	Fine	Scin	LiF(200)	
Zr	45/40	W	Fine	Scin	LiF(200)	

FPC = Flow Proportional Counter
Scin = Scintillation Counter

Table E-2 - Standards (concentrations in %) used in constructing calibration curves

Standards	SiO_2	TiO_2	Al_2O_3	Fe_2O_{3T}	MgO	CaO	K_2O
GSP-1	67.38	0.66	15.25	4.33	0.96	2.02	5.53
AGV-1	58.99	1.04	17.25	6.76	1.53	4.90	2.89
JG1	72.24	0.26	14.21	2.21	0.73	2.18	3.96
GA	69.90	0.38	14.50	2.83	0.95	2.45	4.03
JB-1	52.09	1.34		9.04	7.70	9.21	1.42
SY-1	59.50	0.49	9.60	8.20	4.20	10.20	2.67
BLCR-1	54.50	2.20	13.61		3.46		1.70
HI-31	58.80	0.88	16.70	6.47		6.50	2.88
LOSP	75.90	0.20	12.3	1.81	0.07	0.93	4.83
G-25		2.60	10.15	12.85	13.3	13.8	1.40

Table E-3 - Influencing elements affecting analyte concentrations

Analyte	Si	Ti	Al	Fe	Mg	Ca	K
Si	X		X	X		X	
Ti		X		X			
Al	X		X	X	X	X	
Fe	X			X		X	
Mg					X	X	
Ca	X			X		X	
K				X		X	X

Table E-4 - Mass absorption coefficients of standards used in determining Rb, Sr, and Zr concentrations

Standard	Mass Absorption Coefficient
AGV1	12.32
GSP1	11.53
GH	8.19
G2	10.22
GA	10.24
JB-1	13.82
SY-1	13.94
BCR-1	15.90

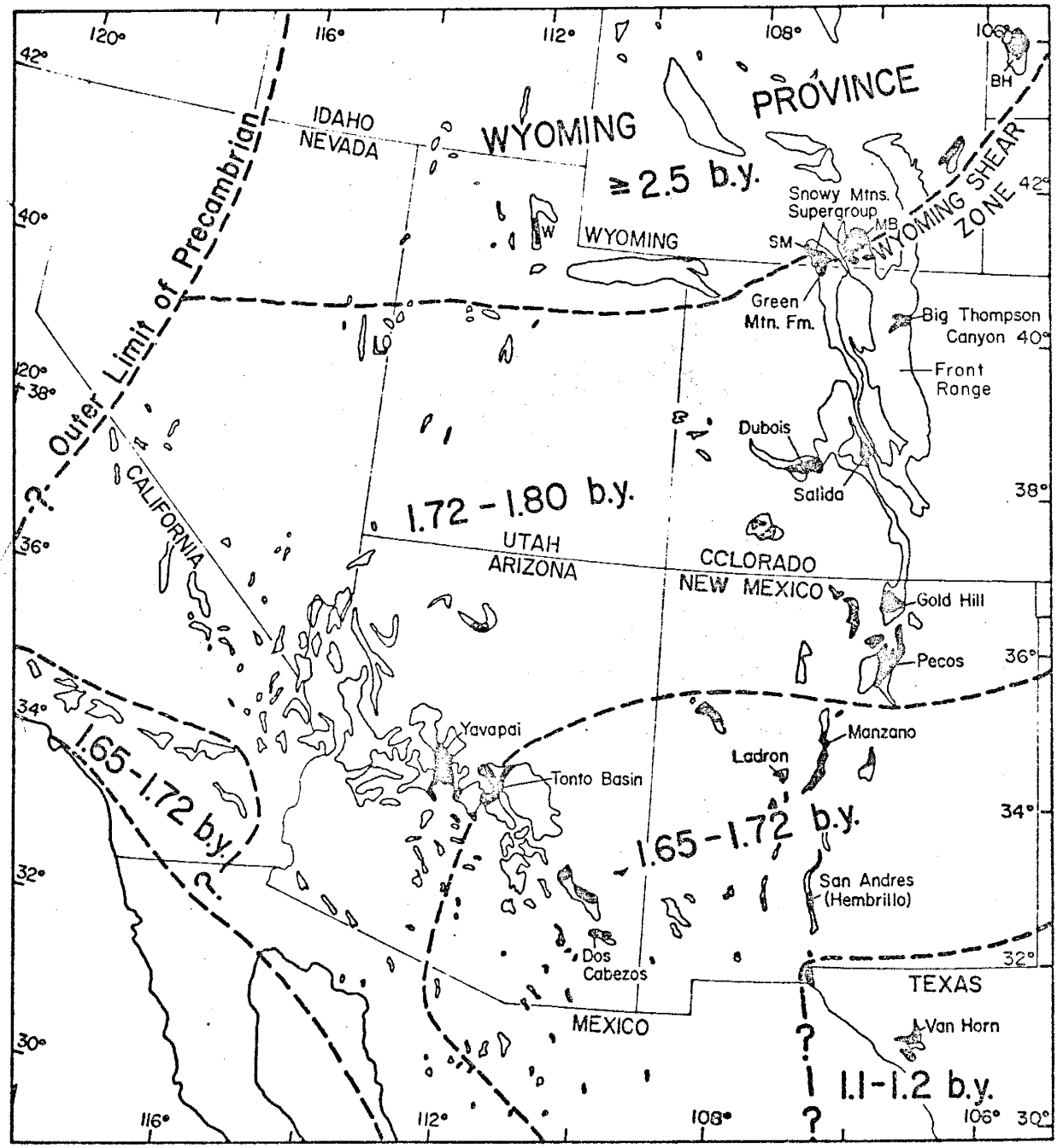

Figure 1: Regional map of the southwestern United States, illustrating the location of the Big Thompson Canyon and the major Precambrian rock age belts (After Condie, 1982)

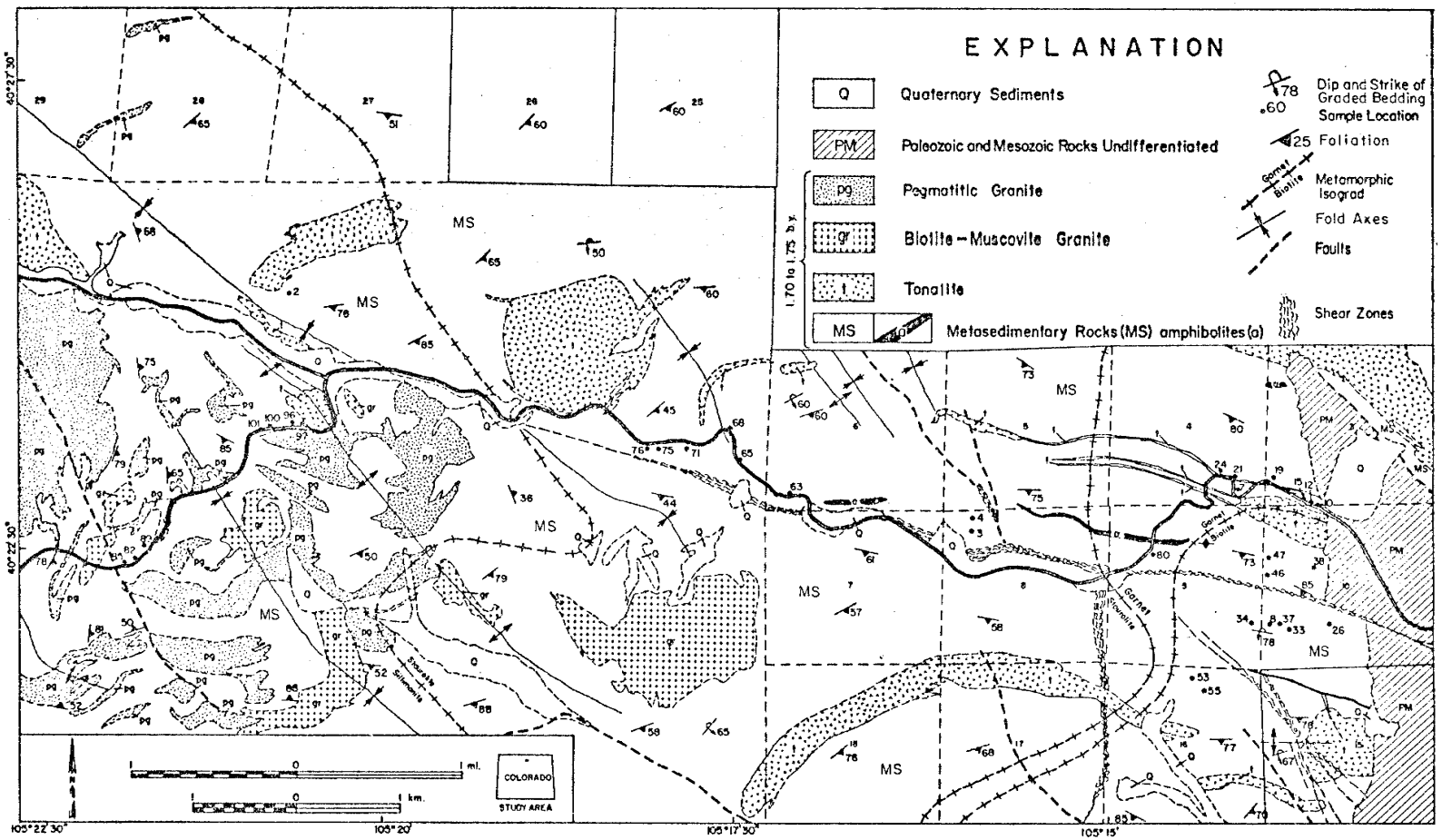

Figure 2: Geologic map of the Big Thompson Canyon area in the Drake and Masonville Quadrangles, Larimer County, Colorado (After Braddock et al, 1970a and 1970b)

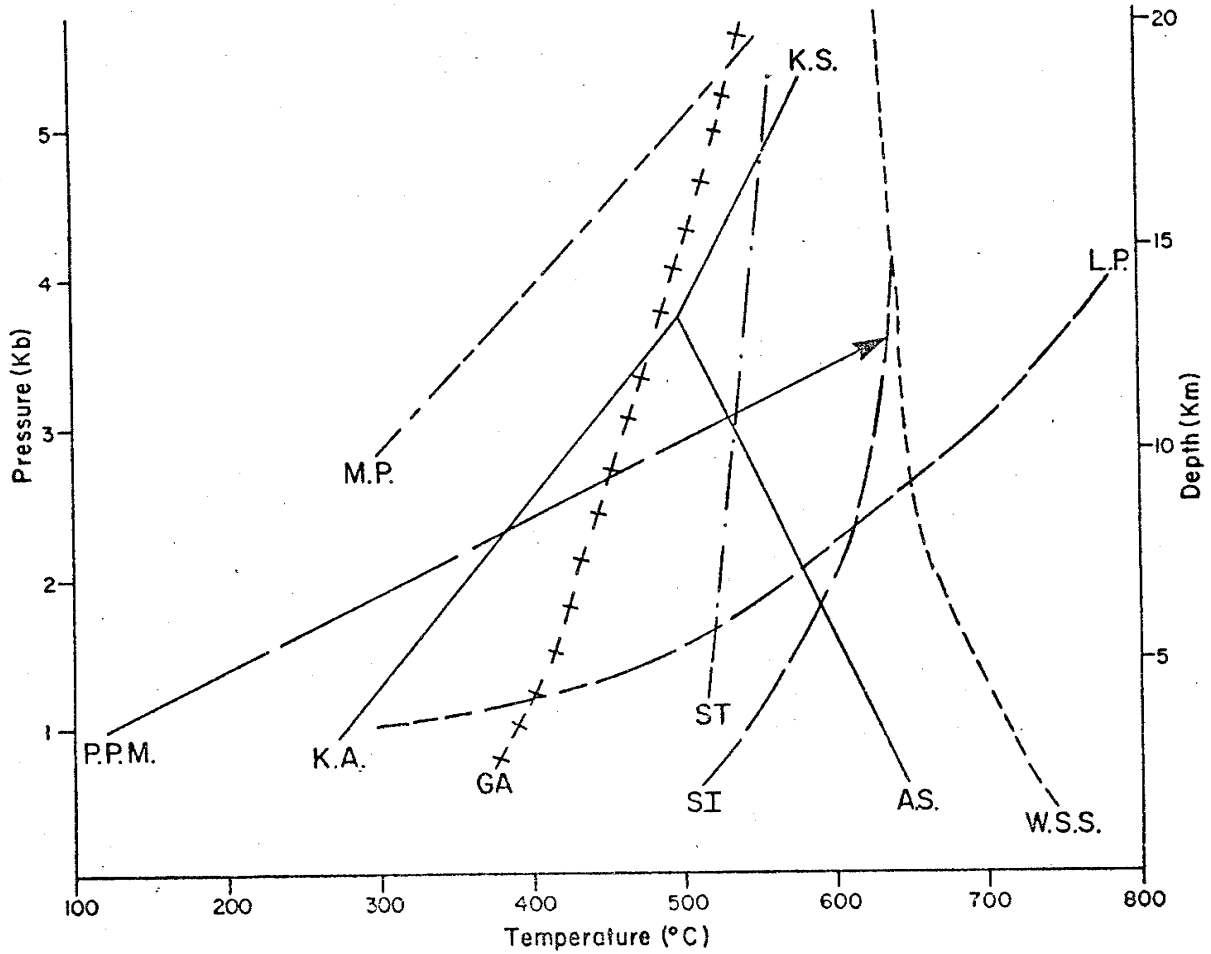

Figure 3: Pressure–temperature diagram of phase relations and probable course of progressive metamorphism in rocks of Big Thompson Canyon. Refer to Table 2I for explanation of symbols (Kyanite–Andalusite–Sillimanite stability triple point is from Holdaway (1971), Other curves are from Miyashiro (1973), Winkler (1979), Condie (1976), Hoseheck (1969), and Luth (1976)).

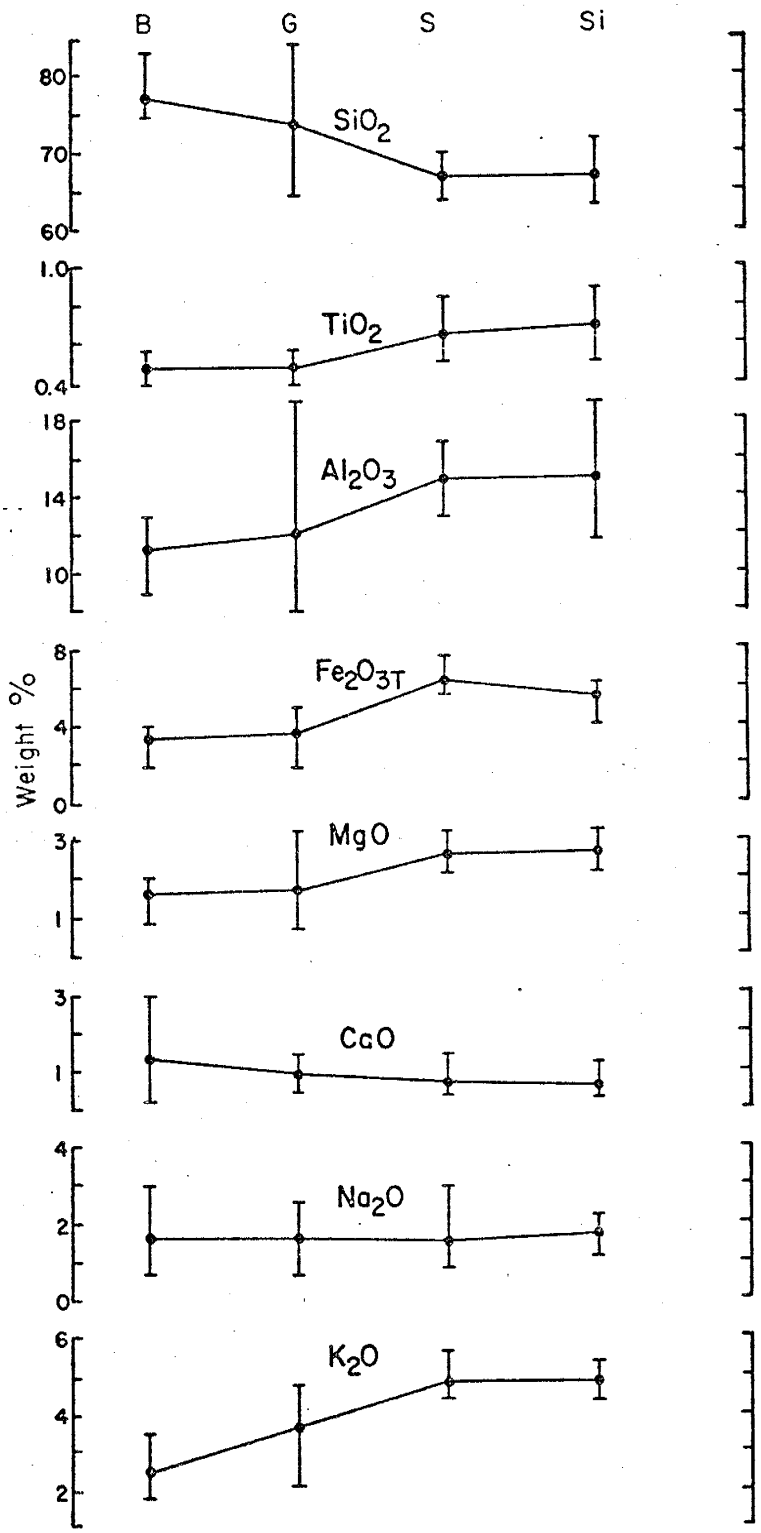

Figure 4: Changes in major element content of metasediments from Big Thompson Canyon as a funation of increasing metamorphic grade, Points represent mean values and brackets denote ranges for each zone, Zones: B, biotite, G, garnet, S, Staurolite, Si, Sillimanite

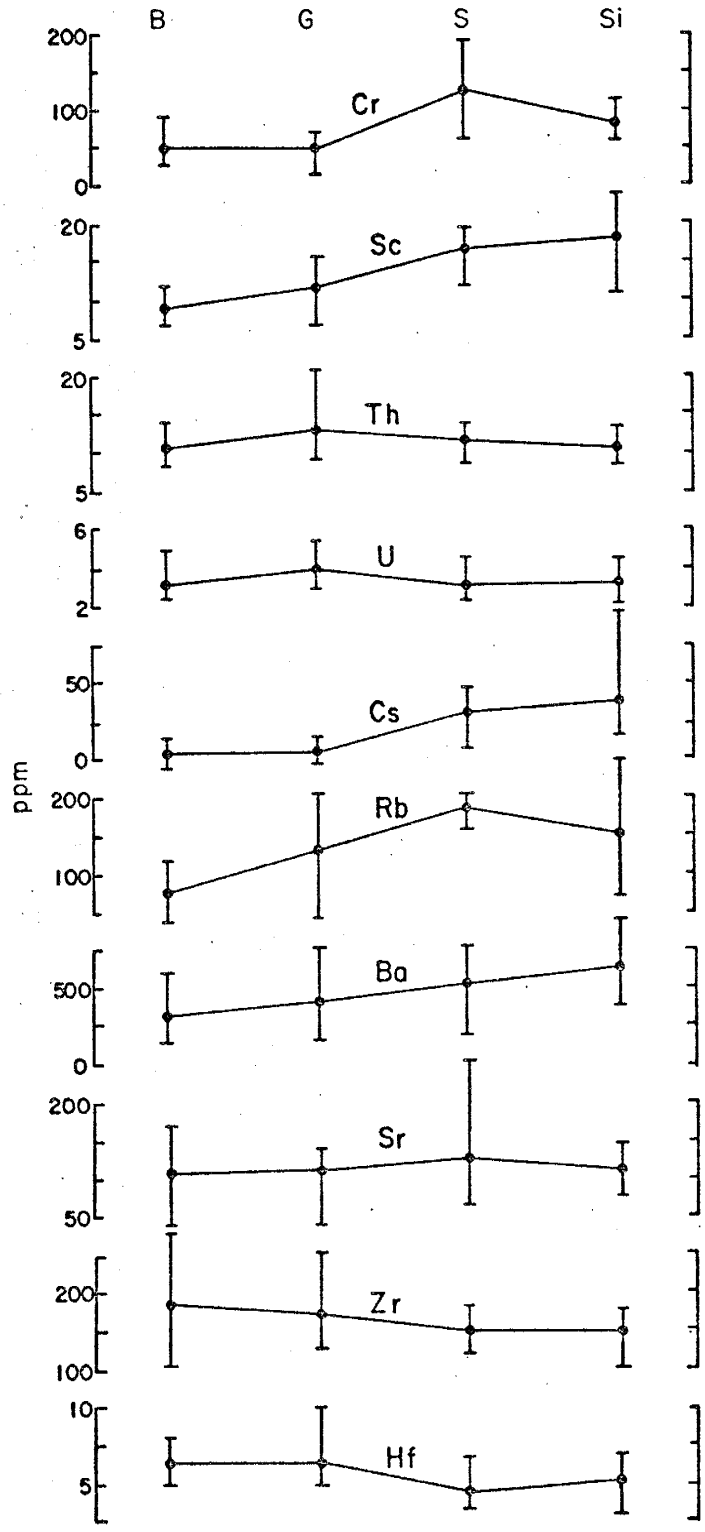

Figure 5: Changes in trace element content of metasediments from Big Thompson Canyon as a function of increasing metamorphic grade, Symbols given in Figure 4.

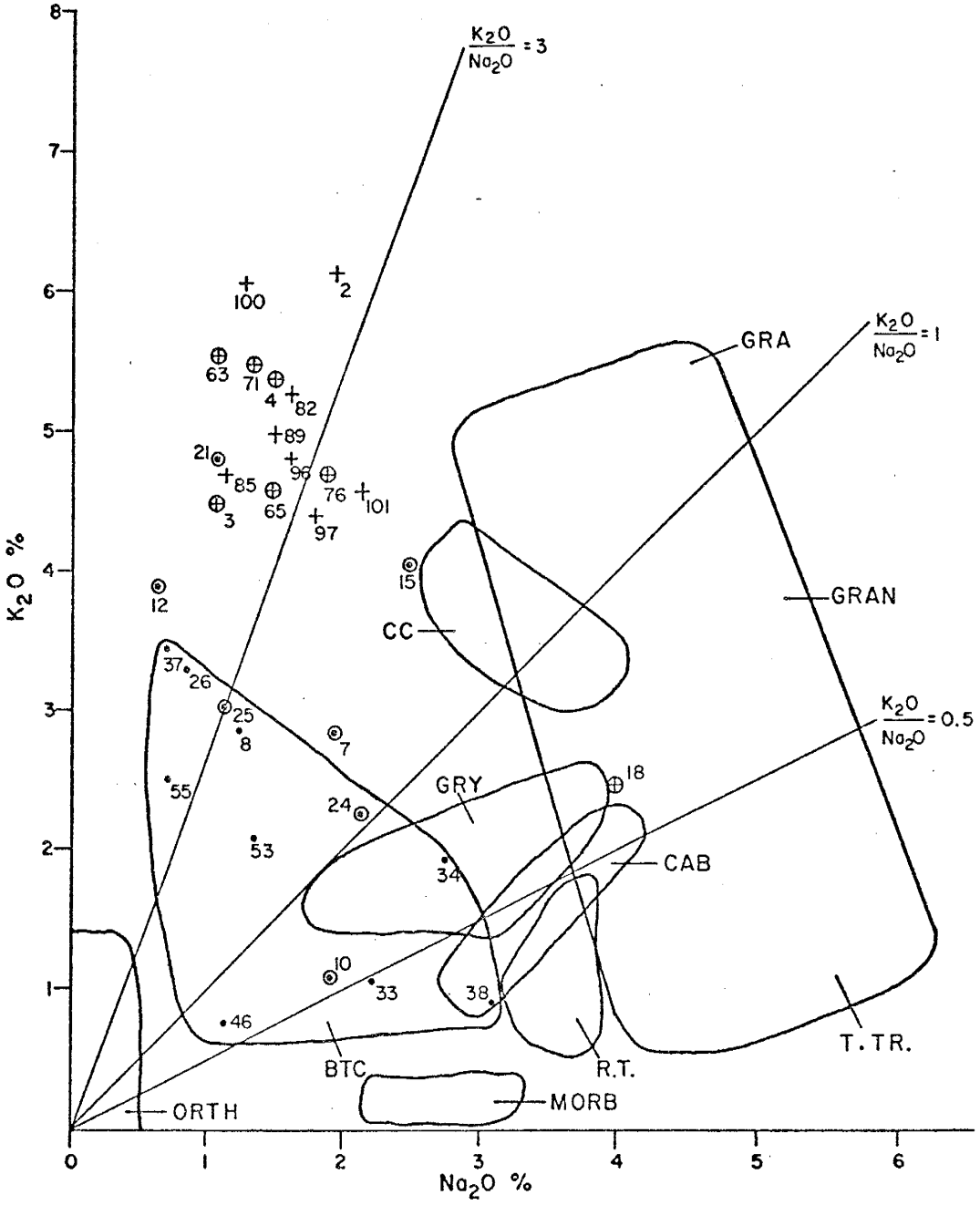

Figure 6: K_2O— Na_2O Plot (Refer to Table 22 for the explanation of symbols on Figures 6–14 and 17. Refer to Table 23 for references of the constructed rock fields of these X–Y element plots.)

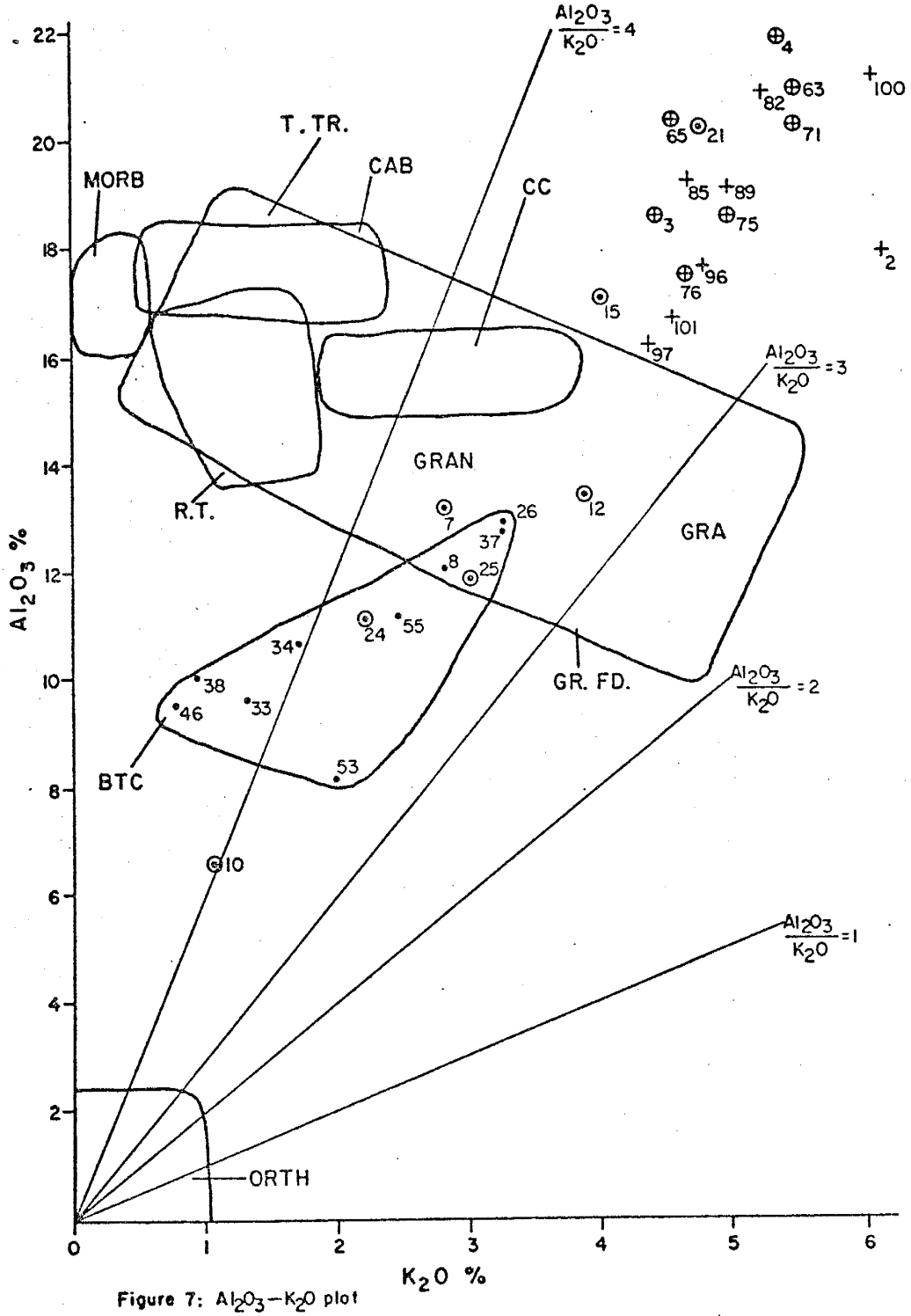

Figure 7: Al_2O_3–K_2O plot

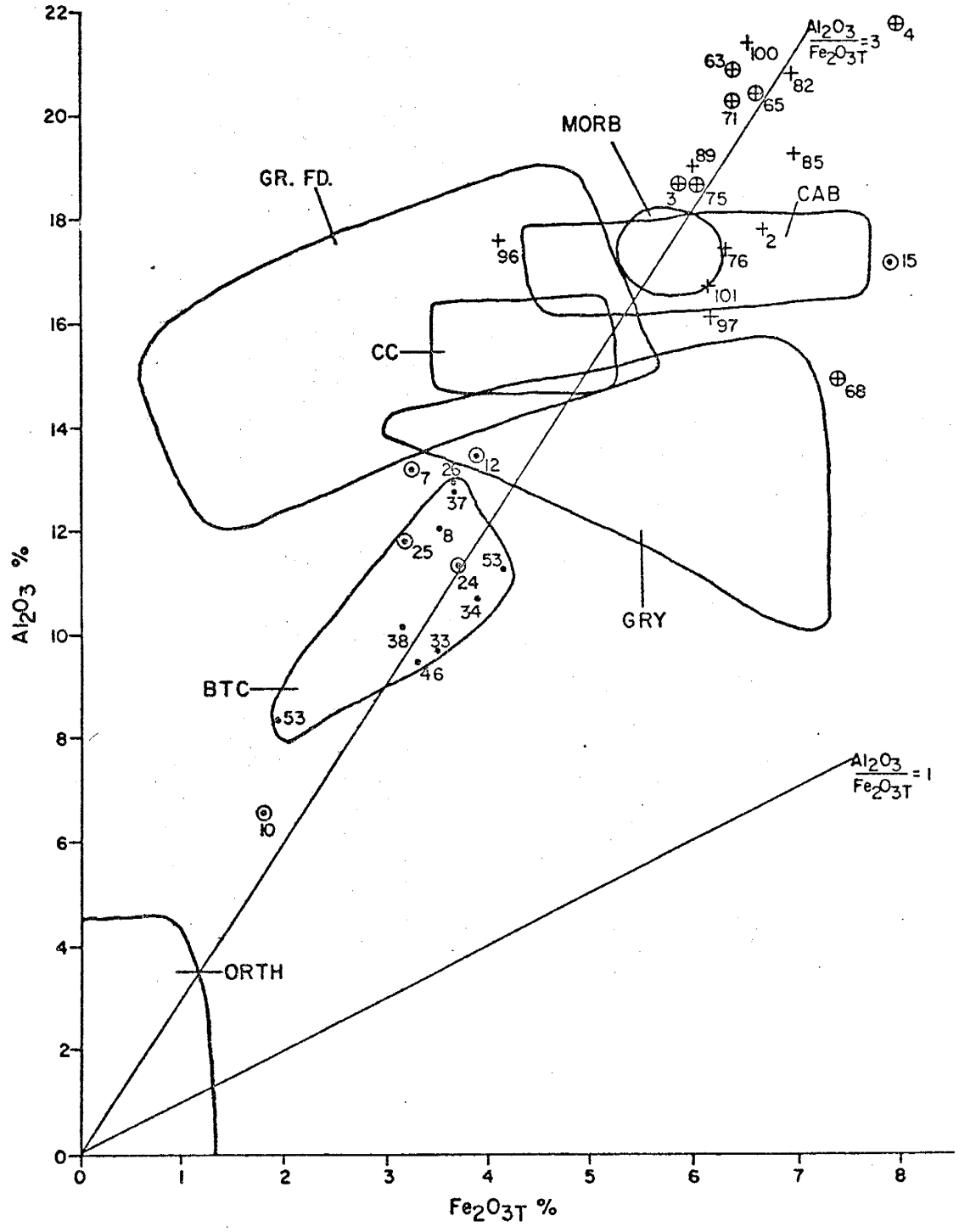

Figure 8: $Al_2O_3-Fe_2O_{3T}$ plot

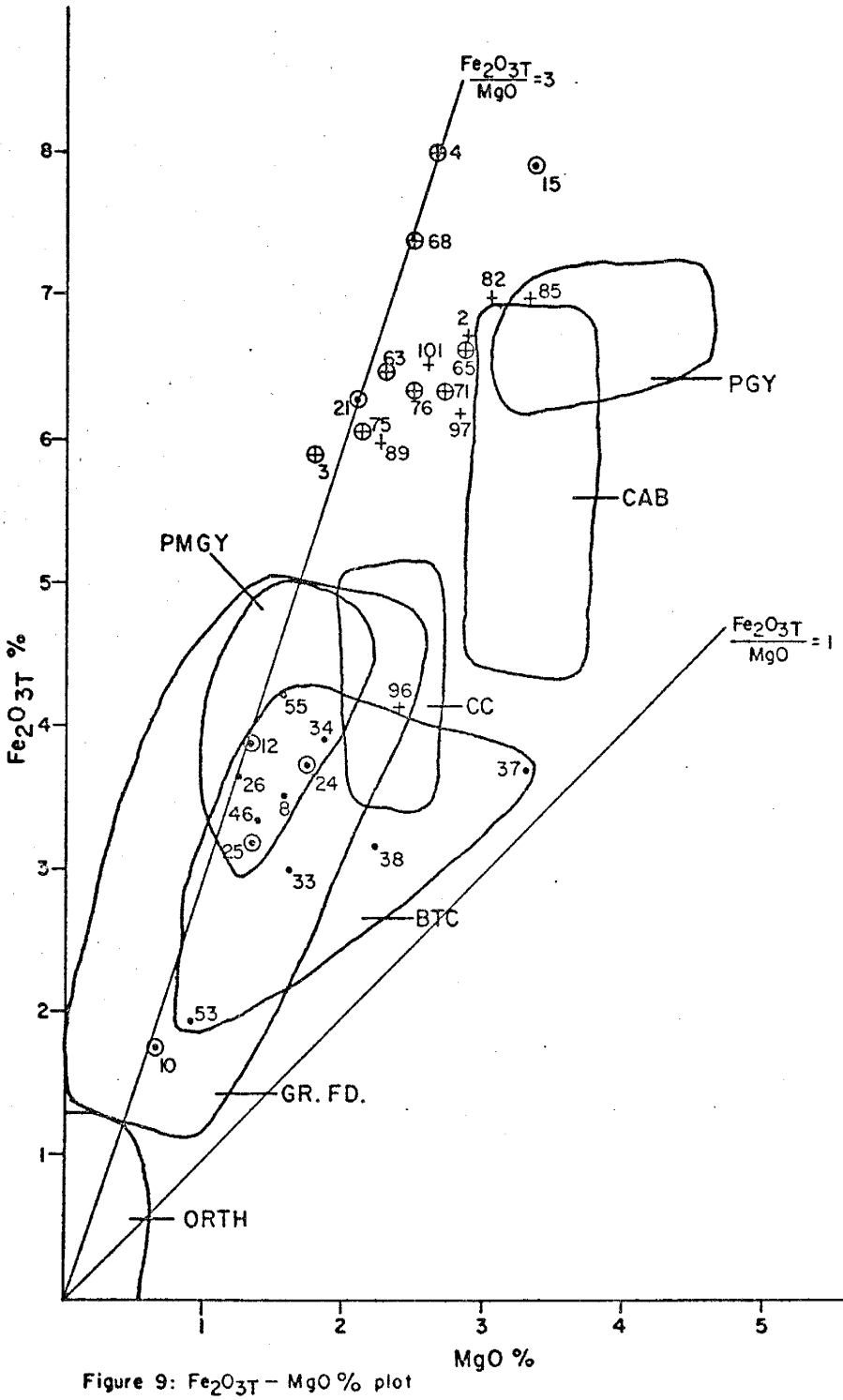

Figure 9: Fe_2O_{3T} – MgO % plot

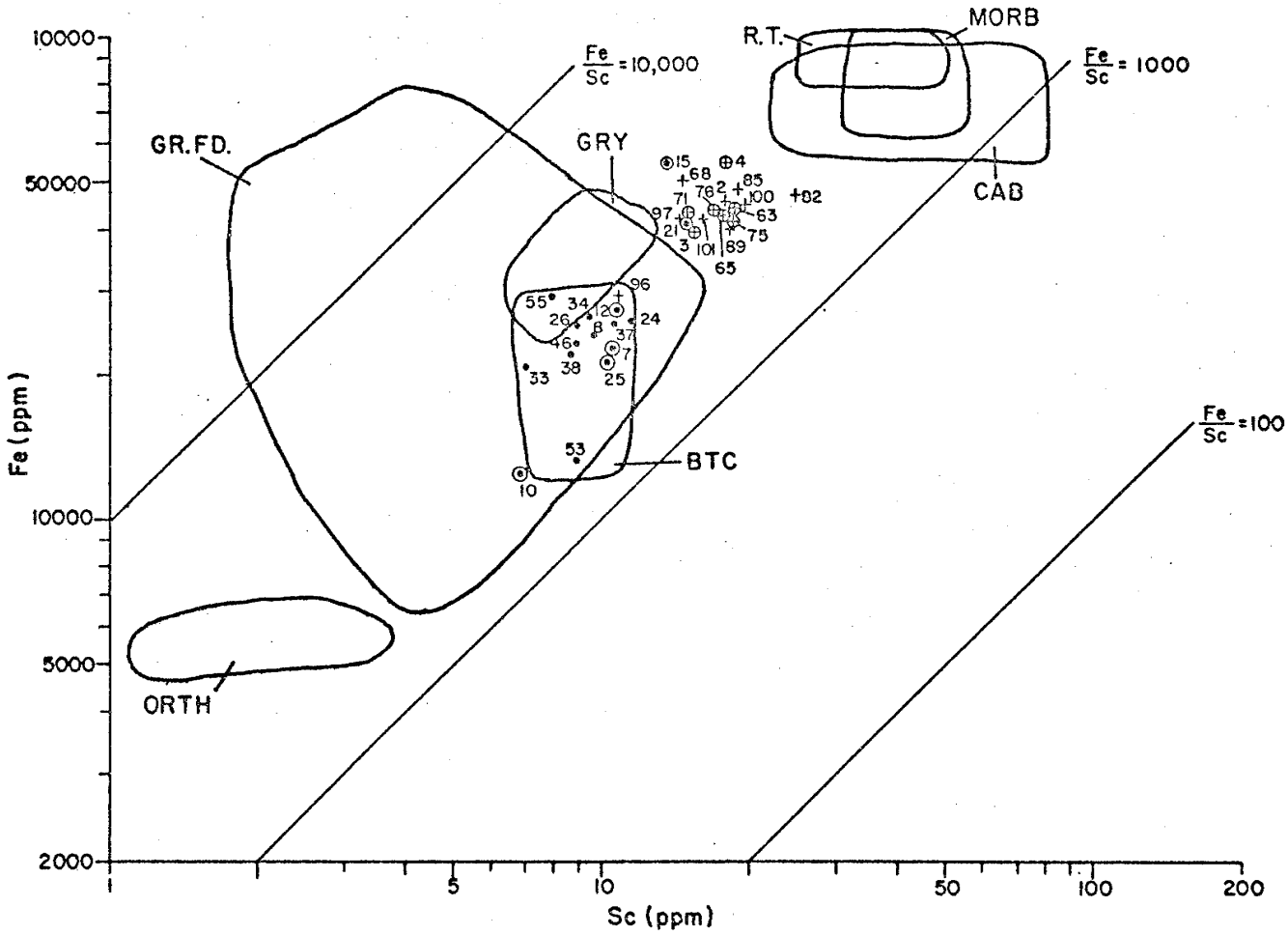

Figure 10: Fe—Sc plot

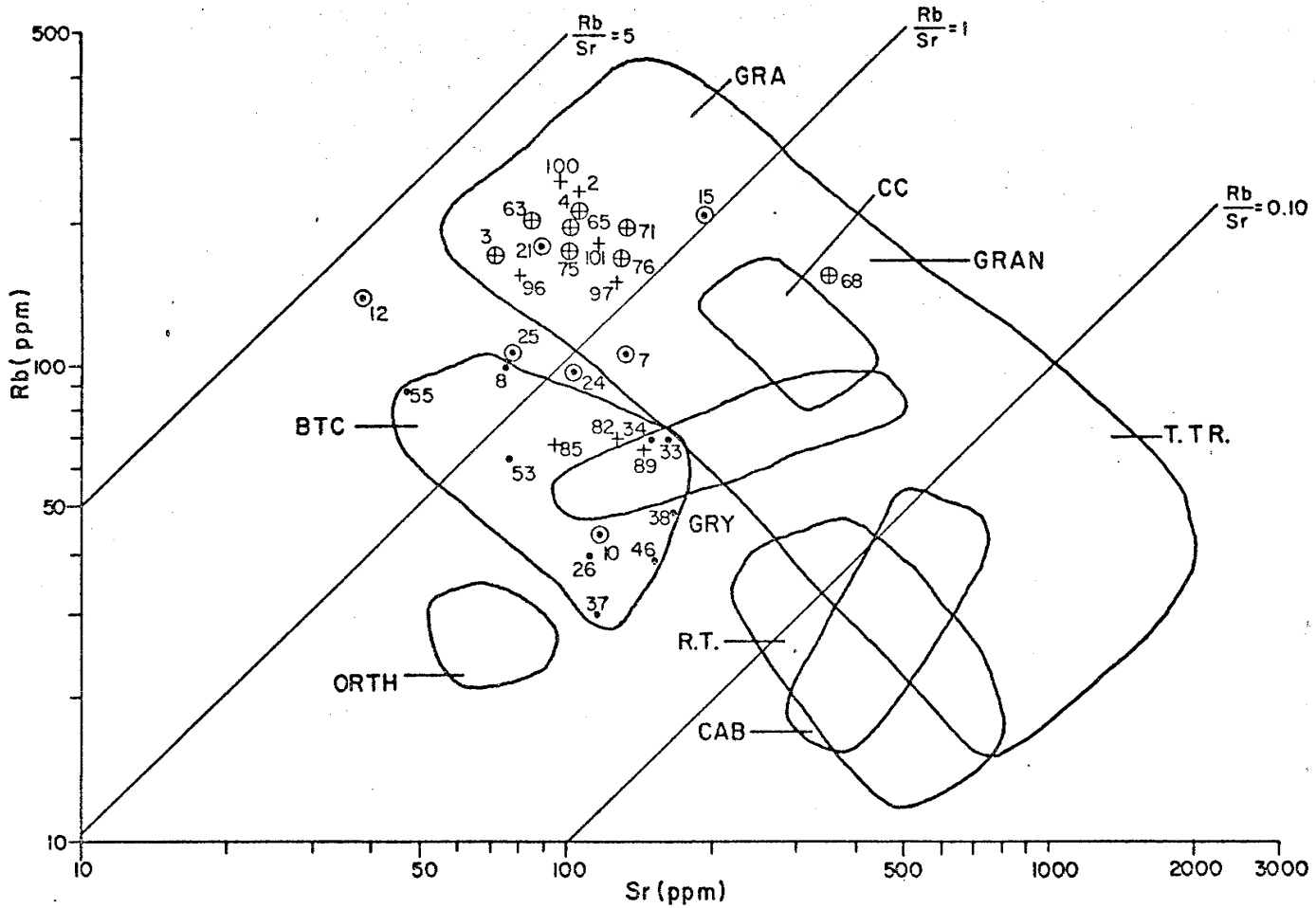

Figure 11: Rb–Sr plot

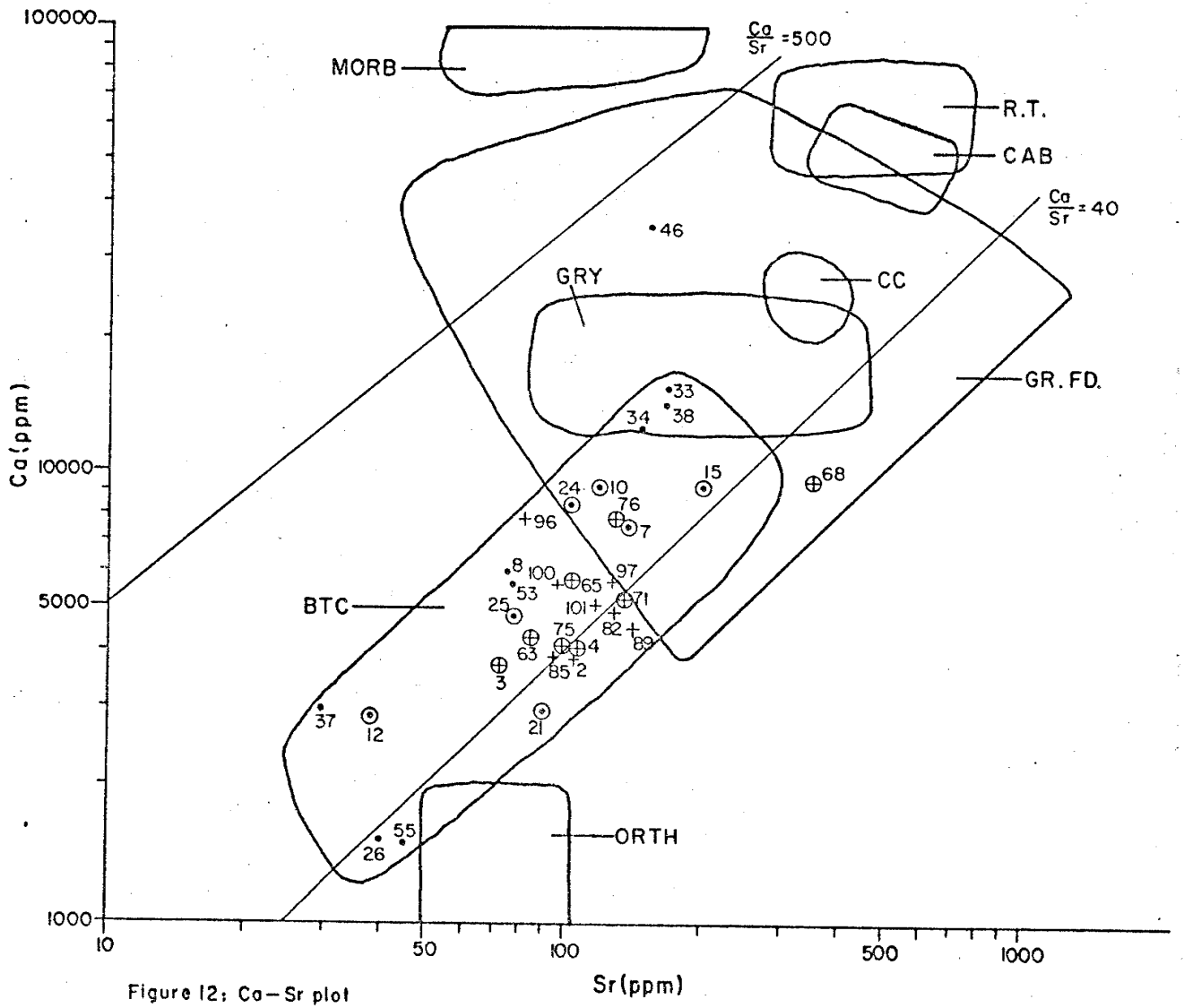

Figure 12: Ca–Sr plot

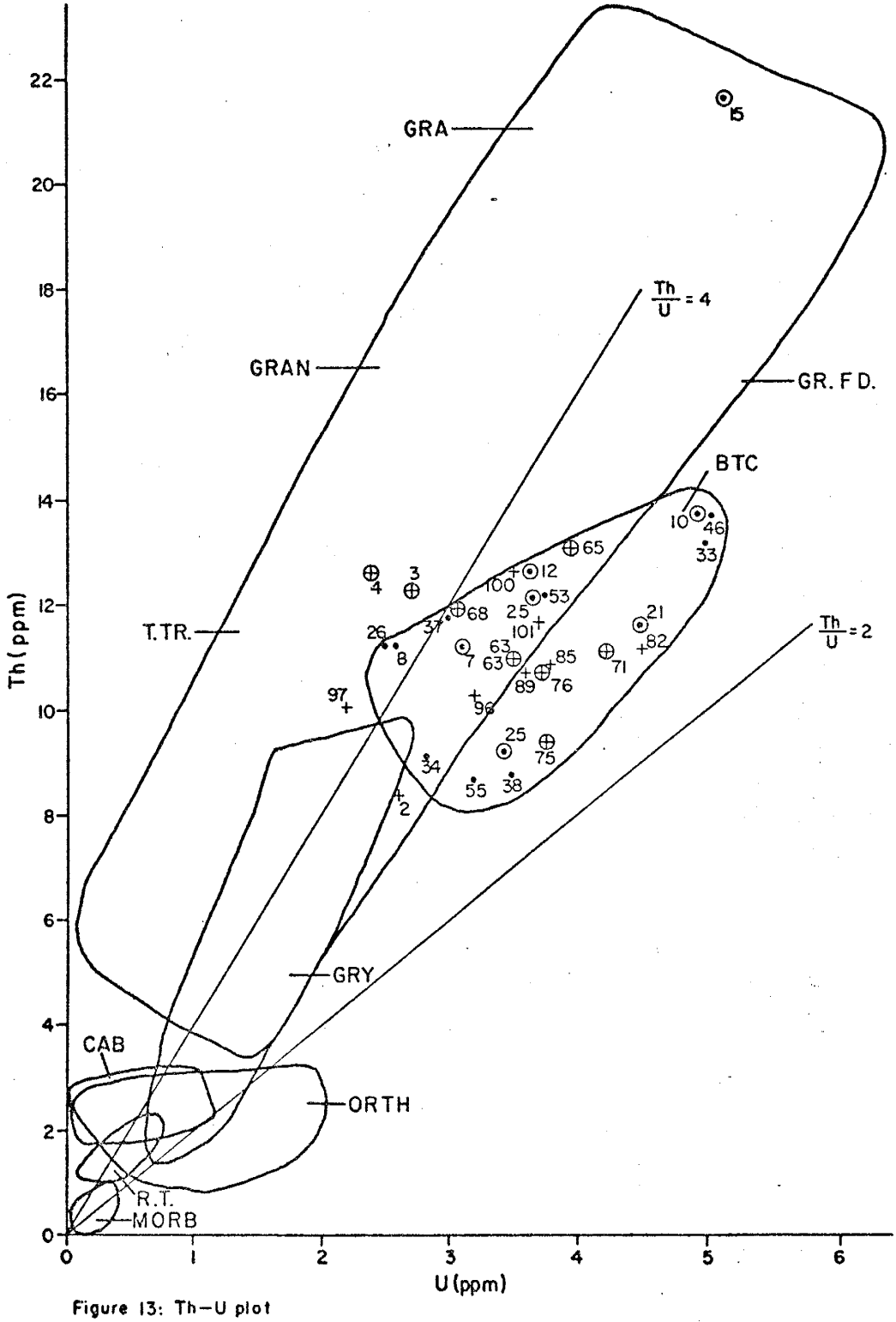

Figure 13: Th–U plot

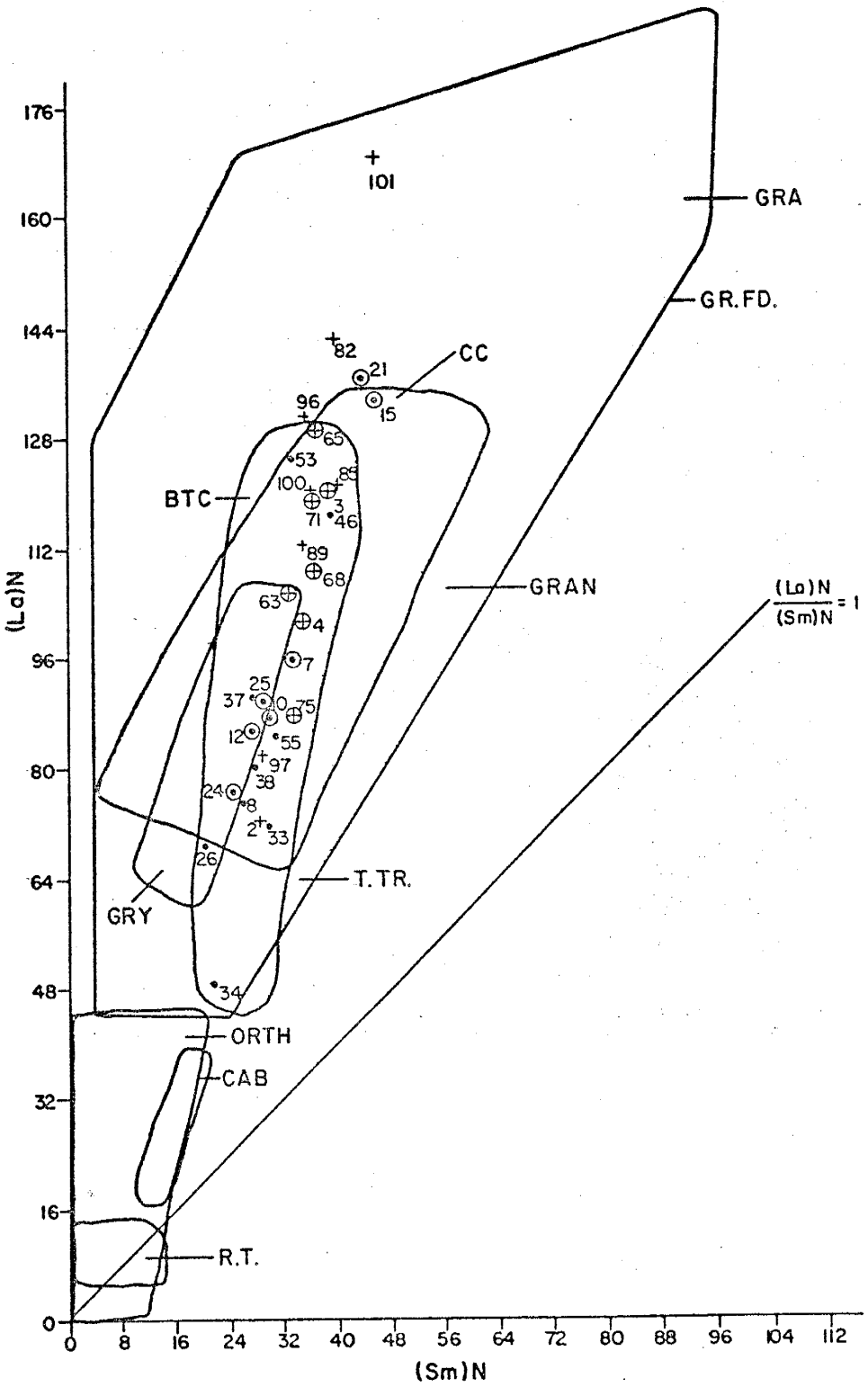

Figure 14: (La)N — (Sm)N plot

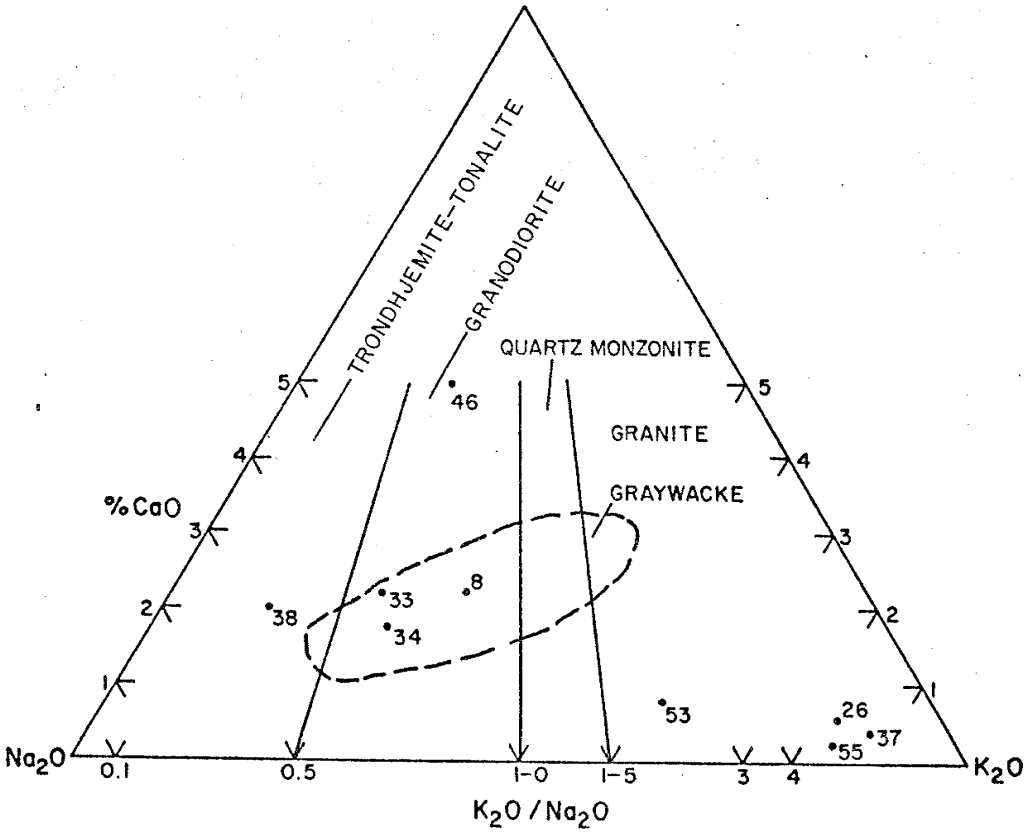

Figure 15: %CaO — K_2O / Na_2O plot delineating position within the Granitic Field (After Condie, 1979)

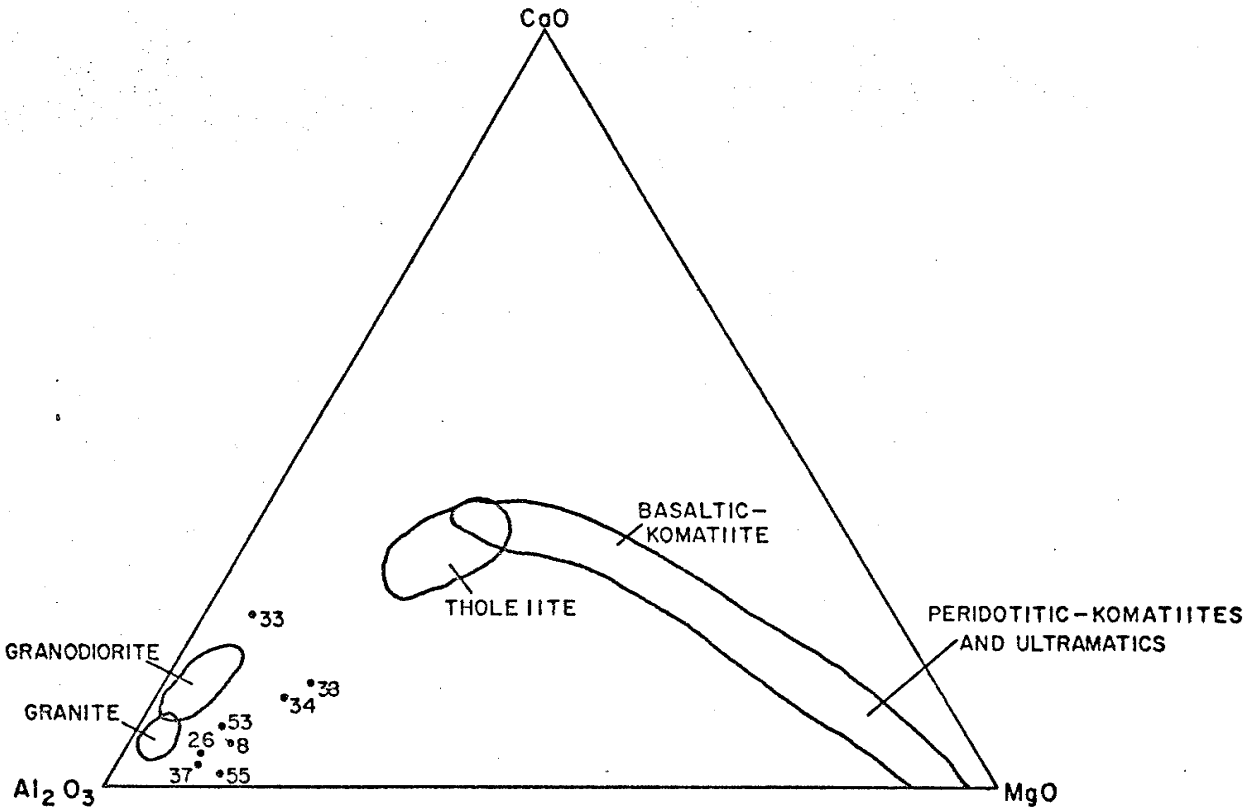

Figure 16: Al_2O_3– CaO – MgO plot illustrating presence of plutonic rock types. (From Bavinton and Taylor, 1980)

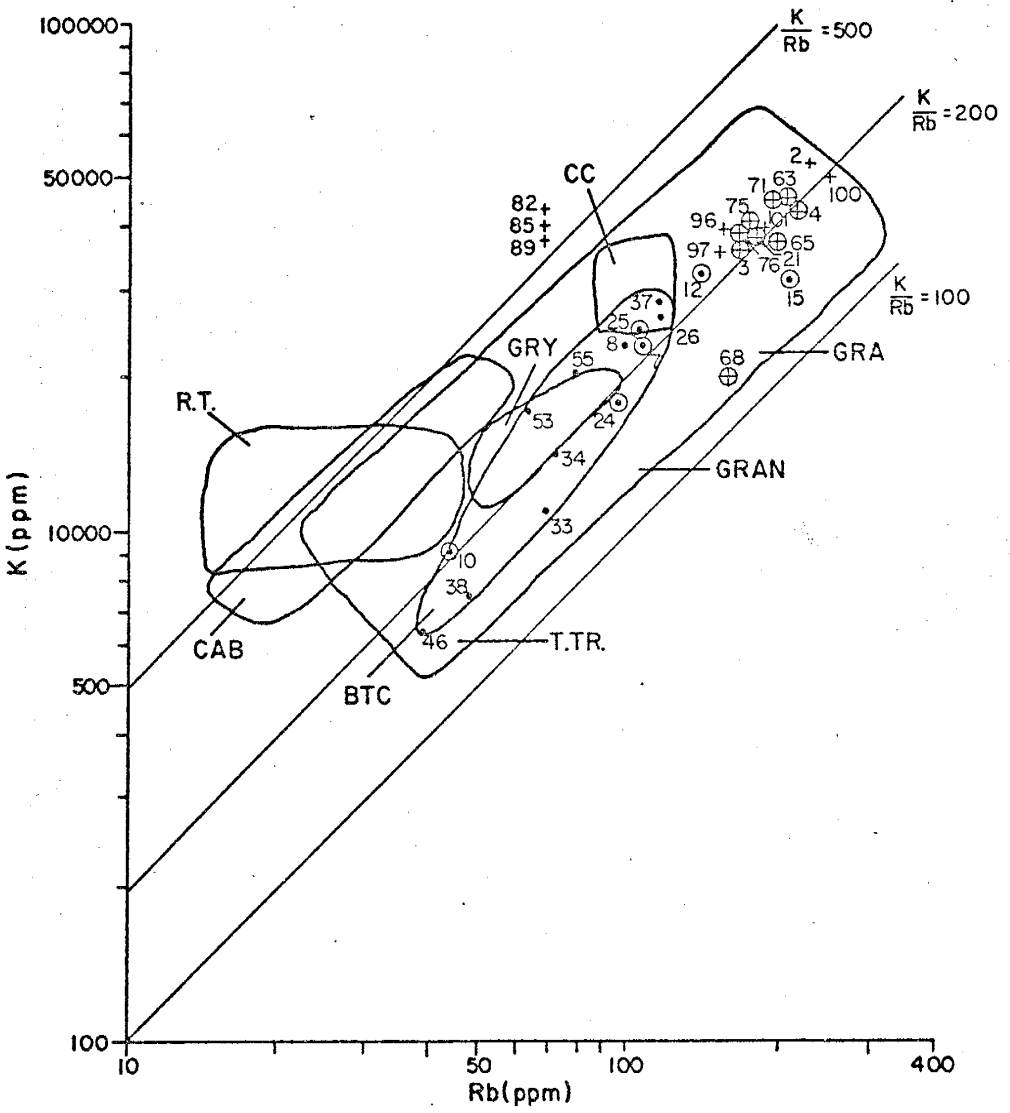

Figure 17: K — Rb plot

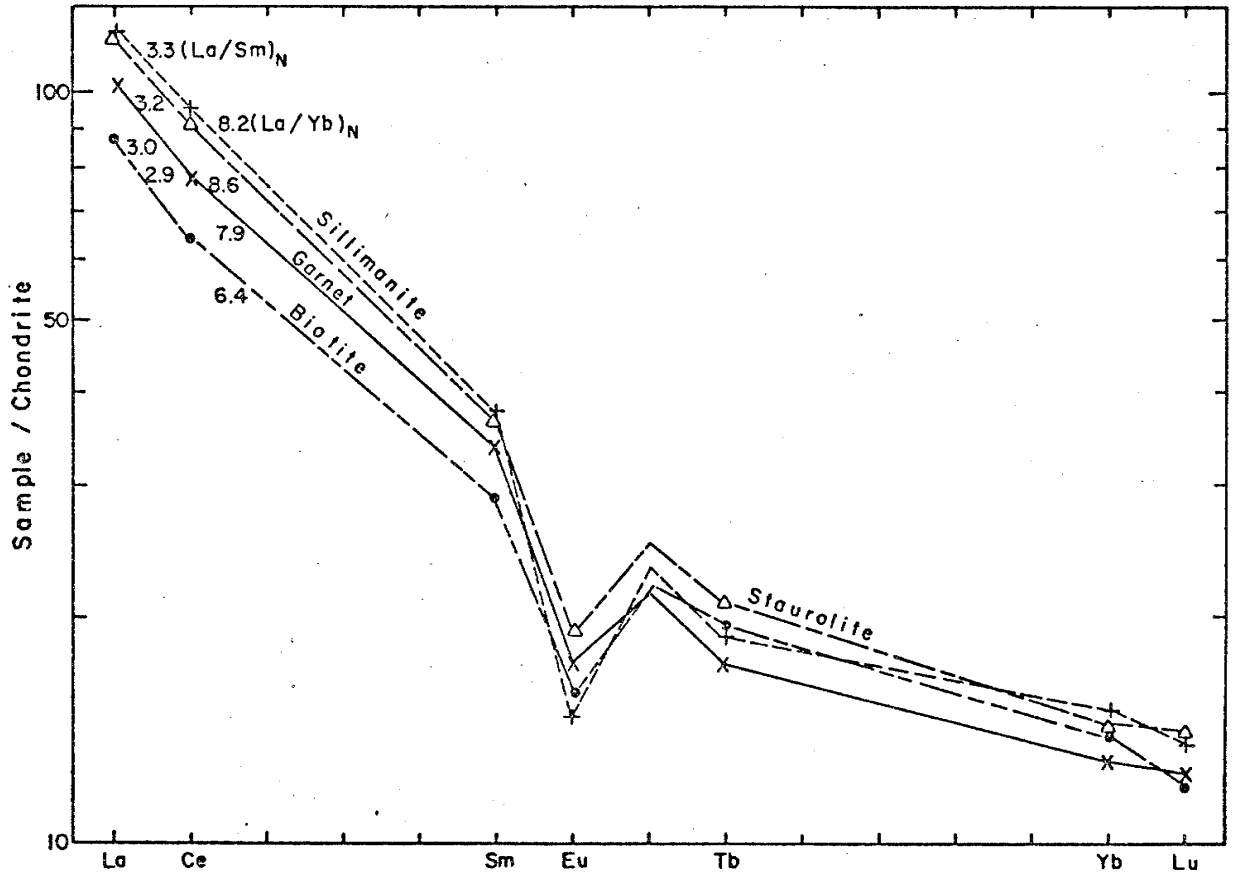

Figure 18: Average REE distribution in metasediments from each metamorphic zone in Big Thompson Canyon, Subscript N refers to Chondrite — normalized ratios

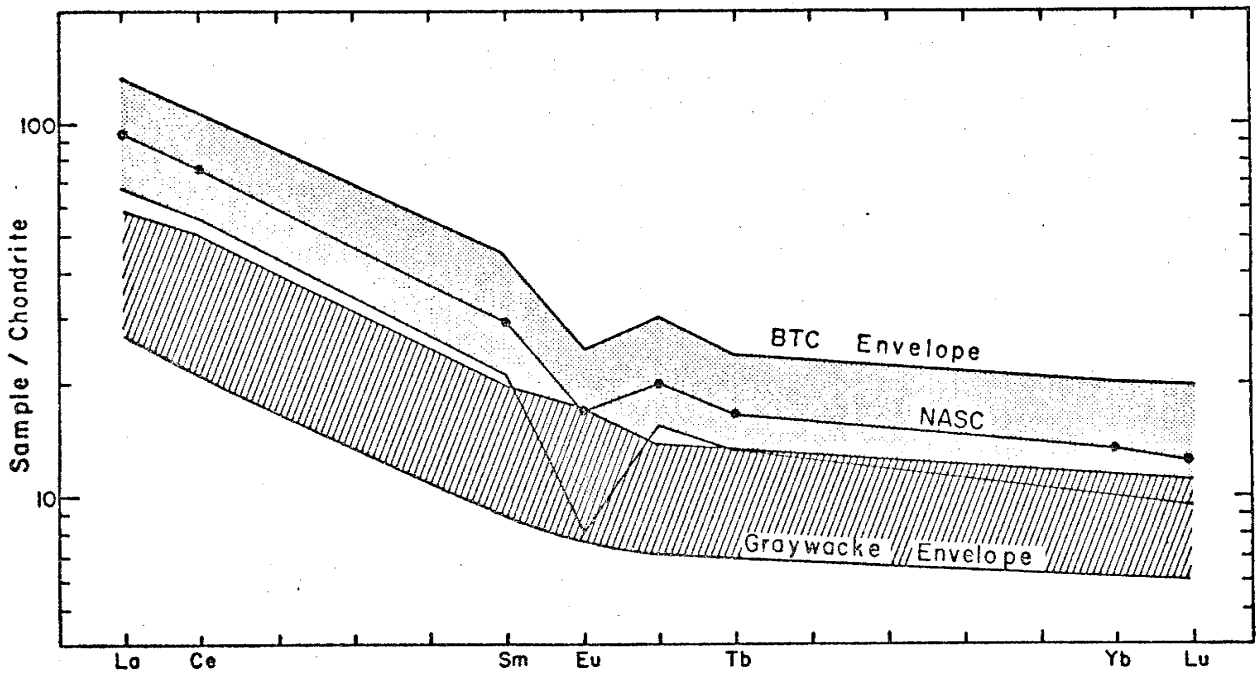

Figure 19: Envelope of REE variation for the Big Thompson Canyon metasediments compared to average North American Shale (NASC) and to the envelope of REE variation in graywackes (NASC composite from Wildeman and Haskin (1979), Graywacke field constructed from data of McLennon et al., (1979), Nance and Taylor (1977, 1976) and Wildeman and Haskin (1973)).

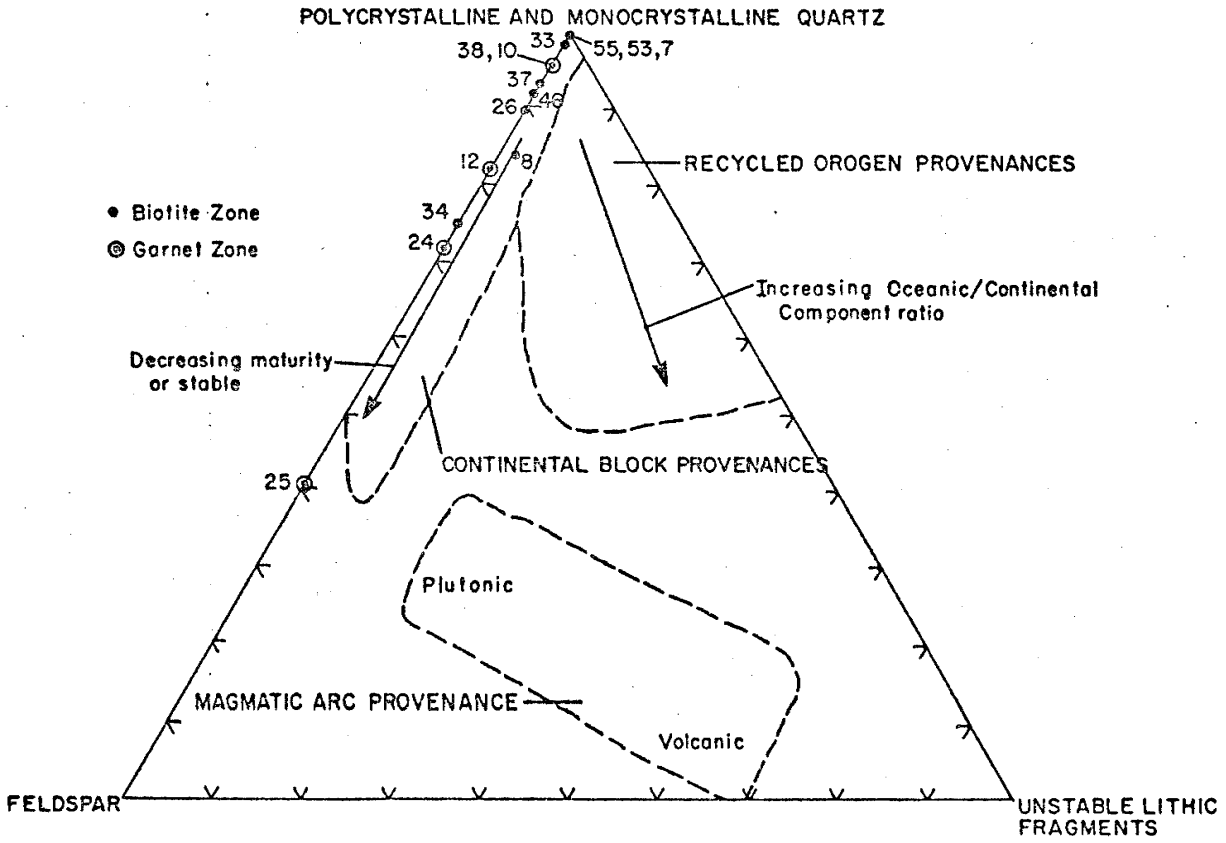

Figure 20: Triangular quartz–feldspar–unstable lithic fragments (sedimentary, metasedimentary, metavolcanic and volcanic varieties) plot showing different types of provenance as a function of framework mode. (From Dickinson and Suczek, 1979)

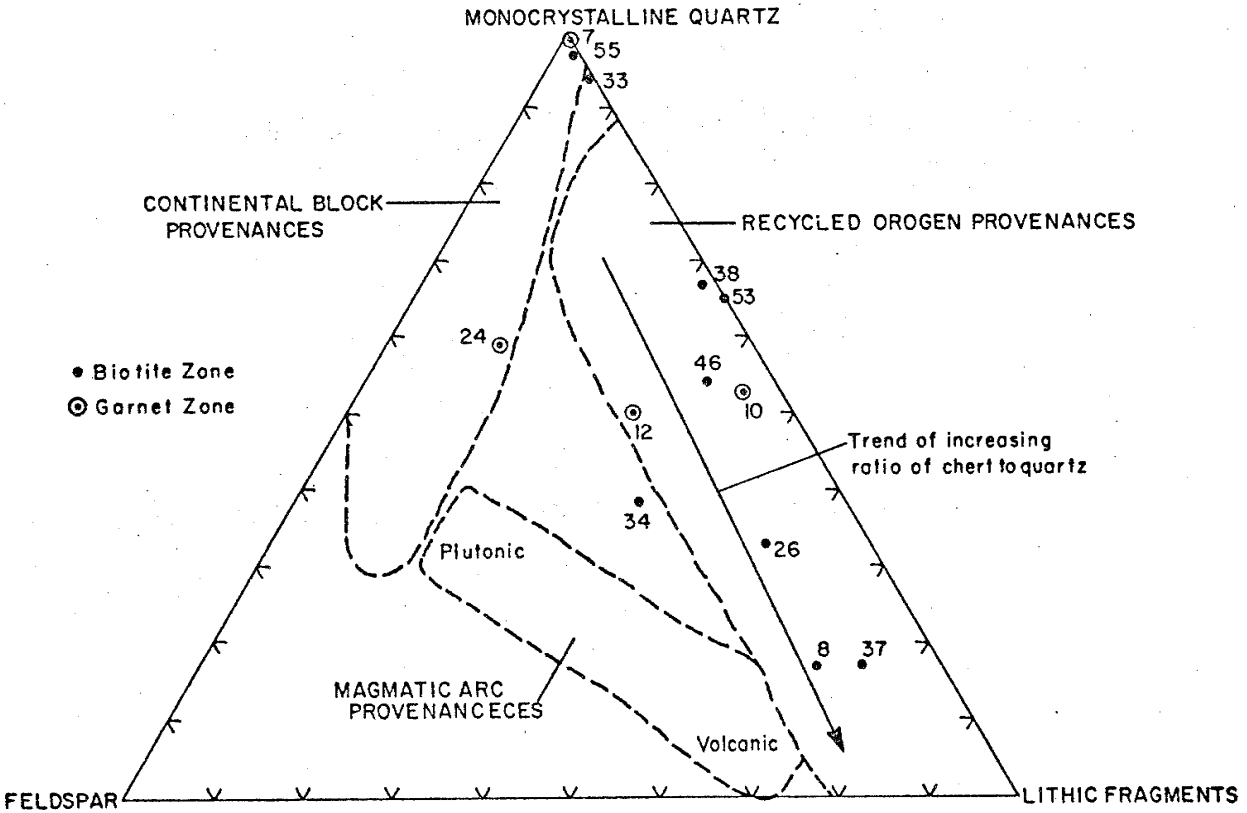

Figure 21: Triangular monocrystalline quartz – total feldspar – lithic fragments (including stable quartzose as well as unstable sedimentary, metasedimentary, metavolcanic and volcanic varieties) plot showing different types of provenance as a function of framework mode (From Dickinson and Suczek, 1979)

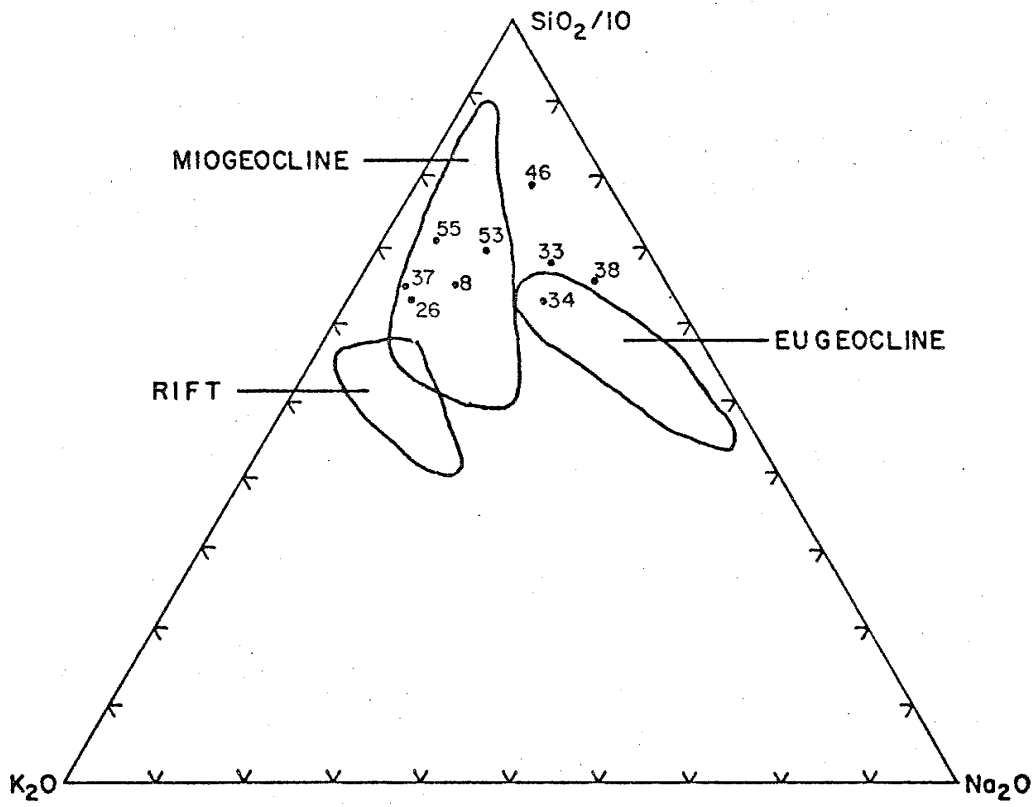

Figure 22: Tectonic setting as a function of SiO_2, K_2O and Na_2O content
'Samples plotted are from the Big Thompson Canyon biotite zone
(After Schwab, 1975)

REFERENCES

Adams, J. A. S., Osmond, J. K., and Rogers, J. J. W., (1959), Physics and Chemistry of the Earth, 3, pg. 299.

Arth, J. G. and Hanson, G. N. (1975), Geochemistry and origin of the early Precambrian crust of northeastern Minnesota. Geol. Soc. of America 39:325-362.

Atherton, M. P. (1964), The garnet isograd in pelitic rocks and its relation to metamorphic facies, American Mineralogist, vol. 49, pp. 1331-1348.

Bavinton, O. A. and Taylor, S. R. (1979), Rare earth element geochemistry of Archean metasedimentary rocks from Kambalda, Western Austrailia, G.C.A., vol. 44, p. 639-648.

Braddock, W. A. (1970), The Origin of Slaty Cleavage: Evidence From Precambrian Rocks in Colorado, Geol. Soc. Am. Bull., 81, pp 589-600.

Braddock, W. A. (1966), Precambrian geology of the east flank of the Front Range near Fort Collins (abstract): Geological Society of America Special Paper 87, p. 277.

Braddock, W. A., Calvert, R. H., Gawarecki, S. J., and Nutalaya, P. (1970a), Geologic map of the Masonville quadrangle, Larimer Co., Colorado, U. S. Geol. Survey Map GQ-832, scale 1:24,000.

Braddock, W. A., Nutalaya, P., Gawarecki, S. J., and Curtin, G. C. (1970b), Geologic map of the Drake quadrangle, Larimer Co., Colorado, U. S. Geol. Survey map GQ-829, scale 1:24,000.

Brown, E. H. (1971), Phase relations of biotite and stilpnomelane in the greenschist facies, Contrib. Mineral. Petrol., vol. 31, pp 275-299.

Brown, P. E. (1967), Major element composition of the Loch Coire migmatite complex, Sutherland, Scotland, Contrib. Mineral. Petrol., vol. 14, pp. 1-26.

Buttram, Frank (1913), The glass sands of Oklahoma, Oklahoma Geol. Survey Bull. 19, 91 p.

Chakraborty, K. R., and Sen, S. K. (1967) Contr. Mineral. Petrol. vol. 16, pp. 210-232.

Clark, S. P. Jr., Peterman, Z. E., and Heier, K. S. (1966), Abundances of uranium, thorium, and potassium, Geol. Soc. Am., Mem 97.

Clark, S. P., and Ringwood, A. E., (1964), Density Distribution and Constitution of the Mantle, Review Geophysics, 2, p. 35.

Collerson, K. D. and Bridgwater D. (1979), Metamorphic Development of an early Archean tonalitic and trondhjemitic gneisses: Saglek area, Labrador. In F. Barker (Editor) Trondhjemites, Dacites and Related Rocks. Elsevier, Amsterdam, pp. 203-274.

Collins, W. H. (1925), North shore of Lake Huron, Canada Geol Survey Mem. 143, 160 p.

Condie, K. C. (1982), A Back-Arc Model For Proterozoic Continental Accretion in the Southwestern United States, Geology, vol. 10. pp. 37-42.

Condie, K. C. (1981), Archean Greenstone Belts, Develoments in Precambrian Geology 3, Elsevier Scientific Publishing Company p. 190.

Condie, K. C. (1976), Plate Tectonics and Crustal Evolution. Pergamon International Library of Science, Technology, Engineering and Social Studies.

Condie, K. C. (1973) Archean magmatism and crustal thickening. Geol. Soc. America Bulletin, 84, pp. 2981-2992.

Condie, K. C., and Budding, A. J., 1979, Geology and geochemistry of Precambrian rocks, central and south-central New Mexico: New Mexico Bureau of Mines and Mineral Resources, Memoir 35.

Condie, Make and Reimer (1970) Petrology and Geochemistry of Early Precambrian Graywackes from the Fig Tree Group, South Africa, Geol. Soc. America Bulletin, vol. 81, p. 2759-2776.

Cooper, A. F. (1972) Progressive metamorphism of metabasic rocks from Haast Schist group of southern New Zealand, J. Petrol., vol. 13, pp. 457-492.

Cooper, J. A., Nesbitt, R. W., Platt, J. P. and Mortimer, G. E., (1978) Crustal development in the Agrew region, Western Australia, as shown by Rb/Sr isotopic and geochemical studies. Precambrian Research, 7:31-59.

Cullers, L. R., Yeh, Long-Tsu and Chaudhuri, Sambhudas (1974) Rare Earth Elements In Silurian Pelitic Schists from N. W. Main, Geochimica et Cosmochimica Acta, vol. 38, pp. 389-400.

Cushing, H. P., Leverett, Frank, Van Horn F. R., Geology and mineral resources of the Cleveland district, Ohio. U. S. Geol. Survey Bull. 818, 138 p (1931).

Deer, W. A., Howie, R. A. and Zussman, J. (1966) An Introduction To The Rock Forming Minerals, Longman Publishing.

Eade, K. E. and Fahrig, W. F. (1973) Regional lithological and temporal variation in abundances of elements in Canadian Shield, Geological Survey Canada Paper, 72-46, 46 pp.

Eade, K. E. and Fahrig, W. F. (1971) Geochemical evolutionary trends of continental plates - a preliminary study of the Canadian Shield Geol. Surv. Can. Bulletin 179.

Elles, G. L., and Tilley, C. E. (1930) Metamorphism in relation to structure in the Scottish Highlands, Trans. Roy. Soc. Edinburgh, vol. 56, pt. 3, pp. 621-646.

Engel, A. E. J., and Engel, C. E. (1964) Composition of Basalts from the Mid Atlantic Ridge, Science, vol. 144, pp. 1330-1333.

Engel, A. E. J. and Engel, G. G. (1960) Progressive Metamorphism and Granitization of the Major Paragneiss, Northwest Adirondack Mountains, New York, Geol. Soc. of America Bulletin, vol. 71, p. 1-58.

Engel, A. E. J. and Engel, C. G. (1958) Progressive Metamorphism and Granitization of the Major Paragneiss, Northwest Adirondack Mountains, New York, Geol. Soc. of America Bulletin, vol. 69, p. 1369-1414.

Engel, A. E. J., Engel, C. G., and Havens, R. G. (1965) Chemical Characteristics of Oceanic Basalts and the Upper Mantle, Geol. Soc. America Bulletin, vol. 76, pp. 719-734.

Eskola, P. (1914) On the petrology of the Orijarvi region of southwestern Finland, Bull. Comm. Geol. Finlande, no. 40.

Evans, B. W. (1965) Application of a reaction-rate method to the breakdown equilibria of muscovite and muscovite plus quartz - American Journal of Science, v. 263, p. 647-667.

Evans, B. W. and Guidotti (1966) The sillimanite-potash feldspar isograd in western Maine, U.S.A., Contrib. Mineral Petrol., vol. 12, pp. 25-62.

Fettke, C. R., Glass Manufacture and the glass sand industry of Pennsylvania. Pennsylvania Topog. and Geol. Survey Rept. 12, 278 p.

Field, D. and Elliot, R. B. (1974) The Chemistry of Gabbro/Amphibolite Transitions in South Norway, Contributions to Mineralogy and Petrology, vol. 47, p. 63-76.

Frycklund, V. C. and Fleischer, M. (1963) The abundance of scandium in volcanic rocks, a preliminary estimate. Geochimica et Cosmochimin Acta vol. 27, 643-664.

Fuller, M. B. (1924) General Features of the Precambrian Structure Along the Big Thompson River in Colorado, Journal of Geology, vol. 32, p. 49-63.

Glikson, A. Y. (1979) Early Precambrian Tonalite-Trondhjemite Sialic Nuclei, Earth Science Reviews, 15, 1-73.

Gordon, G. E., Randle, K., Goles, C. G. et. al. (1968) Instrumental activation analysis of standard rocks with high-resolution gamma-ray detectors, Geochemica et Cosmochimica Acta, vol. 32, pp. 309-396.

Green, T. H., Brunfelt, A. O. and Heir, K. S. (1972) Rare Earth Element distribution and K/Rb ratios in granulites, mangerites and anorthosites, Lofoten-Vesteraalen, Norway, Geochimica et Cosmochimica Acta, vol. 36, pp. 241-257.

Gunn, B. M. and Watkins, N. D. (1970) Geochemistry of the Steens Mountain Basalts, Oregon. Geological Society of American Bulletin, v. 81, p. 1497-1516.

Hart, S. R. (1971) K, Rb, Cs, Sr, and Ba contents and Sr isotope ratios of ocean floor basalts, Philos. Tran. R. Soc. Lond., Ser. A, 268, 573.

Haskin, L. A., Wildeman, T. R., Frey, F. A. Collins, K. A., Keedy, C. R. and Haskin, M. A. (1966) Rare earths in sediments. Journal Geophys. Res. 71, 6091-6105.

Hawkins, J. W. (1970) Petrology and Possible Tectonic Significance of Late Cenozoic Volcanic Rocks, Southern California and Baja California. Geol. Soc. of America Bulletin, v. 81, p. 3323-3338.

Hedge, C. E., Peterman, Z. E. and Braddock, W. A. (1967) Age of the Major Precambrian Regional Metamorphism in the Northern Front Range, Colorado, Geol. Soc. of America Bulletin, vol. 78, p. 551-558.

Heier, K. S. (1965a) Radioactiactive elements in the continental crust. Nature 208, 479-480.

Heier, K. S. (1965b) Metamorphism and chemical differentiation of the crust. Geol. Foren. Stockhdm, Forhandl. 87, pp. 249-256.

Heir, K. S., and Carter, J. L. (1964) Uranium, thorium, and potassium contents in basic rocks and their bearing on the nature of the upper mantle. In Adams, J. A. S. and Louder, W. M. (eds), The natural radiation environment, p. 75, Chicago University Press.

Heier, K. S., McDougall, and Adams, J. A. S. (1964). Th, U and K in Hawaiian lavas, Nature 201, pp. 254.

Heier, K. S., and Rhodes, J. M. (1966) Thorium, uranium and potassium concentrations in granites and gneisses of the Rum Jungle complex, Northern Territory, Australia, Econ. Geol., vol. 61, pp. 563-571.

Heier, K. S. and Rogers, J. W. (1963) Radiometric determination of Thorium, uranium and potassium in basalts and in two magnatic differentiation series. Geochimica et Cosmochimica Acta, vol. 27, No. 2, pp. 137-154.

Helmke, P. A. and Haskin, L. A. (1973) Rare-earth elements, Co, Sc and Hf in the Steens Mountain basalts, Geochimica et Cosmochimica Acta, vol. 37, pp. 1513 to 1529.

Hellman, P. L., Smith, R. E. and Henderson, P. (1979) The Mobility of the Rare Earth Elements: Evidence and Implications From Selected Terrains Affected by Burial Metamorphism, Contributions to Mineralogy and Petrology, vol. 71, p. 23-44.

Hills, F. A. and Houston, R. S. (1979) Early Proterozoic tectonics of the central Rocky Mts., North America, in Contributions to Geology, University of Wyoming, v. 17, no. 2, p. 89-109.

Holdaway, J. J. (1971) Stability of andalusite and the aluminumo silicate phase diagram, Am. J. Sci., vol. 271, pp. 97-131.

Holland, J. G. and Lambert, R. St. (1972) Major element chemical composition of shields and the continental crust, Geochimica et Cosmichimica Acta, vol. 36, pp. 673-683.

Hoschek, G. (1969) The stability of staurolite and chloritoid and their significance in metamorphism of pelitic rocks, Contrib. Mineral. Petrol., vol, 22, pp. 208-232.

Kay, R. W. and Gast, P. W. (1973) The rare earth content and origin of alkali-rich basalts, Journal of Geology, vol, 81, p. 653-682.

Kay, R. W., Hubbard, N. J. and Gast, P. W. (1970) Chemical characteristics and origin of oceanic ridge volcanic rocks. Journal of Geophysical Research, 1583.

Larsen, E. S., 3rd and Gottfried, D. (1960) Uranium and Thorium in selected suites of igneous rocks, American Journal of Science, vol, 258-A, p. 151-169.

Leith, C. K., Van Hise, C. R. (1911) The geology of the Lake Superior region. U. S. Geol. Survey Mono. 52, 641 p.

Lovering, T. S. (1929) Geologic History of the Front Range, Colorado: Colo. Sci. Soc. Proc., vol. 12, p. 61-111.

Lovering, T. S. and Goddard, E. N. (1950) Geology and Ore Deposits of the Front Range, U. S. Geol. Survey Prof. Paper 223.

Luth, W. C. (1976) Granitic rocks, in Bailey, D. K., and MacDonald, R. eds, The evolution of the crystalline rocks, New York, Academic Press, pp. 335-417.

Lyons, J. B. (1955) Geology of the Hanover quadrangle, New Hampshire - Vermont, Geol. Soc. America Bulletin, vol. 66, pp. 105-146.

MacLeod, N. S. and Pratt, R. M. (1973) Petrology of volcanic rocks recovered on Leg 18, in Initial Reports of the Deep Sea Drilling Project, 935.

Mahdavi, A. (1964) Thorium, Uranium and potassium contents of Atlantic and Gulf Coast beachsands. In: J. A. S. Adams and W. M. Louder (eds), The natural radiation environment, p. 87. Chicago University Press.

Mason, B. (1962) Metamorphism in the Southern Alps of New Zealand, Am. Nat. Hist. Mus. Bull, v. 123, Art. 4, p. 217-247.

Mason, R. (1978) Petrology of the Metamorphic Rocks, George Allen and Unwin/Thomas Murby.

McDougall, Ian (1976) Geochemistry and Origin of basalt of the Columbia River Group, Oregon and Washington: Geol. Soc. of America Bulletin, vol. 87, p. 777-792.

McGregor, V. R., (1979) Archean gray greisses and the origin of the Continental Crust: evidence from the Godthaab Region, West Greenland, In: F. Barker (editor), Trondhjemites, Dacites and Related Rocks. Elsevier, Amsterdam, pp. 169-204.

McLennan, Fryer and Young (1979) Rare earth elements in Huronian (Lower Proterozoic) sedimentary rocks: Composition and evolution of the post-Kenoran upper crust, Geochimica et Cosmochimica Acta, vol. 43, pg. 375-388.

Miyashiro, Akiho (1973) Metamorphism and Metamorphic Belts, George Allen and Unwin.

Muecke, G. K., Pride, C., Sarkar, P. (1979) Rare Earth Element Geochemistry of Regional Metamorphic Rocks, Physics and Chemistry of the Earth, vol. 11.

Murray, E. G., and Adams, J. A. S. (1958), Amount and distribution of thorium, uranium and potassium in sandstones. Geochimica et Cosmochimica Acta 13, 260.

Murray, H. H., Patton, J. B. (1953) Preliminary report on high-silica sand in Indiana Dept. Conserv. Geol. Survey Rept. Prog. 5, 35 p.

Nance, R. and Taylor, S. R., (1977) Rare Earth element patterns and crustal evolution - II. Archean sedimentary rocks from Kalgoorlie, Austrilia. Geochimica et Cosmochimica Acta, vol. 41, pp. 225-231.

Nance, R. and Taylor, S. R. (1976) Rare Earth element patterns and crustal evolution - I. Austrialian post-Archean sedimentary rocks, Geochimica et Cosmochimica Acta, vol. 40, pp. 1539-1551.

Noorish, K., and Hutton, J. T. (1969) An accurate x-ray spectrographic method for the analysis of a wide range of geologic samples, Geochimica et Cosmochimica, vol. 33, pp. 431-453.

Norman, J. C. and Haskin, L.A. (1968) The Geochemistry of Sc: A comparison to the rare earths and Fe. Geochimica et Cosmochimica Acta, 32, 93.

Oversby, V. M. (1976) Isotopic Ages and Geochemistry of Archaean acid igneous rocks from the Pilbara, Western Australia. Geochimica Cosmochimica Acta, 40:817-829.

Peterman, Z. E., Hedge, C. E. and Braddock, W. A. (1968) Age of Precambrian Events in the Northeastern Front Range, Colorado. Journal of Geophysical Research, vol. 73, No. 6.

Pettijohn, F. J., 1975, Sedimentary Rocks, Third Edition, Harper & Row, Publishers, New York.

Pettijoh, F. J. Potter, P. E., and Siever, R. (1973) Sand and Sanston, Springer-Verlag, New York, Heidelberg, Berlin.

Phair, G. and Gottfried, (1964). The Colorado Front Range, Colorado, U. S. A., as a uranium and thorium, province: In: J. A. S. Adams and Louder (eds), The natural Radiation environment p. 7, Chicago: Chicago University Press.

Piller, R. and Adams, J. A. S. (1962) The distribution of thorium, uranium and potassium in the Mancos Shale. Geochimica Cosmochimica Acta, 26, 1115.

Rogers, J. W. and Richardson, K. A. (1964) Thorium and uranium contents of some sandstones. Geochimica et Cosmochimica Acta, vl. 28, pp. 2005 to 2011.

Ronov, A. B., Balashov, Y. A. and Migdisov, A. A. (1967) Geochemistry of the rare earths in the sedimentary cycle, Geochemistry International 4, 1-17.

Ronov, A. B., Migdisov, A. A. and Lobach-Zhuchenko, S. B. (1977) Reginonal Metamorphism and Sediment Composition Evolution, Geochemistry Internationa, Geochemistry International 14, 90-112.

Rothrock, E. P. (1944) A geology of South Dakota, part 3, Mineral Resources. South Dakota Geol. Survey Bulletin 15, 255p.

Shaw, D. M. Dostal, J. and Keays, R. R. (1976) Additional estimates of continental surface Precambrian sheild composition in Canada. Geochimica et Cosmochimica Acta, vol. 40, pp. 73-83.

Shaw, D. M. Reilly, G. A., Muysson, J. R., Pattenden, G. E., and Campbell, F. E. (1967) An estimate of the chemical composition of the Canadian Precambrian Shield. Can. J. Earth Sci. 4, 829-854.

Schwab, F. L., 1975, Framework mineralogy and chemical composition of continental margin-type sandstone: Geology, v. 3, p. 487-490.

Schwarcz, H. P. (1966) Chemical and Mineralogic Variations in an Arkosic Quartzite During Progressive Regional Metamorphism, Geol. Soc. America Bulletin, vol. 77, pp. 509-530.

Schwartz (1978) Secular trends in the composition of sedimentary rock assemblages - Archean through Phanerozoic time. Geology v. 6, 532-536.

Shaw, D. M. (1956) Geochemistry of pelitic rocks, part III, Major Element Geochemistry, vol. 67, p. 919-934.

Shaw, D. M. (1954) Trace Elements in metamorphic rocks, part I - Variations during Metamorphism, Geological Society of America Vol 65, p. 1151-1165.

Simonen, Ahti, Kuovo, Olavi, (1955), Sandstones in Finland. Comm. geol. Finlande, Bull. 168, p. 57-87.

Spry, ALan, (1969) Metamorphic Textures. Pergomon International Library of Science, Technology, Engineering and Social Studies.

Tatsumoto, M., Hedge, C., and Engel, A.E.J. (1965), Potassium, rubidium, strontium, thorium, uranium and the ratio of strontium-87 to strontium-86 in oceanic tholeiitic basalts, Science 150, p. 866.

Taylor, S. R. (1969) Trace element chemistry of andesites and associated calc-alkaline rocks in Proceedings of the Andesite Conference, International upper Mantle Project Scientific Report 16. pg. 43-63.

Taylor, S. R. Capp, A. E. and Graham, A. L. (1969) Trace elements abundances in andesites, II. Saipan, Bougainville and Fuji, Contributions Mineralogy and Petrology 23, 1,26.

Taylor, S. R., and White, A. J. R., 1966, Trace element abundances in andesites: Bulletin Volcanoloqique, vo. 29, p. 177-194.

Thiel, G. A., Sedimentary and petrographic analysis of the St. Peter Sandstone. Geol. Soc. America Bull. 46, 559-614.

Thompson, J. B. (1957) The graphical analysis of mineral assemblages in pelitic schists, Am. Mineralogist, vol. 42, pp. 842-858.

Thompson, J. B. and Norton, S. A. (1968) Paleozoic regional metamorphism in New England and adjacent areas. In E-An Zen et al. eds. Studies of Appalachian Geology. Interscience Publisher (John Wiley and Sons), New York.

Tilley, C. E.: Metamorphic zones in the southern Highlands of Scotland, Geol. Soc. London Quart. J., vol. 81, pp. 100-112.

Tilling, R. I. and Gottfriield, D. (1969) Distribution of thorium, uranium, and potassium in igneous rocks of the Boulder Batholith Region, Montana, and it's bearing on Radiogenic Heat Production and Heat Flow, Geological Survey Professional Paper 614-E.

Turkekian, K. K., and Wedepohl, K. H., 1961, Distribution of elements in some major units of the earth's crust: Geological Society of America, Bull., v. 72, p. 175-192.

Turner, F. J. (1981) Metamorphic Petrology: Mineralogical, Field, and Tectonic Aspects, Second Edition. Hemisphere Publishing Corporation.

Turner, F. J. and Verhoogen, J. (1960) Igneous and Metamorphic Petrology, McGraw-Hill Book Co., New York, 694 pp.

Tweto, Ogden (1977) Nomenclature of Precambrian rocks in Colorado: U.S. Geological Survey, Professional Paper 1422-D, 22p.

Waters, A. C. (1962) Basalt magma types and their tectonic associations: Pacific northwest of the United States, in MacDonald, G. A., and Kuno, H. Editors, The Crust of the Pacific Basin: Am. Geophys. Union Geophys. Mon. Ser., no. 6, p. 158-176.

Wildeman, T. R., and Condie, K. C. (1973) Rare earths in Archean graywackes from Wyoming and from the Fig Tree Group, South Africa, Geochimica et Cosmochimica Acta, vol. 37, p. 439-453.

Wildeman, T. R. and Haskin, L. A. (1973) Rare Earths in Precambrian sediments, Geochimica et Cosmochimica Acta, Vol, 37, pp. 419-438.

Williamson, D. H. (1953) Petrology of chloritoid and staurolite rocks north of Stonehaven, Kincardineshire, Geol. Mag., vol. 90, pp. 353-361.

Winkler, H. G. F. (1979) Petrogenesis of Metamorphic Rocks, Fifth Edition, Springer-Verlog, New York. Heidelberg. Berlin.